

**Interaction of Aza-aromatic Compounds with Porous Silica Beads  
and Controlled Porous Glasses as Studied by Absorption  
and Fluorescence Spectroscopy**

**Absorptions- und fluoreszenzspektroskopische Untersuchungen  
der Wechselwirkung von Aza-aromaten mit porösen  
Kieselgelen und kontrolliert porösen Gläsern**

Dissertation

der Fakultät für Chemie und Pharmazie  
der Eberhard Karls Universität Tübingen  
zur Erlangung des Grades eines Doktors  
der Naturwissenschaften

2006

vorgelegt von

**Abeer Salah Eldeen Elsherbiny**

Tag der mündlichen Prüfung:	27.6.2006
Dekan :	Prof. Dr. S. Laufer
1- Berichterstatter :	Prof. Dr. D. Oelkrug
2- Berichterstatter :	PD. Dr. H.-J. Egelhaaf

Die vorliegende Arbeit wurde am Institut für Physikalische und Theoretische Chemie der Universität Tübingen unter Anleitung von Herrn Prof. Dr. Dieter Oelkrug durchgeführt, dem ich für seine Unterstützung und sein Stetiges Interesse danke.

**To**

**MY PARENTS AND MY FAMILY**

## ACKNOWLEDGMENT

I am deeply thankful to God, by the grace of whom the progress of this work was possible. I wish to express my gratitude thanks to Prof. Dr. D. Oelkrug for his great interest, encouragement and his stimulating discussions throughout the progress of this work.

I would like to thank Dr. H.-J. Eglhaaf for suggesting the topic point, continuous guidance, great efforts and fruitful advice during the work. Also, I would like to thank Prof. Dr. K. Albert group for supplying the porous and coated silica and help during the HPLC measurements. Also, I wish to express my deep thanks to Graduiertenkollegs 'Chemie in Interphasen' for supporting this work.

I wish also to extend my thanks to the authorities of Institute of Physical and Theoretical Chemistry, Tübingen University for facilities afford, without which the present work would never have been completed. Also, I wish to thanks my husband for his stand beside me during this work.

# Contents

Page

<b>1. Introduction</b> .....	1
1.1. Stationary phase .....	2
1.2. Probe molecules.....	5
<b>2. Theory</b> .....	7
2.1. Electronic absorption spectroscopy.....	7
2.2. Fluorescence spectroscopy.....	8
2.3. Fluorescence anisotropy.....	9
2.3.1. Effect of multiple scattering on fluorescence anisotropy.....	10
2.3.2. Effects of rotational diffusion on fluorescence anisotropy:	
The Perrin equation.....	11
2.4. Fluorescence lifetime or decay time.....	11
2.5. Collisional quenching of fluorescence.....	12
2.6. Kinetics of opposing reactions in interphase systems.....	13
2.7. Simplified description of reaction kinetics and equilibria	
in interphase systems.....	15
2.7.1. Neglect of back reaction.....	17
2.8. Selectivity factor in chromatography.....	18
<b>3. Experimental</b> .....	20
3.1. Materials.....	20
3.1.1. Fluorescent probes (adsorbates).....	20
3.1.2. Solvents.....	21
3.1.3. Stationary phases.....	21
3.1.3.1. Silica.....	21
3.1.3.1.1. Non-modified (bare) silica.....	21
3.1.3.1.2. Modified (Coated) silica.....	22
3.1.3.1.2.1. Modified with alkyl chains (C30 – alkyl chains).....	22
3.1.3.1.2.2. Modified with active groups (amino groups).....	22
3.1.3.1.2.3 Modified with polymers.....	24
3.1.3.2 Determination the amine concentration at the modified silica surfaces.....	25
3.1.3.3. Controlled Porous Glass (CPG).....	25
3.1.3.3.1. Geltech Controlled Porous Glass (PGG).....	25

3.1.3.3.2. Porous Vycor Glass (PVG).....	25
3.2. Instruments.....	26
3.2.1. Absorption spectrophotometer.....	26
3.2.2. Fluorometer.....	26
3.2.3. Centrifuge.....	27
3.2.4. High-performance liquid chromatography (HPLC).....	27
3.3. Measurements.....	27
3.3.1. Characterization of the adsorption.....	27
3.3.1.1. Silica as stationary phase.....	27
3.3.1.1. CPG as a stationary phase.....	27
3.3.2. Kinetics measurements.....	29
3.3.2.1. Silica as adsorbent.....	29
3.3.2.2. Silica as reactant.....	29
3.3.2.3. PVG as adsorbent.....	29
<b>4. Results and Discussions.....</b>	<b>31</b>
4.1. <b>Characterization of probes in solution.....</b>	<b>31</b>
4.1.1. Selection of probes.....	31
4.1.2. Electronic transitions.....	31
4.1.2.1. Spectra of neutral probes.....	32
4.1.2.2. Influence of solvent acidity on probe spectra.....	34
4.1.2.3. Fluorescence quantum yields and decay times.....	39
4.1.2.4. Fluorescence anisotropy of probes.....	41
4.2. <b>Spectroscopic characterization of the adsorbed state.....</b>	<b>47</b>
4.2.1. Controlled porous glass as adsorbent.....	49
4.2.1.1 Porous Vycor glass .....	49
4.2.1.2. Porous Geltech glass .....	54
4.2.3. Non-modified silica beads as adsorbent.....	58
4.2.4. Modified silica as adsorbent.....	67
4.2.4.1 Silica modified with alkyl chains (silica C30).....	67
4.2.4.2. Silica modified with polymers.....	71
4.2.4.2.1. TBB-coated silica .....	71
4.2.4.2.2. Polymerized divinylbenzene (DVB)-coated silica .....	72
<b>Discussion .....</b>	<b>74</b>
4.3. <b>Adsorption equilibria.....</b>	<b>77</b>

4.3.1. Controlled porous glass as adsorbent.....	77
4.3.1.1. Porous Vycor glass (PVG) .....	77
4.3.1.2. Porous Geltech glass (PGG) .....	77
4.3.2. Non-modified silica beads as adsorbent.....	78
4.3.3. Modified silica beads as adsorbent.....	82
4.3.3.1. Modified with polymer.....	82
4.3.3.1.1. TBB-coated silica.....	82
4.3.3.1.2. Polymerized divinylbenzene (DVB)-coated silica .....	84
4.3.4. HPLC measurements.....	84
<b>Discussion</b> .....	87
<b>4.4. Adsorption kinetics</b> .....	89
4.4.1. Adsorption at porous Vycor glass (PVG).....	89
4.4.1.1. Adsorption of AC at PVG.....	89
4.4.1.2. Adsorption of 1-DBA at PVG.....	92
4.4.1.3. Adsorption of 3-DBA at PVG.....	96
4.4.2. Adsorption at non-modified silica beads.....	100
<b>Discussion</b> .....	107
<b>4.5. Accessibility of probes attached to silica surfaces</b> .....	108
4.5.1. Influence of O <sub>2</sub> on the fluorescence intensity and lifetime of adsorbates.....	109
4.5.1.1. Acridine.....	109
4.5.1.2. Dibenzacridines.....	112
4.5.1.2.1. 1,2,7,8-Dibenzacridine.....	112
4.5.1.2.2. 3,4,5,6-Dibenzacridine.....	117
<b>Discussion</b> .....	119
4.5.2. Chemical reactivity at silica surfaces.....	120
4.5.2.1. Introduction.....	120
4.5.2.2. Binding and mobility.....	122
4.5.2.3. Reaction kinetics.....	125
<b>Discussion</b> .....	129
<b>Summary</b> .....	130
<b>References</b> .....	134



# 1. Introduction

The term of interphase was first introduced in reverse-phase chromatography [1, 2]. For the application of interphases in chromatography, catalysis, and organic synthesis, the same rationale is inherent [3]. An interphase system is formed when the mobile phase penetrates into the stationary phase in molecular level without forming a homogeneous solution [3]. The stationary phase is composed of an inert matrix, a flexible spacer, and a reactive center, whereas the mobile phase consists of a solvent or a gaseous, liquid, or dissolved reactant.

In recent years, various types of photophysical and photochemical phenomena on solid surfaces have been the subject of a number of investigations from both a fundamental as well as an applied approach. At the same time, surface photochemistry and photocatalysis on various substrates have also been actively investigated in the gas and liquid phases. The materials utilized include powders with high surface areas and microporous structures such as  $\text{SiO}_2$ ,  $\text{Al}_2\text{O}_3$  and zeolites.

It has been shown that fluorescence spectroscopy is a useful tool to characterize chemical processes at the interfaces of stationary phases, such as molecular aggregation [4-6], electron transfer [7], proton transfer [8-12], or photochemical transformations [13]. Silica gels are certainly most widely used as substrates for fluorescence investigations.

The present work describes how aromatic compounds can be used as fluorescent probes to characterize the solute-surface interactions at chromatographic or catalytic interfaces, namely nonmodified silica, modified (coated) silica, and controlled porous glasses. By comparing the absorption and fluorescence spectra of the probe molecules in solution to the spectra of the adsorbed species we are able to distinguish between various surface binding sites of different acidity. It will be shown how the nature of the substrate affects the type of the prevalent binding site for the solute molecules. The mobility of the adsorbed probe molecules on the surfaces is determined by the fluorescence anisotropy. The kinetics of the adsorption of the probes on the surfaces (porous Vycor glass and silica) will be measured by absorbance and fluorescence spectroscopy, respectively. The accessibility of the adsorbed species on the surfaces to the oxygen quenching and the accessibility of the active groups in

the modified silica surface will be studied by fluorescence spectroscopy. The ability of the coating polymer to shield the surface silanol groups of silica is measured by fluorescence and fluorescence excitation anisotropy spectra and compared to the results obtained for high-performance liquid chromatography (HPLC).

Description of the materials used during this study will be given:

## 1.1. Stationary phases

The stationary phases of this investigation are silica beads and monolithics. Silica is the most important stationary phase in liquid chromatography. The surface properties of silica have been studied extensively over a long period of time, but there are still many controversies and ambiguities about the origin of the surface acidity, the molecular interactions between solutes and the silica surface, and the surface polarity of silica.

The surface of silica is composed of isolated silanol and strained Si-O-Si (siloxane) groups. Surface silanol groups are mainly responsible for interactions between the silica surface and adsorbates. There are three types of silanol groups: free silanols, hydrogen-bonded silanols and geminal silanols [14] as shown in Fig. 1.

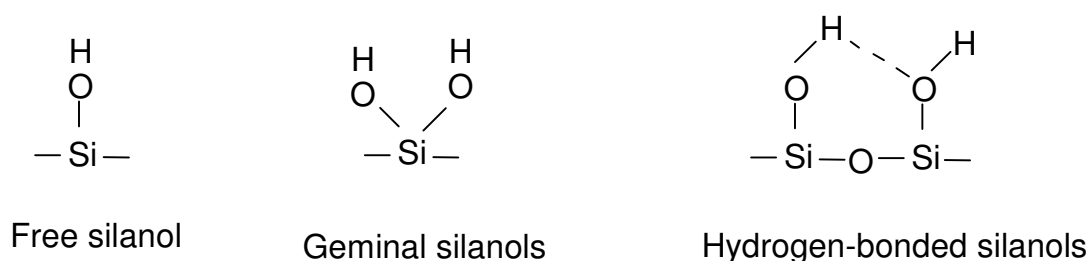


Fig. 1. Different types of silanol groups.

These different types of silanol groups have different acidities. It is generally believed that free silanol groups are more acidic than hydrogen-bonded silanols [15, 16]. Strong evidence was given [17] that geminal silanols were the acidic sites responsible for the abnormal chromatographic behaviour for basic solutes on silica [18-19].

Pure silica gel is inactive for demanding acid-catalyzed reactions, evidently because surface SiOH groups have only a feeble acid strength. The  $pK_a$  values of such groups fall

somewhere in the range of 4 to 7, depending on the mode of measurement [20-22]. Infrared studies of bases chemisorbed on silica gel also show that the SiOH groups are only weakly acidic. Another infrared study shows that silica gel has weak Bronsted acid sites which react with n-butyl amine but are inert towards pyridine under the same conditions [23]. When silica gel is degassed at temperatures higher than 500°C, most surface SiOH groups are removed as well as the weak Bronsted acidity associated with such groups [23]. Reactive sites are formed when silica gel is dehydroxylated, as confirmed by a recent infrared study [24]. The authors find that the new sites chemisorb H<sub>2</sub>O, NH<sub>3</sub>, and CH<sub>3</sub>OH to form SiOH, SiNH<sub>2</sub>, and SiOCH<sub>3</sub> groups, respectively, and suggest that such reactive sites consist of strained Si-O-Si bridges.

There are several methods for the determination of surface acidity, like contact angle titration [25], gaseous base or acid adsorption methods [26], and titration methods using pH indicators [27]. The methods differ in the chemical and physical principles on which they are based, and none of them can be regarded as the universal. Methods using pH indicators have been applied in this field for several decades [26, 28-34]. A precise method for acidity measurements based on pH indicators applicable to pharmaceutical excipients was developed [35]. In this method, indicators were mixed with excipients. The acid strength was determined by recording the spectra of these excipient-indicator mixtures in diffuse reflectance and correlating these spectra to the spectra of indicators in aqueous solution. As a result, a pH-equivalent (pH<sub>eq</sub>) was obtained as a measure for the acid strength.

The surface acidity of some hydrated stationary chromatographic phases was determined by using the same method in [35]. The acidity were given as pH-equivalent (pH<sub>eq</sub>) [36] and the authors found that, the highly purified silica gels always react neutral with a pH<sub>eq</sub> between 6.5 and 7.

Silica-based stationary phases are commonly used in high-performance liquid chromatography (HPLC) and thin-layer chromatography (TLC) [37]. A serious undesirable property of silica is its surface acidity due to free silanols. Effects of silanols on HPLC and TLC retention are difficult to control, especially in the chromatographic behaviour of basic analytes. The problem relates to even the most modern highly purified silica supports and this is due to the strong interactions with the basic analyte which leads to tailing of the peaks in a chromatogram. Hence, modification of the composition of the mobile phase (careful adjustment of pH and / or addition of ionic substances) is necessary [38,39]. The addition of ionic substances to the mobile phases provides coverage of only one third of all the silanol

groups [40-42] Improved separation selectivity can also be obtained by tailoring the properties of the column packing materials [43,44]. End-capping is a process, whereby short-chain chlorosilanes are used to cover the silanol groups. However, even this process leaves some of the silanol groups unreacted. It is also possible to coat silica particles by means of a physically adsorbed polymer [45-47]. Hence, a reduction of unwanted analyte-silanol interactions is expected [48,49]. Polymer resins with a low degree of cross-linking suffer from mass transfer limitations as well as swelling problems, which can lead to poor chromatographic performance [50].

In addition to porous silica beads, also controlled porous glasses are used as stationary phase in chromatography [51, 52]. Controlled porous glasses (CPG's) and the related Vycor glasses have excellent mechanical properties and can be prepared with a wide range of porosities and pore sizes [53]. They can be modified to include a variety of functional groups, and the adsorption strength of the glasses can be adjusted over a wide range of values [52]. Although CPG's were developed for use in size-exclusion chromatography, derivative glasses can show a high chemical affinity for certain biomolecules, and even can be used as catalytic agents or bioreactors [51].

The original preparations and characterizations of CPG's were done by Haller [54]. The starting material is 50-75% SiO<sub>2</sub>, 1-10% Na<sub>2</sub>O, and the remainder B<sub>2</sub>O<sub>3</sub>. The molten glass mixture is phase-separated by cooling to between 500 and 750 °C. The time taken for this treatment determines the extent of phase separation and the resulting average pore size. The borate phase is leached out by acid solutions at high temperatures. The remaining glass contains colloidal silica particles, which are removed by a treatment with NaOH followed by washing with water. The final glass has porosity between 50% and 75% and an average pore size between 4.5 nm and 400 nm. CPG's have surface areas between 10 and 350 m<sup>2</sup>/g, depending on the pore size [52]. Vycor glasses are prepared by a similar procedure [53]. Vycor glasses have a porosity of nearly 28%, an average internal pore diameter 4 and 6 nanometres, and a surface area between 90 and 200 m<sup>2</sup>/g [53]. Vycor porous glass resembles silica gel [55-57], but one difference should be noted. Because of its preparation method, Vycor porous glass, in contrast to silica gel, possesses surface B<sub>2</sub>O<sub>3</sub> Lewis acid sites [57]. The number of these sites depends on the extent of acid leaching, but some estimates suggest that as much as one-third of the surface could be B<sub>2</sub>O<sub>3</sub> [57].

Porous glasses are usually characterized by using standard nitrogen adsorption techniques. Although there has been considerable interest in the physics of flow, diffusion and adsorption in these materials, there have been relatively few complete characterizations of porous glasses and much of their structure is not yet well understood [58].

## 1.2. Probe molecules

The photophysical properties of molecules adsorbed on heterogeneous surfaces were investigated using stationary and time resolved fluorescence spectroscopy [59,60]. In these studies, aromatic amines were used to characterize the solute-surface interaction at chromatographic interfaces. The adsorbed molecules were acridine and some of its derivatives.

Acridine (AC) is an important aza-aromatic compound mainly used as a staining dye for biological tissues. Its derivatives show significant antibacterial and potential antiviral activity and have been widely used in pharmacology [61,62]. Due to their prominent chelating properties, acridines also have been used as ligands for heavy metals in different areas of chemistry [63]. Electronic relaxation processes of excited acridine were investigated in polar and nonpolar solvents [64-68]. It was found that the fluorescence intensity depends on the type of the solvent; strong fluorescence is observed in protic solvents such as water and very weak fluorescence in aprotic solvents such as hydrocarbons at room temperature [69-71]. The solvent dependence of  $\Phi_F$  was interpreted in terms of hydrogen bond interaction which causes an interchange of the electronic character in the lowest excited singlet state:  $\pi-\pi^*$  character in protic solvents and  $n-\pi^*$  character in aprotic solvents [71-73].

The adsorption of AC at silica surfaces was studied by fluorescence spectroscopy [74-76, 36]. Fluorescence studies [77-78] were found that on silica gel preheated at 180°C AC formed hydrogen-bonded complexes which undergo protonation in the excited state via fast proton transfer reaction. Other authors found that on highly porous silica gel preheated at 600°C, AC is adsorbed as H-bonded species and also traces of protonated species were formed in the ground state [36].

The adsorption of 1,2,7,8-dibenzacridine (1-DBA) and 3,4,5,6-dibenzacridine (3-DBA) on silica and alumina surfaces have been investigated [74,75]. It was concluded that 1-

DBA forms hydrogen-bonded complexes on silica surfaces and protonated cations on alumina surfaces. 3-DBA is not protonated on alumina and forms hydrogen-bonded complexes. It was also observed that 1-DBA aggregates on silica when the liquid-phase adsorption is followed by evaporation of the solvent, but adsorption from high vacuum results in isolated adsorbates.

The adsorption of acridine orange (AO) on silica surface is accompanied by a long wavelength shift of its emission spectrum and a dependence of the maximum position on the excitation wavelength [79]. At the same time, there is also another characteristic shift in the spectrum of AO which is related to the formation of associates of the AO dye. The effect of concentration of AO on its electronic spectra in solution was studied in [80].

## 2- Theory

### 2.1. Electronic absorption spectroscopy

The absorbance  $A$  of a sample of molar concentration  $[j]$  is

$$A = \log \frac{I_0}{I} = \varepsilon [j] l \quad (1)$$

where  $I_0$  is the light intensity incident on the sample,  $I$  is the intensity of the light after passing through the sample,  $\varepsilon$  is the molar absorption coefficient (extinction coefficient) of the species and it depends on the frequency of the incident light. Its dimension is  $1 / (\text{concentration} * \text{length})$ , and  $l$  is the path length of the sample.

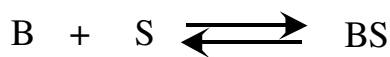
The ratio of the transmitted intensity  $I$  to the incident intensity  $I_0$  at a given frequency is called the transmittance  $T$  of the sample at that frequency;

$$T = \frac{I}{I_0} = 10^{-A} \quad (2)$$

If there is a mixture of absorbing species  $i$  in the solution, the total absorbance at certain wavelength is given by

$$A(\lambda) = \sum_i A_i(\lambda) = \sum_i \varepsilon_i(\lambda) [j_i] l \quad (3)$$

In a two-component system



Where  $B$  is a neutral base which has absorbance at  $\lambda_2$ ,  $S$  are the silanol groups in the stationary surface (glass sheet), and  $BS$  is the protonated or the H-bonded form of the base on the surface which has absorbance at  $\lambda_1$  and  $\lambda_2$ . The absorbance at  $\lambda_2$  in presence of the glass sheet is  $A_2(\lambda_2)$  which is a mixture of the absorbance of the protonated form,  $A_{BS}(\lambda_2)$  at  $\lambda_2$  and the absorbance of the nonadsorbed base in solution,  $A_B(\lambda_2)$  at  $\lambda_2$ , i.e.

$$A_2(\lambda_2) = A_B(\lambda_2) + A_{BS}(\lambda_2) \quad (4)$$

At time,  $t \rightarrow \infty$ , the ratio of the absorbance of the protonated form at  $(\lambda_1)$  and  $(\lambda_2)$  is constant,  $c$ ; so

$$\text{At } t \rightarrow \infty, \frac{A_{BS}(\lambda_2)}{A_{BS}(\lambda_1)} = c \quad \text{and} \quad A_{BS}(\lambda_2) = c \cdot A_{BS}(\lambda_1) \quad (5)$$

Inserting Eq. 5 into Eq. 4 one obtains

$$A_B(\lambda_2) = A_2(\lambda_2) - c \cdot A_{BS}(\lambda_1) \quad (6)$$

## 2.2. Fluorescence spectroscopy

Luminescence is the emission of light from any substance and occurs from electronically excited states. Luminescence is formally divided into two categories, fluorescence and phosphorescence, depending on the nature of the excited state. In the excited singlet states, the electron in the excited orbital is of opposite spin to the second electron in the ground-state orbital. Consequently, return to the ground state is spin-allowed and occurs rapidly by emission of a photon. The emission rates of fluorescence are  $10^7$ - $10^9$  s<sup>-1</sup>, so that a typical fluorescence lifetime is in the nanosecond range. The lifetime  $\tau_F$  of a fluorophore is the average time between its excitation and its return to the ground state.

Fluorescence spectral data are generally presented as emission spectra. A fluorescence emission spectrum is a plot of the fluorescence intensity versus wavelength (nanometres, nm) or wavenumber (cm<sup>-1</sup>).

The fluorescence Intensity is given by

$$I_F = I_{abs} \cdot \phi_F \quad (7)$$

where  $I_{abs}$  is the intensity of the absorbed light by the fluorophore and  $\phi_F$  is the fluorescence quantum yield of the fluorophore, i.e. the ratio of the number of photons emitted to the number absorbed. The absorbed light intensity can be expressed by

$$I_{abs} = I_0(1 - T) \quad (8)$$

where  $T$  is the transmittance according to Eq. 2, and  $I_0$  is the intensity of the incident light.

So the fluorescence intensity is given by

$$I_F = I_0(1 - 10^{-A}) \cdot \phi_F \quad (9)$$



The fluorescence quantum yield is governed by the emissive rate of the fluorophore ( $\Gamma$ ) and the rate of nonradiative depopulation of the excited state ( $k_{nr}$ ).

$$\phi_F = \frac{\Gamma}{\Gamma + k_{nr}} \quad (10)$$

If there are more than one fluorophore in solution, the total fluorescence intensity is given by

$$I_F = \sum_i I_{Fi}, \text{ and } I_{Fi} \text{ is given by} \quad (11)$$

$$I_{Fi} = I_0 \frac{A_i}{A} (1 - 10^{-A}) \cdot \phi_{Fi} \quad (12)$$

where  $A_i$  is the absorbance of  $i^{\text{th}}$  fluorophore, and  $A$  is the total absorbance of the mixture.

### 2.3. Fluorescence anisotropy

The measurement of fluorescence anisotropy is illustrated in Fig. 2.

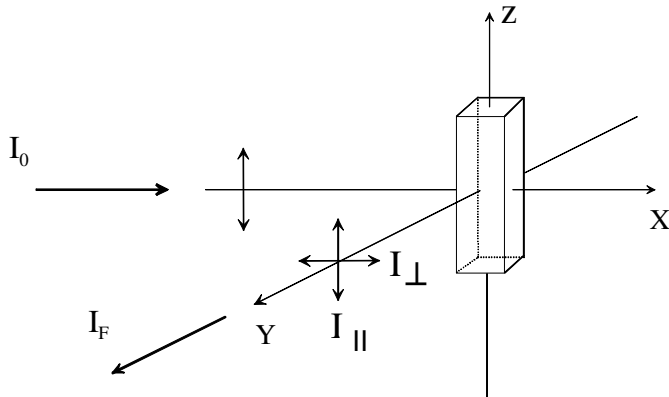


Fig. 2. Schematic diagram for measurement of fluorescence anisotropy.

Where  $I_0$  is the intensity of incident light and  $I_F$  is the total fluorescence intensity

The sample is excited with vertically polarized light. The electric vector of the excitation light is oriented parallel to the vertical or z-axis. One then measures the intensity of the emission through a polarizer. When the emission polarizer is oriented parallel ( $\parallel$ ) to the direction of the polarized excitation, the observed intensity is called  $I_{\parallel}$ . Likewise, when the polarizer is perpendicular ( $\perp$ ) to the excitation, the intensity is called  $I_{\perp}$ . These values are used to calculate the anisotropy:

$$r = \frac{(I_{\parallel} - I_{\perp})}{(I_{\parallel} + 2I_{\perp})} \quad (13)$$

The anisotropy is a dimensionless quantity which is independent of the total intensity of the sample because the difference  $(I_{\parallel} - I_{\perp})$  is normalized to the total intensity, which is

$$I_F = I_{\parallel} + 2I_{\perp}.$$

The fundamental anisotropy of a fluorophore is given by

$$r_0 = \frac{3 \cos^2 \beta - 1}{5} \quad (14)$$

where  $\beta$  is the angle between the absorption and emission dipoles. The fundamental anisotropy is the anisotropy observed in the absence of other depolarizing processes such as rotational diffusion or energy transfer. For a system of randomly oriented fluorophores, the value of the fundamental anisotropy curves are in the range of  $-0.2 \leq r_0 \leq 0.4$  for single-photon excitations.

There are several phenomena that reduce the measured anisotropy to lower than the maximum theoretical values. These phenomena are rotational diffusion, energy transfer and multiple scattering.

### 2.3.1. Effect of multiple scattering on fluorescence anisotropy

The rotational diffusion of a fluorescence probe attached to silica surface cannot exactly be determined on the basis of Eq. 13, because the multiple scattering effects are not negligible, when light travels through the opaque phase. Correction should be done to obtain the real value of fluorescence anisotropy. The real value of fluorescence anisotropy  $R$  can be calculated from the following equation [81]:

$$R = \frac{r}{(P(\lambda_1)P(\lambda_2))^{0.5}} \quad (15)$$

where  $r$  is the measured anisotropy and  $P(\lambda_1)^{0.5}$  and  $P(\lambda_2)^{0.5}$  are the experimental values of anisotropy due to scattering observed at same wavelength as incident and emitted light ( $\lambda_1$  and  $\lambda_2$  nm, respectively).

### 2.3.2. Effects of rotational diffusion on fluorescence anisotropy:

#### The Perrin equation

Rotational diffusion of fluorophores is a dominant cause of fluorescence depolarization. This mode of depolarization is described in the simplest case for spherical rotors by the Perrin equation

$$\frac{r_0}{r} = 1 + \frac{\tau_F}{\tau_R} = 1 + 6D\tau_F \quad (16)$$

where  $\tau_F$  is the fluorescence life time,  $\tau_R$  is the rotational correlation time, and  $D$  is the rotational diffusion coefficient. If  $\tau_R \gg \tau_F$ , the measured anisotropy ( $r$ ) is equal to the fundamental anisotropy ( $r_0$ ), if the correlation time is much shorter than the lifetime ( $\tau_R \ll \tau_F$ ) then the anisotropy is zero.

### 2.4. Fluorescence lifetime or decay time

Suppose a sample containing the fluorophore is excited with an infinitely sharp ( $\delta$ -function) pulse of light. This results in an initial population ( $n_0$ ) of fluorophores in the excited state. The excited-state population decays with a rate  $\Gamma + k_{nr}$  according to

$$\frac{dn(t)}{dt} = -(\Gamma + k_{nr}) n(t) \quad (17)$$

where  $n(t)$  is the number of excited molecules at time  $t$  following excitation,  $\Gamma$  is the emissive rate, and  $k_{nr}$  is the nonradiative decay rate. Emission is a random event, and each excited fluorophore has the same probability of emitting within a given period of time. This results in an exponential decay of the excited-state population,  $n(t) = n_0 \exp(-t/\tau_F)$ .

In a fluorescence experiment we do not observe the number of excited molecules, but rather a fluorescence intensity, which is proportional to  $n(t)$ . Hence, Eq. 17 can also be written in terms of a time-dependent intensity  $I_F(t)$ . Integration of Eq. 17 yields the usual expression for a single exponential decay

$$I_F(t) = I_0 \exp(-t/\tau_F) \quad (18)$$

where  $I_0$  is the intensity at time zero. The lifetime  $\tau_F$  is the inverse of the total decay rate:  $\tau_F = (\Gamma + k_{nr})^{-1}$ . In general, the inverse of the lifetime is the sum of the rates which

depopulate the excited state. The fluorescence lifetime can be obtained in two ways, one from the time at which the intensity decreases to  $1/e$  of its initial value. The more common method is to determine the lifetime from the slope of a plot of  $\log I_F(t)$  versus  $t$ .

Multi-exponential analysis of the fluorescence decay curves is given by

$$I_F(t) = \sum_i B_i \exp\left(-t/\tau_{Fi}\right) \quad (19)$$

where  $\tau_{Fi}$  is the fluorescence decay time of the *i*th component,  $B_i$  is the amplitude of the components decay curve, i.e. it's intensity at  $t = 0$ .

The lifetime is also the average amount of time a fluorophore remains in the excited state after excitation. This can be seen by calculating the average (mean) fluorescence decay times  $\langle \tau_F \rangle$  were obtained from multi-exponential decay analysis:

$$\langle \tau_F \rangle = \frac{\sum_i B_i \tau_{Fi}^2}{\sum_i B_i \tau_{Fi}} \quad (20)$$

## 2.5. Collisional quenching of fluorescence

Collisional quenching of fluorescence is described by the Stern-Volmer equation,

$$\frac{I_{F_0}}{I_F} = 1 + k_q \tau_F [Q] = 1 + K_D [Q] \quad (21)$$

where  $I_{F_0}$  and  $I_F$  are the fluorescence intensities in the absence and presence of a quencher, respectively,  $k_q$  is the bimolecular quenching constant,  $\tau_F$  is the lifetime of the fluorophore in the absence of quencher, and  $[Q]$  is the concentration of the quencher. The Stern-Volmer quenching constant is given by  $k_q \tau_F$ . If the quenching is known to be dynamic, the Stern-Volmer constant will be represented by  $K_D$ .

Quenching data are usually presented as plots of  $I_{F_0}/I_F$  versus  $[Q]$ . This is because the ratio  $I_{F_0}/I_F$  is expected to be linearly dependent upon the concentration of quencher.

## 2.6. Kinetics of opposing reactions in interphase systems

A reaction may proceed to an equilibrium state that differs appreciably from completion. The adsorption of a base on silica beads or glass sheets can be summarized in Fig. 3.

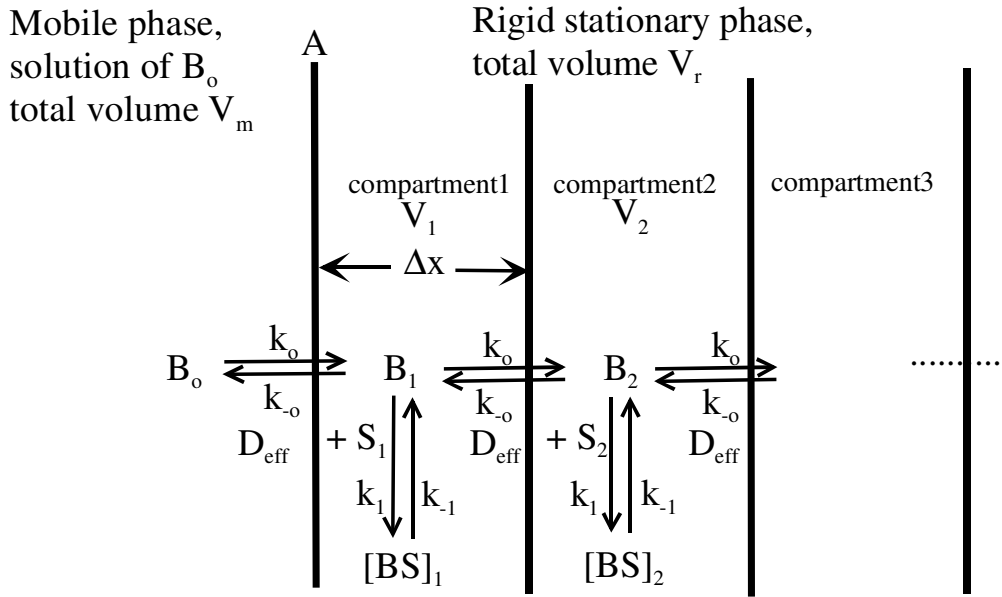


Fig. 3. Schematic diagram for the diffusion and adsorption of a dissolved base  $B_o$  into silica beads or glass sheets.  $D_{eff}$  The effective diffusion coefficient of the dissolved base in the compartments of the silica beads or the glass sheets.

Here, the silica sphere or the glass sheet is divided into  $i$  sufficiently thin concentric spherical shells (subshells) or planar compartments (subsheets),  $i = 1, 2, 3 \dots, i_{max}$ .

$V_m$  is the volume of the mobile phase.

$V_r = \sum_{i=1}^{i_{max}} V_i$  is the volume of the rigid stationary phase (silica beads or glass sheets).

$[B_o]$  is the concentration of a base solution in cyclohexane.

$[B_i]$  is the base concentration inside the compartment  $i$  of the silica beads or the glass sheets.

$[S_i]$  refers to the concentration of the acidic centres at the internal surface of  $SiO_2$  in compartment  $i$  of the silica beads or the glass sheets.

$[BS]_i$  is the concentration of the complex which is formed on the silica beads or on the glass sheets due to the reaction between the base of concentration  $[B_i]$  and acidic centres  $[S_i]$  in compartment  $i$ .

$D_{eff}$  is the effective diffusion coefficient of  $B$  inside the compartments of the beads or of the sheets.

$\Delta x$  is the thickness of the each compartment.

$A$  is the surface area of the silica beads or the glass sheets that is exposed to the cyclohexane solution,

$A = \frac{V_r}{d}$  where  $d$  is the thickness of the glass sheets and  $A = \pi d^2$  where  $d$  is the diameter of the beads.

If the experiment is started using a base solution of concentration  $[B_o]$ , the base starts to diffuse inside the compartments of the silica beads or the glass sheets, reacts with the acidic centres  $[S_i]$  in the beads or the sheets and forms the adsorbed complex  $[BS]_i$ , at a time  $t > 0$ .

The net rate of the change of base concentration  $[B_o]$  is

$$-\frac{\Delta[B_o]}{\Delta t} = k_o [B_o] - k_{-o} [B_1] \quad (22)$$

Since the silica beads or the glass sheets are porous, so there is diffusion of  $[B_o]$  into the compartments of the beads or the sheets and then we have:

$$k_o = k_{-o} = \frac{A \cdot D_{eff}}{\Delta x} \quad (23)$$

Substitution of Eq. 23 into Eq. 22 leads to

$$-\Delta[B_o] = \frac{A \cdot D_{eff}}{\Delta x} \cdot \Delta t ([B_o] - [B_1]) \quad (24)$$

the net rate of the change in base concentration  $[B_1]$  in compartment 1, is

$$\Delta[B_1] = \frac{A \cdot D_{eff}}{\Delta x} \cdot \Delta t ([B_o] - 2[B_1] + [B_2]) - k_1 \cdot [B_1] \cdot [S_1] \cdot \Delta t + k_{-1} \cdot [BS]_1 \cdot \Delta t \quad (25)$$

where the first term in Eq. 25 is the due to the diffusion of the base  $B_o$  from the mobile phase(cyclohexane) into compartment 1, the diffusion of the base  $B_1$  from compartment 1 into the compartment 2 and to the mobile phase and the diffusion of  $B_2$  into compartment 1.

The second term is due to the reaction of  $B_1$  with acidic centres  $S_1$  in the bead or the sheet and formation the complex  $[BS]_1$ . The third term is due to the back reaction of  $[BS]_1$ .

Then the general equation for all compartments inside the sheet is

$$\Delta[B_i] = \underbrace{\frac{A \cdot D_{eff}}{\Delta x} \cdot \Delta t ([B_{i-1}] - 2[B_i] + [B_{i+1}])}_{diffusion\ term} - \underbrace{k_1 \cdot [B_i] \cdot [S_i] \cdot \Delta t + k_{-1} \cdot [BS]_i \cdot \Delta t}_{reaction\ term} \quad (26)$$

This equation is solved numerically to obtain the simulated kinetics of diffusion and reaction of a base on silica bead or glass sheet.

If the system is at complete equilibrium, the base concentrations in all compartments are equal:  $[B_o]_\infty = [B_1]_\infty = [B_2]_\infty = \dots = [B_{max}]_\infty$ , and  $\Delta B_i = 0$ . For this reason the diffusion term in Eq. 26 will be zero. Also, the concentrations of the acidic centres in all compartments will be equal;  $[S_1]_\infty = [S_2]_\infty = \dots = [S_{max}]_\infty$  and the concentrations of formed complex in all compartments will be equal;  $[BS_1]_\infty = [BS_2]_\infty = \dots = [BS_{max}]_\infty$ . Then Eq. 26 becomes

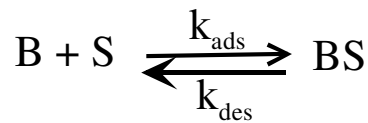
$$k_1 \cdot [B_o]_\infty \cdot [S]_\infty = k_{-1} \cdot [BS]_\infty \quad (27)$$

and the equilibrium constant will be

$$K = \frac{k_1}{k_{-1}} = \frac{[BS]_\infty}{[B_o]_\infty \cdot [S]_\infty} \quad (28)$$

## 2.7. Simplified description of the reaction kinetics and equilibria in interphase systems

The reaction between two between species, base  $B$  and the active centres at silica surfaces  $S$  in the interphase systems is expressed in the simplest approximation as:



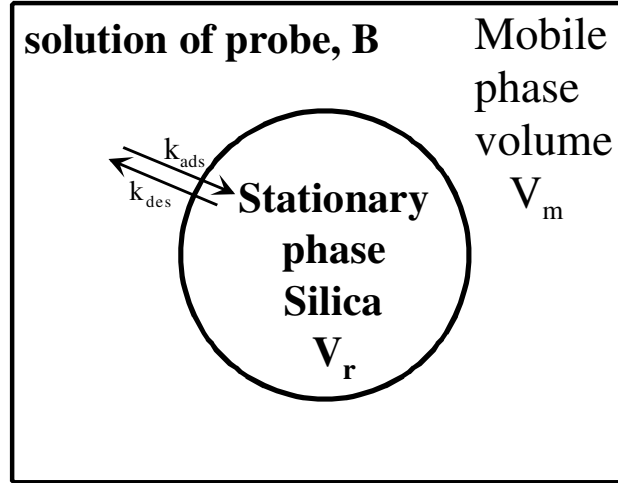


Fig. 4. A simple scheme of reversible adsorption of a dissolved base  $B$  from mobile phase of volume  $V_m$  into silica beads or glass sheets of volume  $V_r$ .

where  $k_{ads}$  is the rate constant of adsorption of the base  $B$  at the silica surfaces, and  $k_{des}$  is the rate of desorption. The net rate of change of concentration of  $B$  is

$$\frac{dB}{dt} = -k_{ads} [S] \cdot [B] + k_{des} \cdot [BS] \quad (29)$$

Under the experimental conditions  $[S]_o \gg [B]_o$ , Eq. 29 becomes

$$\frac{d[B]}{dt} = -k_{eff} \cdot [B] + k_{des} \cdot [BS] \quad (30)$$

where  $k_{eff}$  is a first-order rate constant and its equal to

$$k_{eff} = k_{ads} \cdot [S]_o \quad (31)$$

where  $S_o$  is the initial concentration of the acidic centres at the internal surface of the stationary phase.

At time  $t > 0$  the concentration of  $B$  is

$$[B]_t = [B]_o - [BS]_t \quad (32)$$

By replacement from Eq. 32 into Eq. 30 and solving this first-order differential equation at time  $t > 0$  one obtains:

$$\frac{[B]_t - [B]_\infty}{[B]_o - [B]_\infty} = e^{-(k_{eff} + k_{des})t} \quad (33)$$

By introducing  $k_{tot}$  in Eq. 33 one obtains

$$\frac{[B]_t - [B]_\infty}{[B]_o - [B]_\infty} = e^{-k_{tot}t} \quad (34)$$



and for formation of  $[BS]$

$$[BS]_t = [BS]_\infty (1 - e^{-k_{tot} t}) \quad (35)$$

$$\text{where } k_{tot} = k_{eff} + k_{des} , \quad (36)$$

$[B]_o$  is the initial concentration of a base  $B$  in the mobile phase,  $[B]_\infty$  and  $[BS]_\infty$  are the concentrations of  $B$  and  $[BS]_\infty$  at time  $t \rightarrow \infty$ , respectively.  $[BS]_t$  is the concentration of the complex  $BS$  at the stationary phase at time  $t > 0$ .

When  $t \rightarrow \infty$  i.e. the reaction reaches to the equilibrium, the concentration of  $[BS]_\infty$  is

$$[BS]_\infty = [B]_o - [B]_\infty \quad (37)$$

where  $[B]_\infty$  is the concentration of  $B$  in the mobile phase at time  $t = \infty$ . At time  $t \rightarrow \infty$ , Eq. 30 becomes

$$k_{eff} \cdot [B]_\infty = k_{des} \cdot [BS]_\infty \quad (38)$$

The ratio of these equilibrium concentrations, which is the equilibrium constant of the above reaction, is

$$K = \frac{k_{eff}}{k_{des}} = \frac{[BS]_\infty}{[B]_\infty} \quad (39)$$

by replacement from Eq. 37 into Eq. 39, gives rise to

$$K = \frac{k_{eff}}{k_{des}} = \frac{[B]_o - [B]_\infty}{[B]_\infty} \cdot \frac{V_m}{V_r} \quad (40)$$

Since the two concentrations  $[B]_o - [B]_\infty$  and  $[B]_\infty$  are in different phases and these phases of different volumes, these concentrations are divided by the volume of the stationary  $V_r$  and the volume of the mobile  $V_m$  phases, respectively.

### 2.7.1. Neglection of back reaction

When there is 1) no back reaction and 2) the diffusion of the base  $B$  inside the stationary phase is much faster than the reaction between base  $B$  and the active centres on the

silica surface (e.g. amino groups)  $S$ . The rate of formation of  $BS$  depends on the concentration of the base  $B$  in the mobile phase and the concentration of the active groups at the silica surface  $S$  as follows:

$$\frac{d[BS]}{dt} = k_b [B][S] \quad (41)$$

where  $k_b$  is a second-order rate constant of the reaction. Under the conditions of  $S \gg B$  the rate equation can be written:

$$\frac{d[BS]}{dt} = k_{eff} [B] \quad (42)$$

where  $k_{eff}$  is a first-order rate constant and is equal to

$$k_{eff} = k_b [S] \quad (43)$$

By solving Eq. 42 at time  $t > 0$  the following Eq. is obtained

$$[BS]_t = [BS]_\infty \cdot (1 - e^{-k_{eff} t}) \quad (45)$$

## 2.8. Selectivity factor in chromatography

The passage of the substance between the mobile  $m$  and the rigid stationary  $r$  phase is determined by the partition equilibrium. One can obtain the partition coefficient  $K$  for this equilibrium using the concentration for the stationary phase  $[c_r]$  and for the mobile phase  $[c_m]$  corresponding to

$$K = \frac{[c_r]}{[c_m]} \quad (46)$$

The partition coefficient describes the equilibrium constant for the distribution of a solute between two immiscible phases. It is also called a partition ratio.

The partition coefficient cannot be directly deduced from the chromatogram. The total retention time  $t_r$  is immediately readable. The retention time  $t_m$  (mobile time or hold-up time) corresponds to the time required for the molecules in the mobile phase to pass through the column.

The adjusted retention time is given by

$$t'_r = t_r - t_m \quad (47)$$

The capacity factor  $k'$  or the retention factor  $k$  is given by

$$k' = K \frac{V_r}{V_m} = \frac{t'_r}{t_M} \quad \text{Or} \quad k' = \frac{K}{\theta} \quad (48)$$

where  $V_r$  is the volume of the stationary phase  $V_m$  is the volume of the mobile phase and  $\theta$  is the phase ratio.

The selectivity factor, also called separation factor, is a measure for the separation of two substances and is indicated by an  $\alpha$  in chromatography. Using the partition coefficients for calculating the selectivity factor for two substances,  $A$  and  $B$  one obtains

$$\alpha = \frac{K_B}{K_A} \quad (49)$$

By incorporating Eq. 48 one obtains:

$$\alpha = \frac{k'_B}{k'_A} \quad (50)$$

Determination of  $\alpha$  from an experimental chromatogram is feasible by substitution of the retention factors in Eq. 50 by Eq. 48 revealing the ratio of adjusted retention times

$$\alpha = \frac{(t'_r)_B}{(t'_r)_A} \quad (51)$$

## 3. Experimental

### 3.1. Materials

#### 3.1.1. Fluorescence probes (adsorbates)

The fluorescent probes are acridine (TCI-Up) with  $pK_a(S_0) = 5.5$  and  $pK_a(S_1) = 10.7$  [82, 83] and its derivatives 1) 1,2,7,8-dibenzacridine, 2) 3,4,5,6-dibenzacridine, (the latter two probes are received from Perkampus; see Perkampus *et al.* (1969) and 3) acridine orange (Aldrich) with  $pK_a(S_0) = 10.5$  [84]. Figs. 5-8 present the chemical formula of the four fluorescent probes.

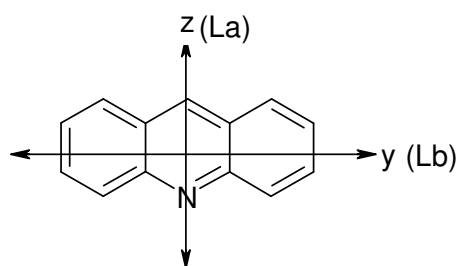


Fig. 5. Acridine (AC)

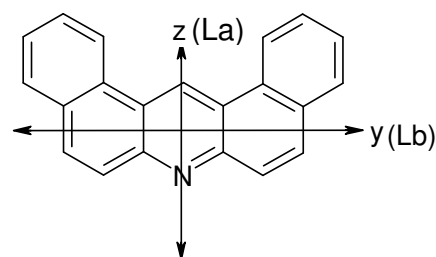


Fig. 6. 1,2,7,8-dibenzacridine (1-DBA)

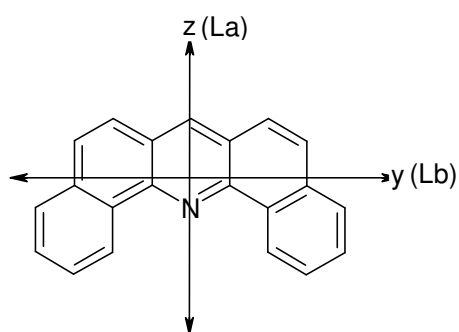


Fig. 7. 3,4,5,6-dibenzacridine (3-DBA)

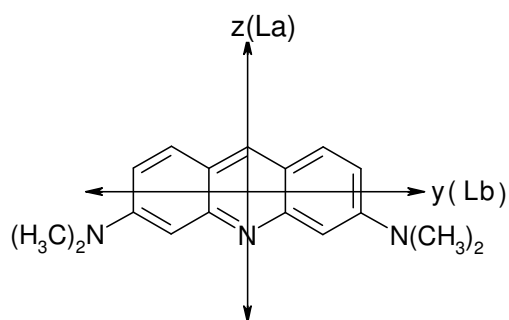


Fig. 8. Acridine orange (AO)

5-(Dimethylamino)-1-naphthalenesulfonyl chloride (DANSyl chloride) and 5-(Dimethylamino)-1-naphthalenesulfonyl amide (DANSyl amide) are received from Fluka, Fig. 9 and 10 respectively.

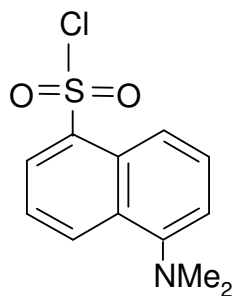


Fig. 9. 5-(Dimethylamino)-1-naphthalenesulfonyl chloride (DANSyl chloride)

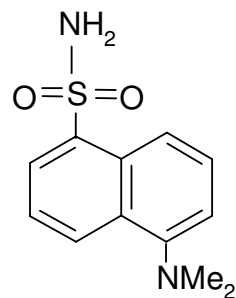


Fig. 10. 5-(Dimethylamino)-1-naphthalenesulfonyl amide (DANSyl amide)

### 3.1.2. Solvents

Dichloromethane, cyclohexane, and ethanol are used as organic solvents. These organic solvents are spectroscopic grade. HPLC grade isopropanol and cyclohexane (Merck, Darmstadt, Germany) are used for the HPLC measurements.

### 3.1.3. Stationary phases

#### 3.1.3.1. Silica

##### 3.1.3.1.1. Nonmodified (bare) silica

Porous silica (Eka-Chemicals) of surface area =  $116 \text{ m}^2/\text{g}$ , average particle size of  $6 \mu\text{m}$ , and pore size of  $300 \text{ \AA}$  is used. Fig. 11 shows the scanning electron microscopy (SEM) for the silica beads.

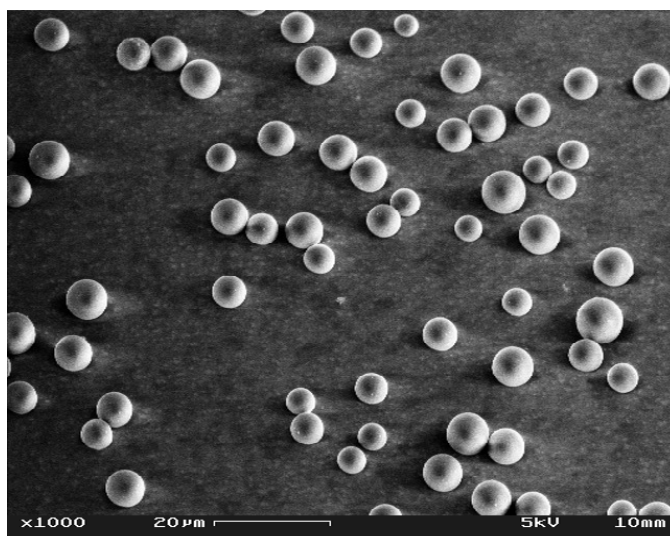


Fig. 11. SEM picture showing the particles of bare silica beads.

### 3.1.3.1.2. Modified (Coated) silica

#### 3.1.3.1.2.1. Modified with alkyl chains (C30 – alkyl chains)

Silica C30 monomeric phase on Lichrospher (particle size of 6  $\mu\text{m}$ ; Merck, Darmstadt, Germany) is synthesized according to procedures described previously [85, 86].

#### 3.1.3.1.2.2. Modified with active groups (amino groups)

Another modification of Porous silica (Eka-Chemicals 6  $\mu\text{m}$ ) surface is done in the group of Prof. H. Mayer. This modification is to put active groups at the silica surfaces and then study this reactivity of silica surfaces by fluorescence spectroscopy. Five different types of active groups are added to the surface resulting in four different types of modified silica surfaces which are: 3-aminopropyl silica, 3-aminopropyl and octyl silica, 3-aminopropyl and phenyl silica and 3-aminopropyl and butyric silica, they are appeared in Fig. 12-15 respectively

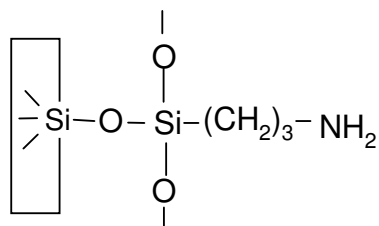


Fig. 12. 3-aminopropyl silica (1)

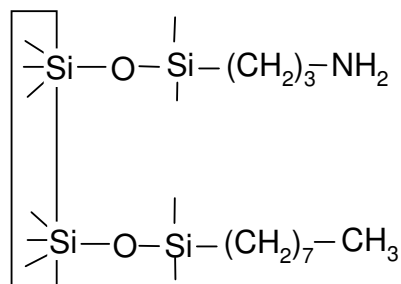


Fig. 13. 3-aminopropyl + octyl silica (2)

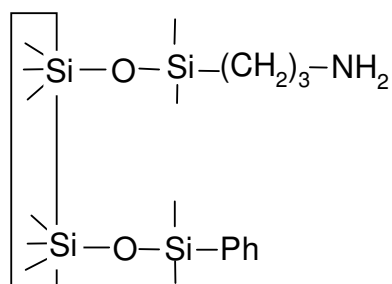


Fig. 14. 3-aminopropyl + phenyl silica (3)

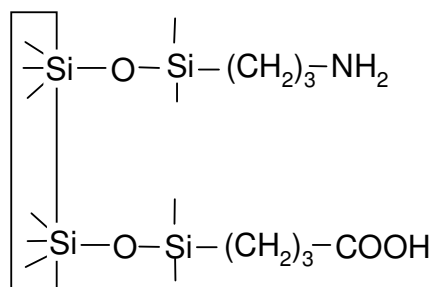


Fig. 15. 3-aminopropyl + butyric silica (4)

These modifications are carried out as the following: the silica (0.5 g) is dried under vacuum at 150°C over night to remove all the adsorbed water from the surface and then it is cooled to room temperature and is stored under Ar atmosphere. The silica is suspended in dry toluene (20 ml) in round bottomed flask equipped with reflux condenser, then a four times excess of the amount of 3-aminopropyl-triethoxy silane (1.36 ml) is added with a syringe and refluxed under Ar atmosphere for 20 h. Then the suspension is cooled to room temperature, centrifuged and washed with aliquots of toluene and n-hexane twice. The 3-aminopropyl silica is dried at 130°C over night.

For preparations of the 3-aminopropyl and octyl silica the following method is used: The silica (0.2 g) is dried under vacuum at 150°C over night to remove all the adsorbed water from the surface and then it is cooled to room temperature and is stored under Ar atmosphere. The silica is suspended in dry toluene (20 ml) in round bottomed flask equipped with reflux condenser, then the amount of 3-aminopropyl-triethoxy silane (26 µl) is added with a syringe and refluxed under Ar atmosphere for 20 h. Then cooled to room temperature, added the amount of octyl trimethoxy silane (29 µl) is added with a syringe and refluxed under Ar atmosphere for 20 h. Then cooled to room temperature, centrifuged and washed with aliquots of toluene and n-hexane twice. The 3-aminopropyl and octyl silica is dried at 130°C over night.

For preparations of the 3-aminopropyl and phenyl silica the following method is used The silica (0.2 g) is dried under vacuum at 150°C over night to remove all the adsorbed water from the surface and then it is cooled to room temperature and is stored under Ar atmosphere. The silica is suspended in dry toluene (20 ml) in round bottomed flask equipped with reflux condenser, then the amount of phenyl trimethoxy silane (55 µl) is added with a syringe and refluxed under Ar atmosphere for 20 h. Then cooled to room temperature, added the amount of 3-aminopropyl-triethoxy silane (68 µl) is added with a syringe and refluxed under Ar atmosphere for 20 h. Then it is cooled to room temperature, centrifuged and washed with

aliquots of toluene and n-hexane twice. The 3-aminopropyl and phenyl silica is dried at 130°C over night.

For preparations of the 3-aminopropyl and butyric silica the following method is used. The silica (0.25 g) is dried under vacuum at 150°C over night to remove all the adsorbed water from the surface and then it is cooled to room temperature and is stored under Ar atmosphere. The silica is suspended in dry toluene (20 ml) in round bottomed flask equipped with reflux condenser, then the amount of cyano triethoxy silane (33 µl) is added with a syringe and refluxed under Ar atmosphere for 20 h. Then it is cooled to room temperature, centrifuged and washed with aliquots of toluene and water twice. Amount (20 ml) of 50% water / H<sub>2</sub>SO<sub>4</sub> (V / V) is added to the silica and refluxed for 3h. Then it is cooled to room temperature, centrifuged and washed with water and dried under vacuum at 95°C over night. The silica is suspended in dry toluene (20 ml) and (25 µl) of 3-aminopropyl-triethoxy silane is added with a syringe and refluxed under Ar atmosphere for 20 h. Then it is cooled to room temperature, centrifuged and washed with aliquots of toluene and n-hexane twice. The 3-aminopropyl and butyric silica is dried at 130°C over night.

### 3.1.3.1.2.3. Modified with polymers

Coated silica is prepared in the group of Prof. K. Albert. Two different types of polymers were used. Coating 1 consists of polymerized divinylbenzene (DVB), see Fig. 16. Two polymer loadings of 200 mg and 500 mg DVB per g silica are employed. The polymeric coating 2 consists of N, N'-diallyl-1-tartardiamide bis-(4-tertbutylbenzoate) (TBB) with loading 0.27 mmol of TBB /g silica, which is depicted in Fig. 17.

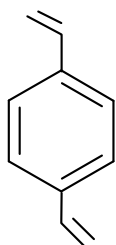


Fig. 16. 1,4-DVB monomer for polymeric coating DVB.



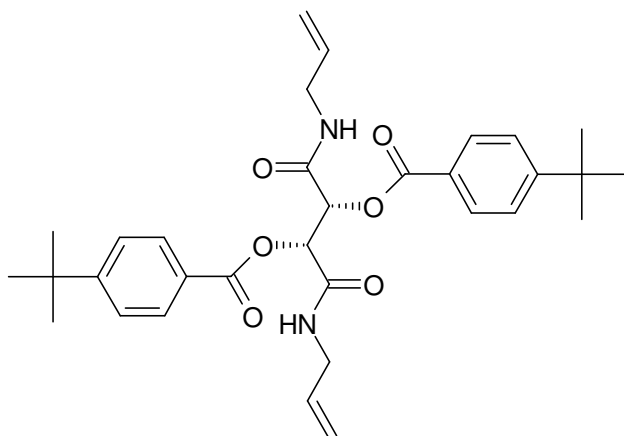


Fig. 17. Structure of monomer (TBB) for polymeric coating 2

### 3.1.3.2. Determination the amine concentration at the modified silica surfaces

The amine-containing silica is treated with a solution of picric acid to form a salt with the silica-bound amino groups. After thorough washing to remove excess of picric acid, the resin is treated with an excess of a strong base which quantitatively releases the picrate from the silica into solution. The concentration of picrate in this solution is determined spectrophotometrically and reflects the amine content of the silica [87].

### 3.1.3.3. Controlled Porous Glass (CPG)

#### 3.1.3.3.1 Geltech Controlled Porous Glass (PGG)

Geltech CPG is a porous silica glass having 25Å pore diameters. It is produced using the sol-gel technique by the Geltech Corporation [88].

#### 3.1.3.3.2. Porous Vycor Glass (PVG)

VYCOR ® Brand Porous Glass 7930 is a porous silica glass having 40Å pore diameters and surface area 250 m<sup>2</sup>/g are produced by a similar procedure [53] by Corning.

Table 1 shows the different surfaces which are used as stationary phase in this study.

Table 1 Different stationary phases are used.

Silica	1- nonmodified (bare) silica 2- silicaC30 3- coated silica: a- TBB coated silica b- DVB coated silica; i- 200 mg DVB/g silica ii- 500 mg DVB/g silica 4- reactive silica a- 3-aminopropyl silica (silica1) b- 3-aminopropyl + octyl silica (silica 2) c- 3-aminopropyl + phenyl silica (silica3) d- 3-aminopropyl + butyric silica (silica 4)
Controlled Porous Glass	1- Geltech Porous glass (PGG) 2- Porous Vycor Glass (PVG)

## 3.2. Instruments

### 3.2.1. Absorption spectrophotometer

The absorption spectra are measured by using a Perkin Elmer Lambda9 spectrophotometer.

### 3.2.2. Fluorometer

Steady state fluorescence spectra are obtained with a SPEX Fluorolog 222 spectrometer. Fluorescence anisotropy is measured with the Fluorog 222 spectrometer equipped with two polarizers. Fluorescence decays were recorded using a time-correlated single-photon counting setup (pico-timing discriminators (Ortec, model 9307), Time-to-Amplitude Converter (Ortec, model 457), pre-amplifier (Ortec, model 9306)) utilizing the emission monochromator of the fluorometer SPEX Fluorolog 222 and same photomultiplier tube. For excitation a picoseconds diode laser (PicoQuant, Germany, model LDH-400 (371 nm) FWHM 70 ps) was used.

### 3.2.3. Centrifuge

Centrifugation is carried out with an eppendorf centrifuge S415C of a speed 10000 r.p.m.

### 3.2.4. High-performance liquid chromatography (HPLC)

Analytical liquid chromatography is performed with a Merck-Hitachi 6200A solvent delivery pump and a Merck-Hitachi L-4000A variable wavelength UV detector. Samples are introduced via a Rheodyne injector equipped with a 20- $\mu$ L loop. The stationary phase is prepared in the group of Prof. Albert. Porous silica (Eka-Chemicals 6  $\mu$ m) was coated by polymeric coating and packed into steel tubes with the dimensions 125 x 4.6 mm, using standard procedures. The polymeric coating consists of N, N'-diallyl-1-tartardiamide bis-(4-tertbutylbenzoate) (TBB) which is depicted in Fig. 17. The two constituents are 1-DBA and 3-DBA. The mobile phases is used during the separations are mixtures of isopropanol/cyclohexane, and all analytes are dissolved in cyclohexane.

## 3.3. Measurements

### 3.3.1. Characterization of the adsorption

#### 3.3.1.1. Silica as stationary phase

Steady state fluorescence, fluorescence anisotropy spectra and the fluorescence decays of the interaction of the fluorescent probes with silica surface are carried out as follows. A certain weight of silica (6-10 mg) is suspended into 2 ml of dry solvent into a fluorescence cell and stirred for 2 min. Then 1 ml of the probe solution of definite concentration is injected and the suspension is stirred during the measurements to avoid sedimentation. Silica is not activated by heat treatment (it is preheated sometimes, in equilibria studies). The depolarization measurements are obtained by exciting the stirred suspension by vertically polarized light parallel to the z-axis. The emitted intensity was measured through a polarizer when the emission polarizer is oriented parallel ( $\parallel$ ) to the excitation, the intensity is called  $I_{\parallel}$ . A second measurement is done with the polarizer perpendicular ( $\perp$ ) to the excitation, the intensity is called  $I_{\perp}$  and the value of the anisotropy was calculated according to Eq. 13.

#### 3.3.1.1. CPG as a stationary phase

Steady state fluorescence, fluorescence anisotropy spectra and the fluorescence decays of the interaction of the fluorescent probes on CPG surface are carried out as following: a

weighted glass sheet (PVG) or disc (PGG) is immersed into a fluorescence cell containing 2 ml of cyclohexane and stirred well for 2 min. Then 1 ml of the probe solution of certain concentration is injected and the solution is stirred well. The fluorescence spectra of the PVG and PGG are measured in the right-angle geometry by putting the sheet by angle in the fluorescence cell, see Fig. 18a. The depolarization measurements are performed by the same method as in section 3.3.1.1. with using two mirrors to avoid the geometric error due to the reflectance of the polarized light in vertical direction since the sheet is parallel to the cell wall as shown in Fig. 18b. Both the glass sheet (PVG) and disc (Geltech) are not preheated.

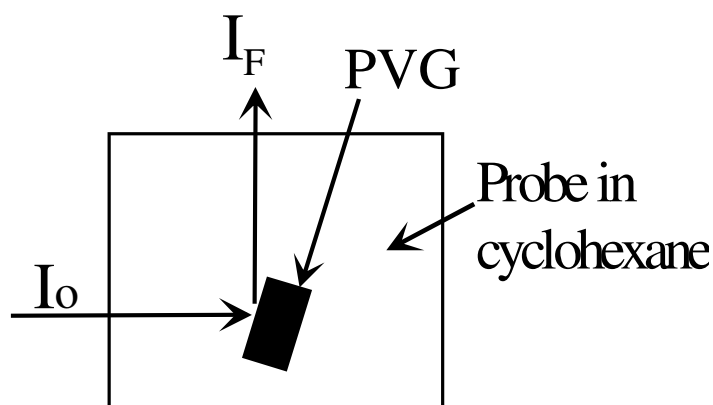


Fig. 18a. Fig. 9. Top view of the cell during the measurements of the fluorescence and fluorescence excitation spectra through the PVG sheet.  $I_0$  is the intensity of the incident light and  $I_F$  is the fluorescence intensity.

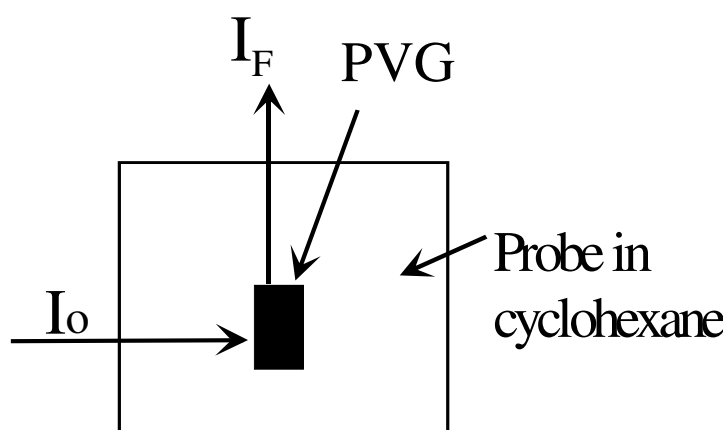


Fig. 18b. Top view of the cell during the measurements of the fluorescence anisotropy spectrum through the PVG sheet.  $I_0$  is the intensity of the incident light and  $I_F$  is the fluorescence intensity.

### 3.3.2. Kinetics measurements

#### 3.3.2.1. Silica as adsorbent

The kinetics of adsorption of AC and 1-DBA at silica bead, (formation of  $[BS]$ , see Fig. 3) are measured as follows: 6 mg of non-modified silica of diameter,  $d = 6 \mu m$  are suspended into 2 ml of dry cyclohexane into a fluorescence cell and stirred for 2 min. Then 1 ml of AC or 1-DBA solution in cyclohexane  $[B_o]$  is injected at time,  $t = t_0$  and the solution is stirred well. The fluorescence intensity of the protonated species on silica surface is measured as a function of time with stirring the system (cyclohexane solution + silica). The kinetics of nonadsorbed 1-DBA is measured by the same method, but a SPEX Fluorolog 222 spectrometer is adjusted at different excitation and emission wave numbers.

#### 3.3.2.2. Silica as reactant

The kinetics of the reaction of DANsyl chloride with amino groups on 3-aminopropyl, 3-aminopropyl + octyl, 3-aminopropyl + phenyl and 3-aminopropyl + butyric silica are measured as follows: 6 mg of the modified silica are suspended into 2 ml of dry dichloromethane into a fluorescence cell and stirred for 2 min. Then 1 ml of DANsyl chloride solution in dry dichloromethane was injected at time,  $t = t_0$  and the solution is stirred well. The fluorescence intensity of the product (DANsyl amide) on the modified silica surface is measured as a function of time with stirring the system (dichloromethane solution + silica). All the measurements are carried out at room temperature.

#### 3.3.2.3. PVG as adsorbent

The kinetics of adsorption of AC, 1-DBA and 3-DBA on PVG,  $[BS]$  are measured as follows: a planar PVG sheet of thickness,  $d = 0.1 \text{ cm}$ , height = 1 cm and width = 0.7 cm ( $V_r = 0.07 \text{ cm}^3$ ,  $A = 1.74 \text{ cm}^2$ ) is immersed into a 1-cm fluorescence cuvette containing 2 ml of cyclohexane and is stirred well for 2 min. Then 1 ml of AC, 1-DBA or 3-DBA solution in cyclohexane  $[B_o]$  is injected at time,  $t = t_0$  and the solution is stirred well. The absorption spectra of the stirred system (cyclohexane solution + PVG) are measured at different times,  $t$  after injection from  $t \approx 1 \text{ min}$  till  $t \approx 300 \text{ min}$  (till 1440 min in case of 3-DBA). Fig. 19 shows the position of the glass sheet in the cell during the absorption measurements of the adsorbed probes on PVG.

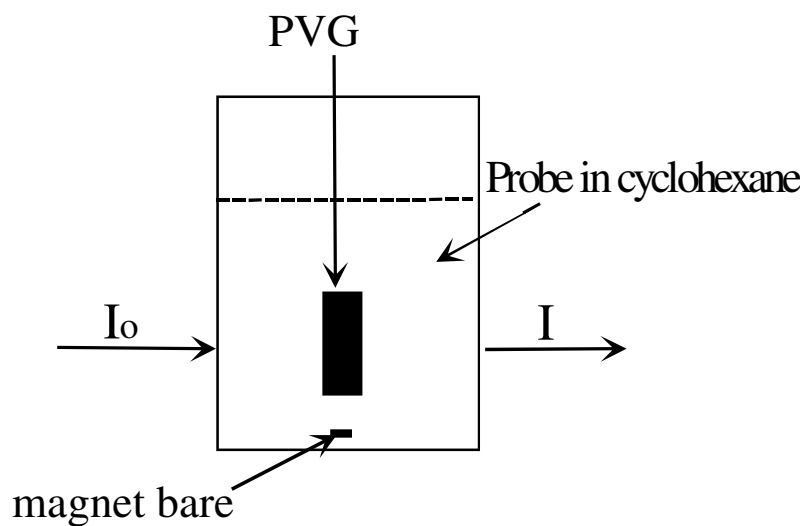


Fig. 19. Side view of the cell during the measurements of the absorption spectrum through the glass sheet.  $I_0$  is the intensity of the incident light and  $I$  is the intensity of the measured light.

## 4. Results and Discussions

### 4.1. Characterization of probes in solution

#### 4.1.1. Selection of probes

In this work, we report a comparative study of the surface acidities of different microporous environments. For this purpose, conjugated molecules with additional electron-donor and proton-acceptor centres are used as adsorbates. Acridine (AC) and some of its derivatives 1,2,7,8-dibenzacridine (1-DBA), 3,4,5,6-dibenzacridine (3-DBA), and acridine orange (AO) are chosen for this study, see Figs. 5-8 (in the experimental part). These probes are used because they are fluorescent molecules with high quantum yields. The positions of the electronic transitions of these molecules are easily to determine. The molecules possess different basicity, since AO has the highest  $pK_a$  value in the ground state ( $pK_a = 10.5$  [84]), AC ( $pK_a = 5.5$  [82,83]) and 1-DBA have approximately the same  $pK_a$  value while 3-DBA has the lowest one. Furthermore, the spectra and the photophysical properties of these molecules exhibit considerable changes upon protonation. They also have long fluorescence lifetimes.

DANSyl chloride is used to quantify the reaction of silica surface modified with amino-groups, since DANSyl chloride is a non-fluorescent probe in dry dichloromethane. DANSyl chloride reacts with the amino-groups at the silica surface and forms DANSyl amide, which is a fluorescent probe.

#### 4.1.2. Electronic transitions

Acridine and its derivatives belong to the point group  $C_{2V}$ , since they have two fold-symmetry axis along the 9-10 position. They have low-lying excited singlet states,  $n-\pi^*$  and  $\pi-\pi^*$  transitions. This  $n-\pi^*$  transition is polarized perpendicular to the molecular plane with very low oscillation structure. It is not further considered in this work.

The  $\pi-\pi^*$  transitions are polarized in the molecular plane and it can be: 1) parallel to the principle z-axis (Figs. 5-8 in the experimental part) in this case it will be of  $A_1$ -symmetry ( $b_1-b_1^*$ ) corresponding to the  ${}^1L_a$ -band in aromatic hydrocarbons, 2) or lie in direction of y-axis,  $B_2$ -symmetry ( $a_2-b_1^*$ ,  $b_1-a_2^*$ ) corresponding to  ${}^1L_b$ -and  $B_b$ -bands in aromatic hydrocarbons [89-90].

#### 4.1.2.1. Spectra of neutral probes

Fig. 20 shows the absorption spectra of the probes in cyclohexane and alkaline ethanol, respectively, where all molecules are dissolved in their neutral forms (only the spectra of 1-DBA are presented, since the spectra of 3-DBA are more or less identical). When AC is dissolved in cyclohexane, the excited states increase in the order  $n-\pi^*$ ,  ${}^1L_a$ ,  ${}^1L_b$ , and  $B_b$ -band. As a consequence, the molecule is almost nonfluorescent, since the  $n-\pi^*$  transition deactivates radiationless very fast [71-73]. In the other molecules, the excited state energy order is  ${}^1L_b$ ,  ${}^1L_a$ , and  $B_b$  [89]. Thus, 1-DBA and 3-DBA emit well structured fluorescence spectra, whereas the absorption and fluorescence spectra of AO are unstructured. This is because the transitions of AO are of appreciable intermolecular charge transfer character (ITC) with a large Stokes shift between the absorption and the fluorescence maximum. The spectrum of neutral AO is obtained only in alkaline ethanol, since it is already protonated in the neutral solvents because of its high  $pK_a$  value ( $pK_a = 10.5$  [84]).

Table 2 summarizes the transition energies and the molar extinction coefficients of AC, 1-DBA and AO in different solvents. The 0-0 transition energies are given for the sharp bands, and for the broad bands their absolute maxima (M) are presented.

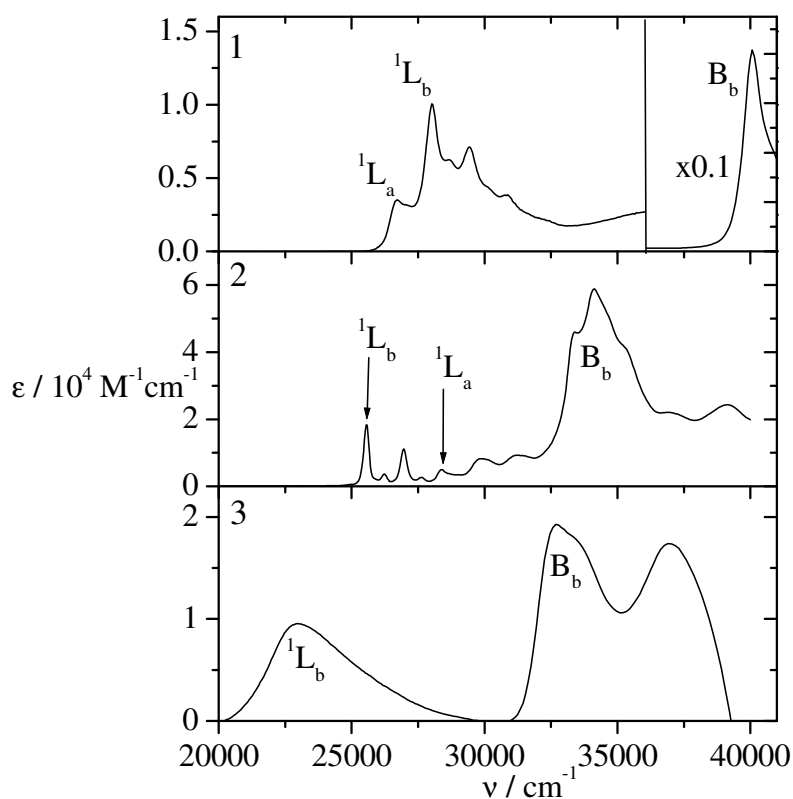


Fig. 20. Absorption spectra of (1) AC in cyclohexane ( $c=1.1 \cdot 10^{-5} M$ ). (2) 1-DBA in cyclohexane ( $c=9.0 \cdot 10^{-6} M$ ). (3) AO in alkaline ethanol ( $c=3.9 \cdot 10^{-6} M$ ).



Table 2. Transition energies (M = absolute maximum, 0-0 = zero-to-zero transition) and maximum molar extinction coefficients  $\epsilon_{\max}$  of AC, 1-DBA and AO respectively in different solvents.

Probe	solvent	$^1L_a$		$^1L_b$		$B_b$	
		$\tilde{\nu}_{\max} / cm^{-1}$	$\epsilon_{\max} / 10^4$ $M^{-1} cm^{-1}$	$\tilde{\nu}_{\max} / cm^{-1}$	$\epsilon_{\max} / 10^4$ $M^{-1} cm^{-1}$	$\tilde{\nu}_{\max} / cm^{-1}$	$\epsilon_{\max} / 10^4$ $M^{-1} cm^{-1}$
AC	Cyclohexane	26700 (M)	0.35	28000 (0-0)	1.00	40100 (0-0)	16.0
		26000 (0-0)					
	Ethanol	26400 (M)	0.28	28200 (0-0)	1.04	40200 (0-0)	18.0
		25400 (0-0)					
	alkaline water	26300 (M)	0.24	28300 (0-0)	1.00	40200 (0-0)	
		25700 (0-0)					
ACH+	acidic ethanol	24800 (M)	0.31	28300(0-0)	1.91	39100 (0-0)	10.4
ACH+	acidic water	25000 (M)	0.31	28300 (0-0)	1.89	39400 (0-0)	10.7

Probe	solvent	$^1L_b$		$^1L_a$		$B_b$	
		$\tilde{\nu}_{\max} / cm^{-1}$	$\epsilon_{\max} / 10^4$ $M^{-1} cm^{-1}$	$\tilde{\nu}_{\max} / cm^{-1}$	$\epsilon_{\max} / 10^4$ $M^{-1} cm^{-1}$	$\tilde{\nu}_{\max} / cm^{-1}$	$\epsilon_{\max} / 10^4$ $M^{-1} cm^{-1}$
1-DBA	cyclohexane	25500 (0-0)	1.80	28300 (0-0)	0.5	34000 (M)	5.90
		26900 (0-1)	1.10				
	ethanol	25300 (0-0)	1.80	28200 (0-0)	0.61	34200 (M)	6.8
		26700 (0-1)	1.10				
1-DBAH <sup>+</sup>	acidic ethanol	23500 (0-0, M)	2.10	28200 (M)	0.39	33400 (M)	7.2

Probe	solvent	$^1L_b$		$^1L_a$		$B_b$	
		$\tilde{\nu}_{\max} / cm^{-1}$	$\epsilon_{\max} / 10^4$ $M^{-1} cm^{-1}$	$\tilde{\nu}_{\max} / cm^{-1}$	$\epsilon_{\max} / 10^4$ $M^{-1} cm^{-1}$	$\tilde{\nu}_{\max} / cm^{-1}$	$\epsilon_{\max} / 10^4$ $M^{-1} cm^{-1}$
AO	alkaline ethanol	23000 (M)	0.95			32700 (M)	1.90
	ethanol	20400 (M)	3.60			32700 (M)	5.20
AOH <sup>+</sup>	acidic ethanol	20200 (M)	5.30			34300 (M)	2.4

#### 4.1.2.2. Influence of solvent acidity on probe spectra

The absorption and fluorescence emission spectra of AC in water at  $\text{pH} \approx 1$  and  $\approx 12$  are presented in Fig. 21. The  ${}^1\text{L}_a$ -band of the acridinium ion exhibits a red shift by about  $\Delta\tilde{\nu} = 2500\text{cm}^{-1}$  compared to that in alkaline water, while the  ${}^1\text{L}_b$ -band does not show any significant shift [76,91], see Table 2. The emission spectrum of the protonated AC is also shifted to the red by about  $\Delta\tilde{\nu} = 2500\text{cm}^{-1}$  compared to that of AC in alkaline water. The maximum values of the emission bands are collected in Table 3.

Table. 3. Positions of the emission  $\tilde{\nu}_{F,\text{max}}$  peaks of AC, 1-DBA and AO in different solvents.

Probe	solvent	$\tilde{\nu}_{F,\text{max}} / \text{cm}^{-1}$
AC	Alkaline water	23200
ACH <sup>+</sup>	Acidic water	20700
1-DBA	ethanol	25100
1-DBAH <sup>+</sup>	Acidic ethanol	22100
AO	Alkaline ethanol	18000
AOH <sup>+</sup>	Acidic ethanol	18900

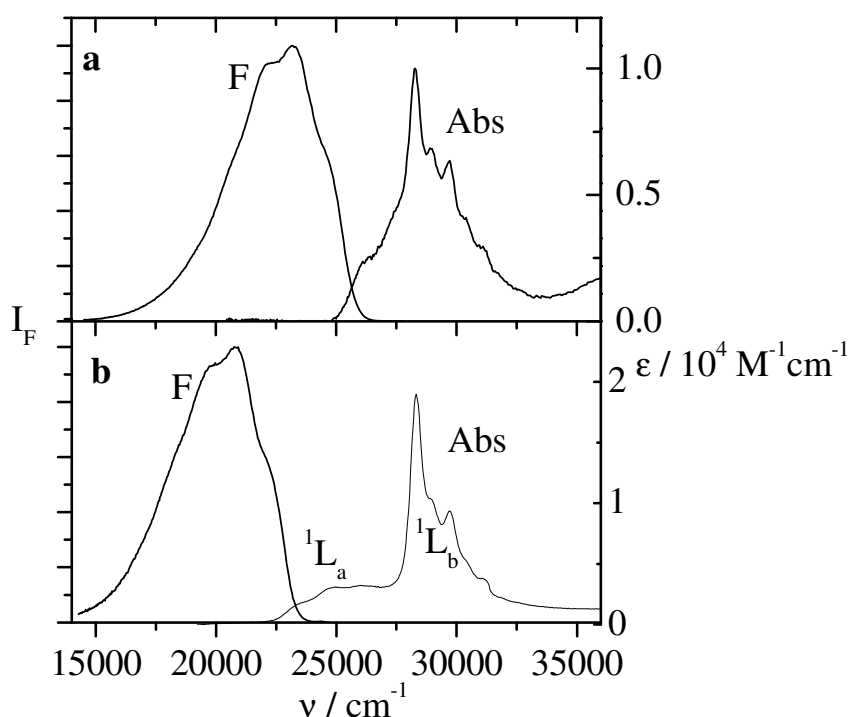


Fig. 21. Absorption (Abs) and normalized fluorescence (F) spectra of AC in water ( $c = 3.9 \cdot 10^{-6} \text{ M}$ ) at different pH-values. a)  $\text{pH} \approx 12$  (the fluorescence spectrum is excited at  $\tilde{\nu}_{\text{ex}} = 28200 \text{ cm}^{-1}$ ), b)  $\text{pH} \approx 1$  (the fluorescence spectrum is excited at  $\tilde{\nu}_{\text{ex}} = 25000 \text{ cm}^{-1}$ ).

The extinction coefficients  $\epsilon$  of neutral and protonated species of AC in ethanol are plotted in Fig. 22 for the  ${}^1L_a$ - and  ${}^1L_b$ -bands. This experiment is done by titration of 27 ml of AC solution in ethanol of concentration  $c = 1.02 \cdot 10^{-5} M$  with a solution of  $0.1 N H_2SO_4$  and measuring the absorbance for each addition of  $H_2SO_4$ . From Fig. 20, it is obvious that the  ${}^1L_a$ -band of protonated acridine exhibits a red shift by about  $\Delta\tilde{\nu} = 2800 cm^{-1}$  compared to that in neutral ethanol. Values of the extinction coefficients of neutral and protonated AC are listed in Table 2.

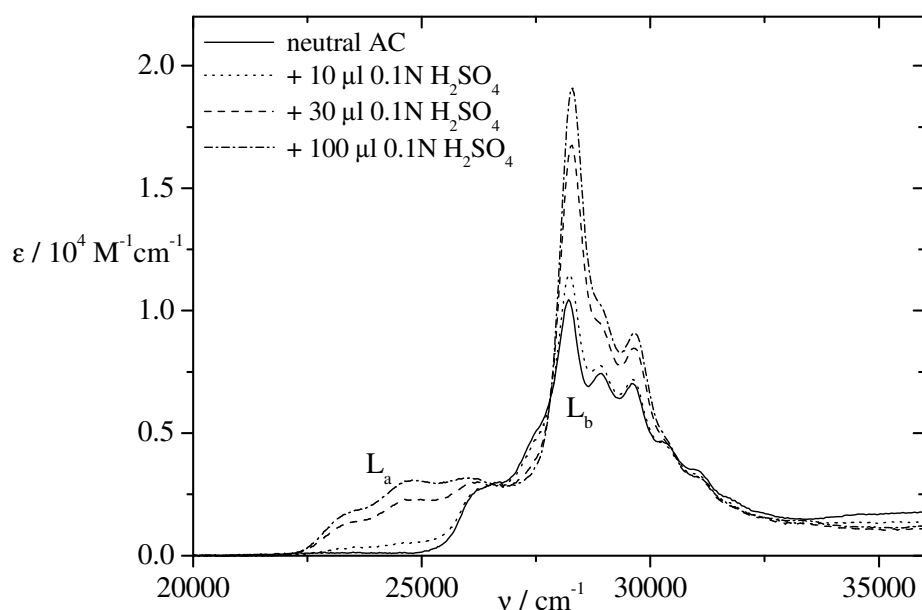


Fig. 22. The change of the extinction coefficient,  $\epsilon$ , of AC in ethanol ( $c = 10.2 \cdot 10^{-6} M$ ) by titration with  $0.1 N H_2SO_4$ .

The absorption and emission fluorescence spectra of 1-DBA in ethanol at  $pH \approx 2, 5.2$  and 6 are presented in Fig. 23. In neutral ethanol, only the neutral species of 1-DBA is present. At  $pH \approx 2$ , in the absorption spectrum, the  ${}^1L_b$ -band shifts to longer wavelength compared to the value in neutral ethanol by about  $\Delta\tilde{\nu} = 1800 cm^{-1}$ . The  ${}^1L_a$ -band decreases in intensity and the  $B_b$ -band has a red shift by about  $\Delta\tilde{\nu} = 800 cm^{-1}$ , see Table 2. In the emission spectrum, there is one broad band at  $22100 cm^{-1}$  which is due to the protonated species of 1-DBA. At  $pH \approx 5.2$ , in the absorption spectrum, the  ${}^1L_b$ -band shifts to longer wavelengths, the  ${}^1L_a$ -band decreases in the intensity and the  $B_b$ -band has a red-shift compared to the value in neutral ethanol, see Table 2. The emission spectrum has a broad band at about

$22300\text{ cm}^{-1}$  which is due to the protonated 1-DBA. The emission band at  $25100\text{ cm}^{-1}$  is due to the neutral 1-DBA in cyclohexane, see Table 3. 3-DBA is much harder to protonate than 1-DBA because of the free electron pair at the nitrogen is sterically shielded by the benzo groups [74] and is can only be protonated by 20%  $\text{H}_2\text{SO}_4$ .

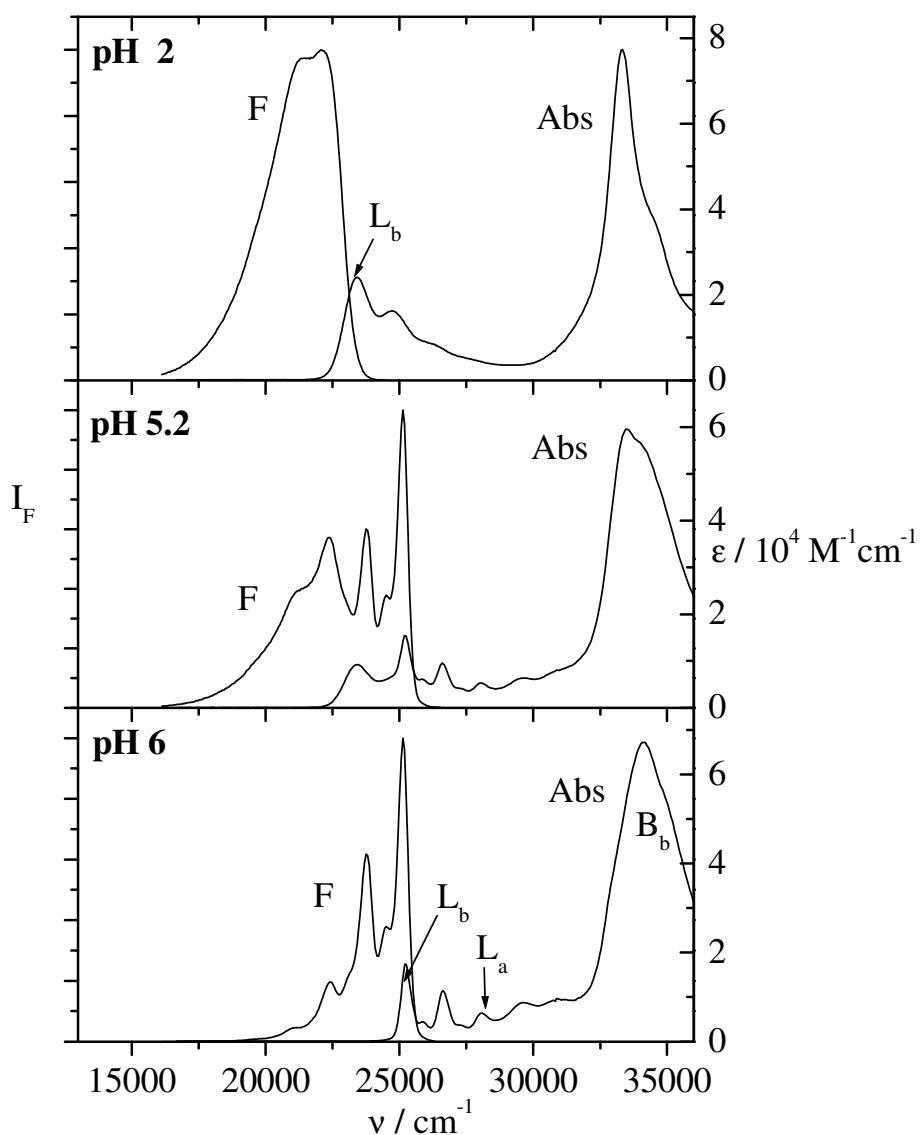


Fig. 23. Absorption (Abs) and normalized fluorescence (F) spectra of 1-DBA in ethanol ( $c=7.8 \cdot 10^{-6}\text{ M}$ ) at different pH-values. pH  $\approx 2$  (the fluorescence spectrum is excited at  $\tilde{\nu}_{ex} = 23400\text{ cm}^{-1}$ ), pH  $\approx 5.2$  (the fluorescence spectrum is excited at  $\tilde{\nu}_{ex} = 26700\text{ cm}^{-1}$ ) and pH  $\approx 6$  (the fluorescence spectrum is excited at  $\tilde{\nu}_{ex} = 26700\text{ cm}^{-1}$ ).

Fig. 24 presents the extinction spectra of neutral and protonated 1-DBA in ethanol. Selected values of the extinction coefficients of neutral and protonated 1-DBA are listed in Table 2.

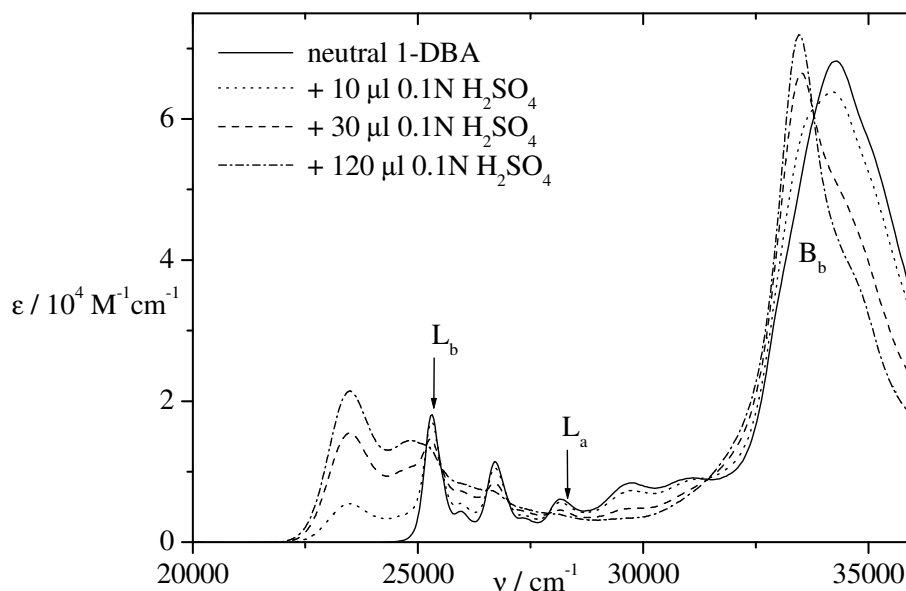
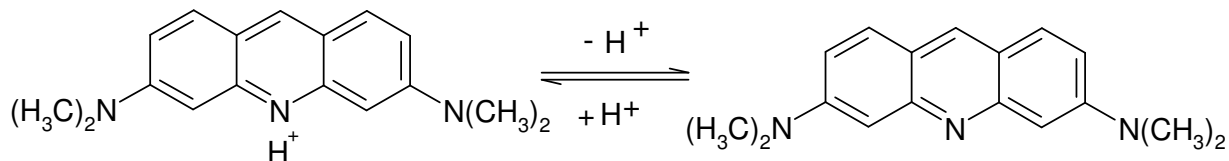


Fig. 24. The change of the extinction coefficient,  $\epsilon$ , of 1-DBA in ethanol ( $c = 9.6 \cdot 10^{-6} M$ ) by titration with  $0.1 N H_2SO_4$ .

Fig. 25 shows the absorption and emission fluorescence spectra of AO in neutral, alkaline and acidic ethanol, respectively. In neutral ethanol, there are two absorption bands of AO, one at  $20400 \text{ cm}^{-1}$  which is due to the protonated form of AO and the other at  $23100 \text{ cm}^{-1}$  which is results from the neutral form of AO. In acidic ethanol, a single band at  $20200 \text{ cm}^{-1}$  is present due to the protonated form of AO [92, 93]. In alkaline ethanol, one band is appears at about  $23000 \text{ cm}^{-1}$  due to the unprotonated species of AO.



There is equilibrium between the protonated and unprotonated form of AO in neutral solution [80]. In the fluorescence spectrum of AO in neutral ethanol, there is one band at

$18900\text{ cm}^{-1}$ , which is due to the protonated form of AO and there is a shoulder at about  $18100\text{ cm}^{-1}$  which is due to the neutral species of AO. In acidic ethanol, only one emission band appears at  $18900\text{ cm}^{-1}$  due to the protonated form of AO, whereas in alkaline ethanol, only the emission band of the neutral AO is present at  $18000\text{ cm}^{-1}$ , see Table 3.

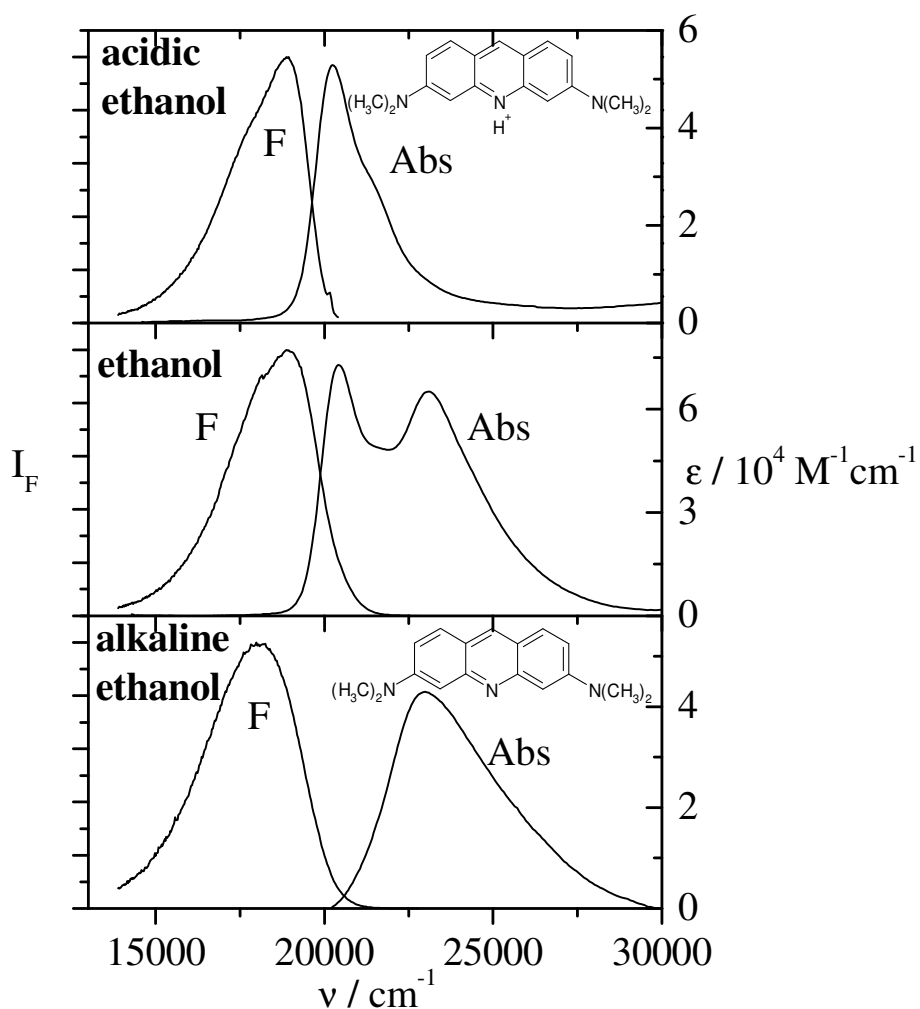


Fig. 25. Absorption (Abs) and normalized fluorescence (F) spectra of AO in ethanol ( $c=3.9 \cdot 10^{-6}\text{ M}$ ) at different pH-values. Acidic ethanol (the fluorescence spectrum is excited at  $\tilde{\nu}_{ex} = 20200\text{ cm}^{-1}$ ), ethanol (the fluorescence spectrum is excited at  $\tilde{\nu}_{ex} = 23000\text{ cm}^{-1}$ ) and alkaline ethanol (the fluorescence spectrum is excited at  $\tilde{\nu}_{ex} = 23000\text{ cm}^{-1}$ ).

### 4.1.2.3. Fluorescence quantum yields and decay times

In table 4, the fluorescence quantum yields and decay times of AC in various solvents are collected. Table 6 indicate that the decay pathway of AC excited states depends on the type of AC species present.

Table 4: Fluorescence quantum yields  $\Phi_F$  and fluorescence lifetimes  $\tau_F$  of AC in various solvents in air

Solvent	$\Phi_F$	$\tau_F$ /ns	ref
Water			
pH $\approx$ 12	0.33-0.37	11.3	[64,94]
pH $\approx$ 1	0.66	34.2	
Ethanol	0.03-0.0079	0.72	[95,96]
n-hexane	0.0009	0.033	[95,96]

Table 5 presents the fluorescence life time of AC in alkaline and acidic water in presence of air, oxygen and nitrogen atmosphere and the quenching rate constants are obtained from the Stern-Volmer plots.

Table 5: Fluorescence lifetime  $\tau_F$  of AC in water at different pH values in presence of air, oxygen and nitrogen atmosphere, concentration of oxygen in water at pressure = 1 bar and the quenching rate constants  $k_q$ , ( $\tilde{\nu}_{ex} = 27000 \text{ cm}^{-1}$ ).

water	$\tilde{\nu}_{em} / \text{cm}^{-1}$	$\tau_F$ /ns (nitrogen)	$\tau_F$ /ns (air)	$\tau_F$ /ns (oxygen)	concentration of $\text{O}_2 / 10^{-3} \text{ M}$	$k_q / 10^9 \text{ M}^{-1}\text{s}^{-1}$
pH $\approx$ 12	23400	11.6	11.3	10.5	1.4	6.4
pH $\approx$ 1	20800	34.3	34.2	33.9	1.4	0.26

The rate constant of quenching of protonated AC by oxygen is smaller than expected for the diffusion limited case ( $k_q \approx 10^{10} \text{ M}^{-1}\text{s}^{-1}$ ).

In table 6 presents the values of the fluorescence lifetime of 1-DBA and 3-DBA in different solvents in air, oxygen and nitrogen atmosphere and the quenching rate constants are obtained from the Stern-Volmer plots. The fluorescence lifetime of the protonated 3-DBA is longer than that of the protonated 1-DBA.

Table 6: Fluorescence decay times  $\tau_F$  of 1-DBA and 3-DBA in various solvents in presence of air, oxygen and nitrogen atmosphere, concentration of oxygen in cyclohexane and ethanol at pressure = 1 bar and the quenching rate constants  $k_q$ , ( $\tilde{\nu}_{ex} = 27000\text{ cm}^{-1}$ ).

Probe	solvent	$\tilde{\nu}_{em} / \text{cm}^{-1}$	concentration of $\text{O}_2 / 10^{-3} \text{ M}$	$\tau_F / \text{ns}$			$k_q / 10^9 \text{ M}^{-1} \text{ s}^{-1}$
				nitrogen	air	oxygen	
1-DBA	Cyclohexane	24000	11.7 [97]	10.1	7.4	3.5	16.7
	Ethanol	24900	10.0 [97]	10.5	8.0	3.6	18.5
	Acidic ethanol	21700	10.0 [97]	7.1	6.7	5.6	4.7
3-DBA	Cyclohexane	25400	11.7	10.0	7.9	3.4	17.8
	Ethanol	25300	10.0	10.1	9.7	3.6	18.3
	Acidic ethanol	20700	10.0	12.5	11.8	11.5	0.87

From Table 5 and 6 it can be seen that the lifetimes of the neutral forms of AC, 1-DBA and 3-DBA are more strongly quenched by oxygen than those of the protonated forms. The reason for this is, that the paramagnetic oxygen contacts with the neutral species of the probes and causes it to undergo intersystem crossing from the singlet ( $S_1$ ) to the triplet ( $T_1$ ) state [98]. In the protonated species the oxygen is not excited and quenched the protonated form because the energy difference between the singlet and the triplet states is not high enough. The fluorescence quantum yield of AO in ethanol is determined and possesses a value of  $\Phi_F = 0.34$  for the neutral species and  $\Phi_F = 0.67$  for the protonated form. The lifetimes and the fluorescence quantum yields of AO in different solvents are listed in table 7.

Table 7: Fluorescence lifetimes  $\tau_F$  of AO and fluorescence quantum yield  $\Phi_F$  in various solvents under air, ( $\tilde{\nu}_{ex} = 27000\text{ cm}^{-1}$ ).

Solvents	$\tau_F / \text{ns}$	$\Phi_F$
Ethanol		
pH $\approx$ 1	3.1	0.67
pH $\approx$ 6	5.3	0.34
pH $\approx$ 14	7.3	
Dichloromethane	4.8	
Glycerol	4	



#### 4.1.2.4. Fluorescence anisotropy of probes

Fig. 26 depicts the emission fluorescence, fluorescence excitation and fluorescence anisotropy spectra of AC in glycerol ( $\eta = 1.25 \text{ g / ml}$  at  $20^\circ\text{C}$ ). The fluorescence anisotropy excitation spectrum of protonated AC in glycerol shows positive anisotropy in the region of the  ${}^1\text{L}_a$ -band, which slowly increases towards longer wavelengths and reaches a maximum value of  $r \approx 0.20$  at  $\tilde{\nu} = 22000 \text{ cm}^{-1}$ . In the  ${}^1\text{L}_b$  region, negative  $r$  values are observed, due to the  ${}^1\text{L}_b$  transition dipole moment being approximately perpendicular to the  ${}^1\text{L}_a$ -band.

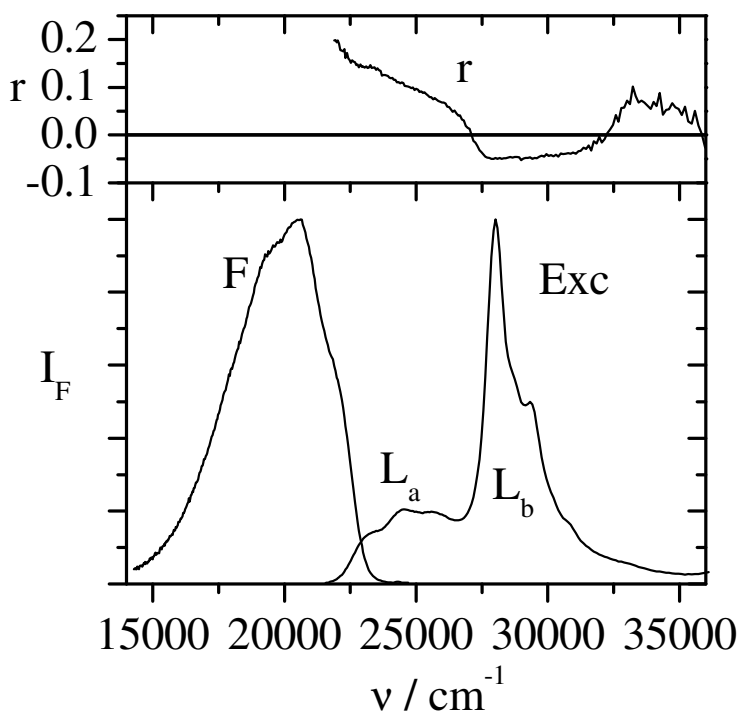


Fig. 26. Fluorescence (F), fluorescence excitation (Exc), and fluorescence anisotropy spectra ( $r$ ) of AC in glycerol ( $c = 13.8 \cdot 10^{-6} \text{ M}$ ). The fluorescence spectrum is excited at  $\tilde{\nu}_{ex} = 25000 \text{ cm}^{-1}$ ; the excitation and the anisotropy spectra are observed at  $\tilde{\nu}_{em} = 20700 \text{ cm}^{-1}$ .

The fluorescence anisotropy spectra of 1-DBA are recorded in liquid Paraffin ( $\eta = 0.90 \text{ g / ml}$  at  $20^\circ\text{C}$ ) and in glycerol ( $\eta = 1.25 \text{ g / ml}$  at  $20^\circ\text{C}$ ). Fig. 27 presents the fluorescence, fluorescence excitation and fluorescence anisotropy spectra of 1-DBA in liquid paraffin, only the unprotonated 1-DBA is presented. The anisotropy reaches a maximum value of  $r \approx 0.07$  at  $26520 \text{ cm}^{-1}$ . The fundamental anisotropy of neutral 1-DBA in glass at low

temperature (77°K) is  $r_0 \approx 0.18$  [89]. The fluorescence, fluorescence excitation and fluorescence anisotropy spectra of 1-DBA in glycerol appear in Fig. 28. In glycerol, only the protonated species of 1-DBA is presented and the maximum anisotropy amounts to  $r \approx 0.34$  at  $23300 \text{ cm}^{-1}$ . The fluorescence anisotropy excitation spectrum in glycerol reveals the presence of at least three bands,  ${}^1L_a$ ,  ${}^1L_b$  and  $B_b$ -bands which are superpositions. The first part from  $22100$  to  $23500 \text{ cm}^{-1}$  is due to the  ${}^1L_b$ -band. The second part from  $23500$  to  $27100 \text{ cm}^{-1}$  is due to the contribution of  ${}^1L_b$  and  ${}^1L_a$ -bands. The third part from  $27100$  to  $31300 \text{ cm}^{-1}$  is due to the contribution of  ${}^1L_a$  and  $B_b$ -bands. The fourth one from  $31300$  to  $34600 \text{ cm}^{-1}$  is due to the  $B_b$ -band.

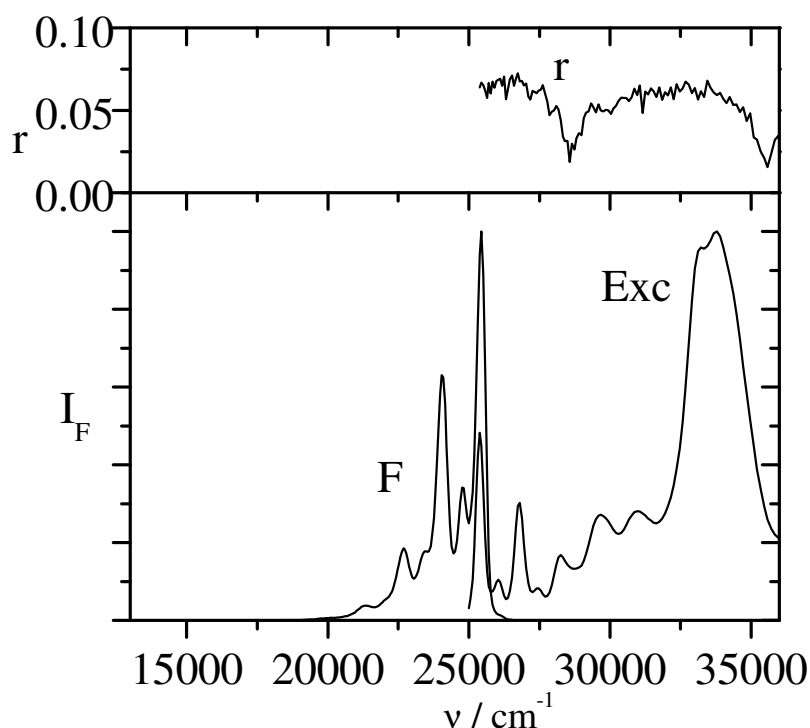


Fig. 27. Fluorescence (F), fluorescence excitation (Exc), and fluorescence anisotropy spectra ( $r$ ) of 1-DBA in paraffin liquid ( $c=2.0 \cdot 10^{-6} M$ ). The fluorescence spectrum is excited at  $\tilde{\nu}_{ex} = 25500 \text{ cm}^{-1}$ , the excitation and the anisotropy spectra are observed at  $\tilde{\nu}_{em} = 23800 \text{ cm}^{-1}$ .

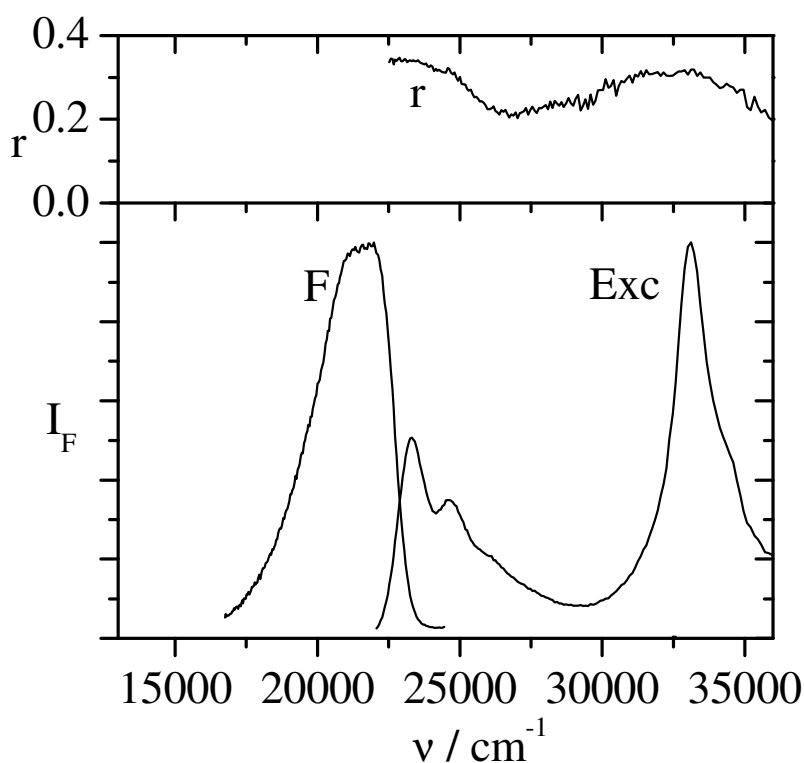


Fig. 28. Fluorescence (F), fluorescence excitation (Exc), and fluorescence anisotropy spectra ( $r$ ) of 1-DBA in glycerol ( $c = 2.0 \cdot 10^{-6} M$ ). The fluorescence spectrum is excited at  $\tilde{\nu}_{ex} = 33110 \text{ cm}^{-1}$ ; the excitation and the anisotropy spectra are observed at  $\tilde{\nu}_{em} = 21600 \text{ cm}^{-1}$ .

The fluorescence emission, fluorescence excitation and fluorescence anisotropy spectra of 3-DBA in glycerol (one drop of concentrated  $\text{H}_2\text{SO}_4$  is added) are given in Figs. 27. In glycerol, only the protonated form of 3-DBA appears and the fluorescence anisotropy amounts to  $r \approx 0.19$  at  $23300 \text{ cm}^{-1}$ . This means slow rotational diffusion, i.e. low mobility of the protonated species of 3-DBA according to Eq. 16. In cyclohexane the fluorescence anisotropy of both 1-DBA and 3-DBA has a value of  $r \approx 0$ . This means fast rotational diffusion, i.e., high mobility of both molecules in cyclohexane.

The fluorescence emission, fluorescence excitation and fluorescence anisotropy spectra of AO in glycerol are shown in Fig. 30. In glycerol, only the protonated species of AO is appeared and the fluorescence anisotropy possesses a value of about  $r \approx 0.34$  at  $21400 \text{ cm}^{-1}$ .

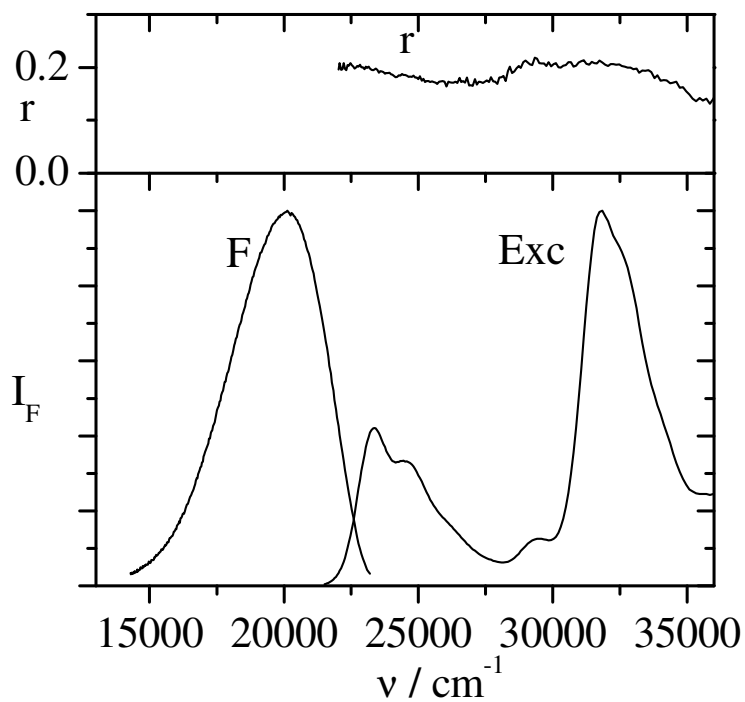


Fig. 29. Fluorescence (F), fluorescence excitation (Exc), and fluorescence anisotropy spectra ( $r$ ) of 3-DBA in glycerol +  $\text{H}_2\text{SO}_4$  ( $c = 11.0 \cdot 10^{-6} \text{ M}$ ). The fluorescence spectrum is excited at  $\tilde{\nu}_{ex} = 23500 \text{ cm}^{-1}$ ; the excitation and the anisotropy spectra are observed at  $\tilde{\nu}_{em} = 20600$

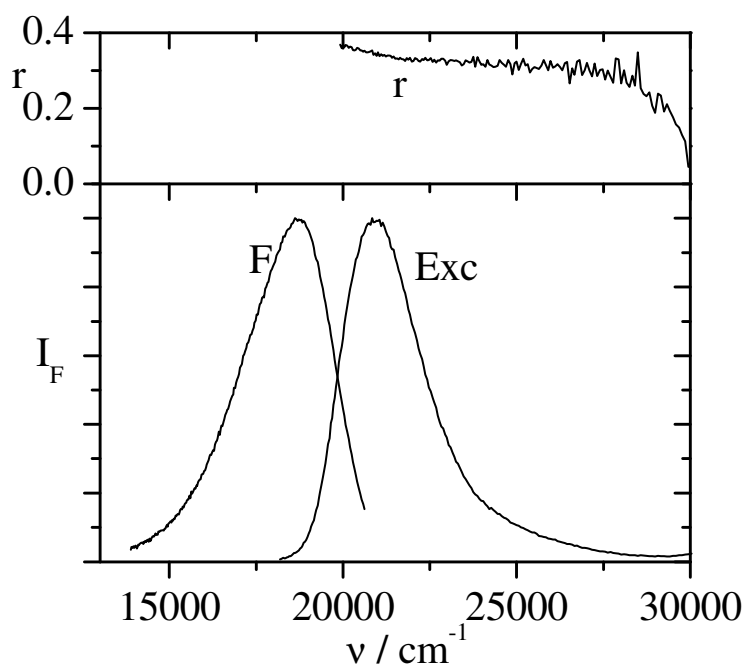


Fig. 30. Normalized fluorescence (F), fluorescence excitation (Exc), and fluorescence anisotropy ( $r$ ) spectra of AO in glycerol ( $c = 3.9 \cdot 10^{-6} \text{ M}$ ). The fluorescence spectrum is excited at  $\tilde{\nu}_{ex} = 20800 \text{ cm}^{-1}$ ; the excitation and the anisotropy spectra are observed at  $\tilde{\nu}_{em} = 18600 \text{ cm}^{-1}$ .

Fig. 31 presents the fluorescence emission and fluorescence excitation spectra of DANSyl amide in dichloromethane. In the measured range, DANSyl amide has one emission peak at  $19000\text{ cm}^{-1}$ . The excitation spectrum possesses its maximum at  $29200\text{ cm}^{-1}$ . The fluorescence anisotropy excitation spectrum shown in Fig. 31 has a value of  $r \approx 0.005$  at  $25000\text{ cm}^{-1}$ , which means fast rotational diffusion, i.e. high mobility of DANSyl amide in dichloromethane.

The fluorescence emission, fluorescence excitation and fluorescence anisotropy of DANSyl amide in glycerol appear in Fig. 32. In glycerol the fluorescence spectrum is shifted to the red compared to that in dichloromethane by about  $1100\text{ cm}^{-1}$ . This is due to the higher polarity of glycerol compared to dichloromethane. The fluorescence anisotropy of DANSyl amide in glycerol is  $r \approx 0.28$  at  $25000\text{ cm}^{-1}$ , which means slow rotational diffusion, i.e. low mobility of DANSyl amide. The values of the anisotropy and the fluorescence lifetimes of the probes in different solvents are listed in Table 8.

Table 8. Maximum values of anisotropy  $r_{\text{max}}$  of the probes and their decay times  $\tau_{\text{F}}$  in different solvents.

Probe	solvent	$r_{\text{max}}$	$\tilde{\nu}_{\text{max}} / \text{cm}^{-1}$	$\tau_{\text{F}} / \text{ns}$
ACH <sup>+</sup>	glycerol	0.20	22000	21.0
1-DBA	paraffin liquid	0.07	26500	
1-DBA	glass at 77°K	$r_0 = 0.18$ [89]	23300	
1-DBAH <sup>+</sup>	glycerol	0.34		6.6
3-DBAH <sup>+</sup>	glycerol	0.19	23300	11.4
AOH <sup>+</sup>	glycerol	0.34	21400	4.0
DANSyl amide	Dichloromethane	0.0	25000	
DANSyl amideH <sup>+</sup>	glycerol	0.28	25000	

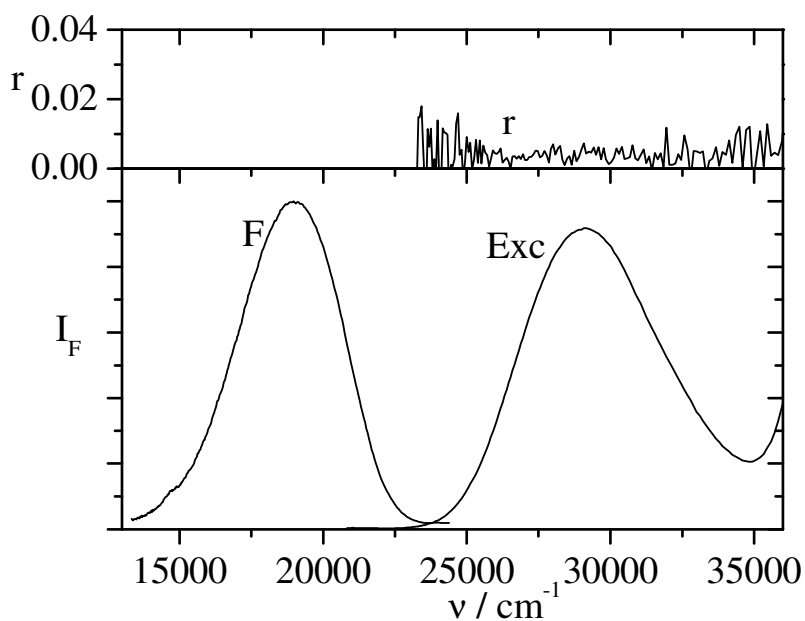


Fig. 31. Normalized fluorescence (F), fluorescence excitation (Exc) and fluorescence anisotropy ( $r$ ) spectra of DANSyl amide in DCM ( $c=5.9 \cdot 10^{-6} M$ ). The fluorescence spectrum is excited at  $\tilde{\nu}_{ex} = 29400 \text{ cm}^{-1}$ ; the excitation and anisotropy spectra are observed at  $\tilde{\nu}_{em} = 20000 \text{ cm}^{-1}$ .

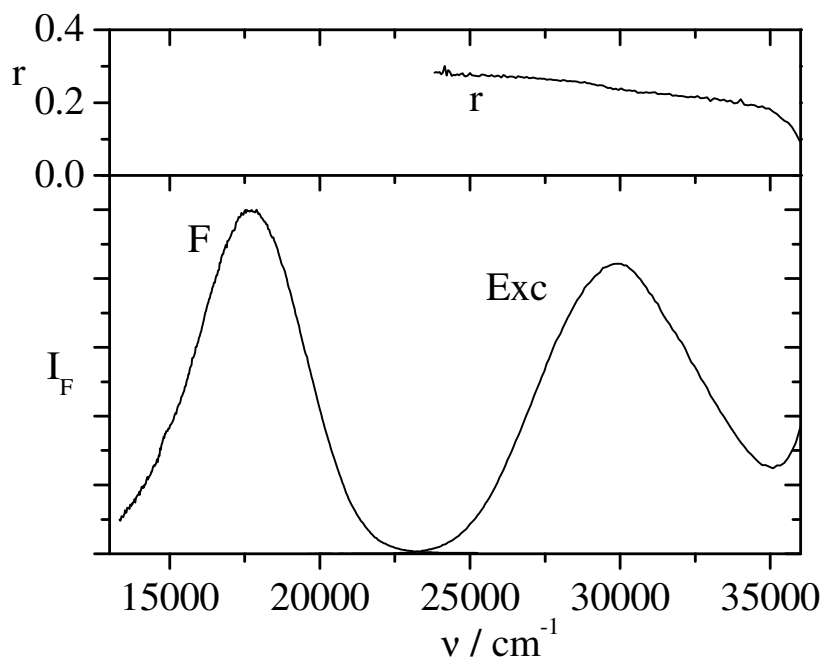
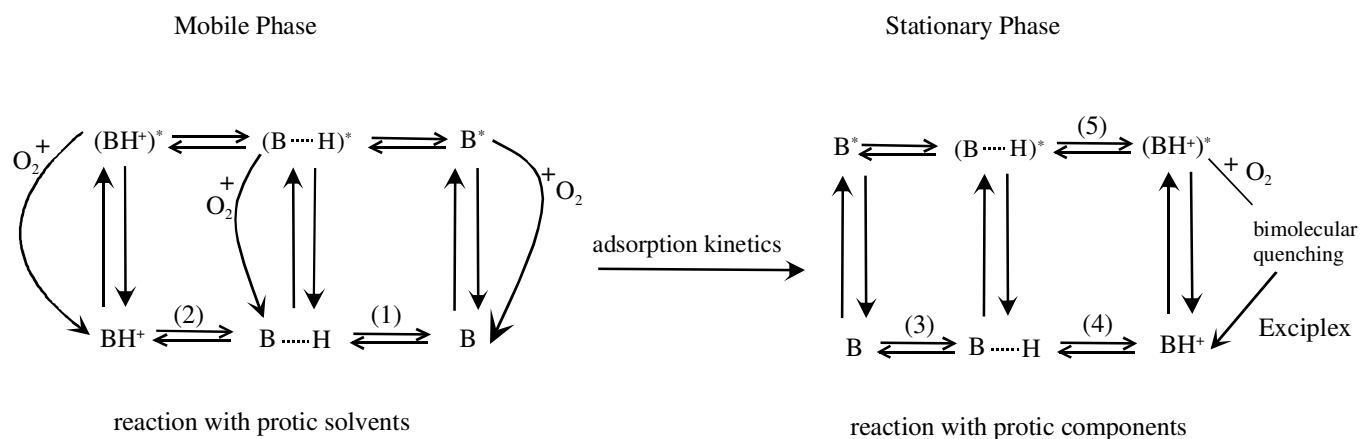


Fig. 32. Fluorescence, fluorescence excitation, and fluorescence anisotropy spectra of DANSyl amide in glycerol ( $c=3.9 \cdot 10^{-6} M$ ). The fluorescence spectrum is excited at  $\tilde{\nu}_{ex} = 29900 \text{ cm}^{-1}$ ; the excitation and the anisotropy spectra are observed at  $\tilde{\nu}_{em} = 18900 \text{ cm}^{-1}$ .

## 4.2. Spectroscopic characterization of the adsorbed state

The interphase concept (see the description in the introduction part, page 1) is applied to the following general scheme:



Scheme 1. The adsorption of base, b from the mobile phase on the stationary phase in interphase systems.

where B is the dissolved fluorescence probe (base = Acridine, 1,2,7,8-dibenzacridine, 3,4,5,6-dibenzacridine and acridine orange) in its ground state and  $B^*$  is the fluorescence probe in its excited state.

In the mobile phase:

When B is dissolved in protic solvents, it forms the hydrogen bonded species B---H in the ground state (step (1)) which can be excited to  $(B \cdots H)^*$ . The protonated species of the fluorescence probe,  $BH^+$ , is formed in the ground state when its solution in protic solvents is acidified to lower pH value (step (2)). The excited fluorescence probe  $B^*$ , its hydrogen bonded species  $(B \cdots H)^*$  and the protonated form  $(BH^+)^*$  are quenched and deactivated to the ground state by bimolecular oxygen. The protonated species are less quenched by oxygen than the neutral base and the hydrogen bonded species.

In the stationary phase:

When the fluorescence probe **B** is dissolved in aprotic solvents and added to the stationary phase (silica beads and controlled porous glass) it adsorbs to the stationary phase and forms the hydrogen bonded species,  $B\cdots H$ , (step (3)) or the protonated species,  $BH^+$ , (step (4)) in the ground state, depending on the  $pK_a$  of the base and the surface acidity of the stationary phase. When the hydrogen bonded species is formed in the ground state after adsorption at the stationary phase, it is transformed to the protonated species upon excitation (step (5)). The protonated species on the surface are quenched and deactivated to the ground state by bimolecular oxygen.



## 4.2.1. Controlled porous glass as adsorbent

### 4.2.1.1. Porous Vycor glass

When AC is adsorbed on different surfaces, it forms various species depending on the surface acidity of the surfaces. There are three species of AC; neutral species in solution, H-bonded species and the protonated form.

Fig. 33 shows the fluorescence emission, fluorescence excitation and the corresponding fluorescence anisotropy spectra of solution of AC in cyclohexane ( $c = 2.2 \cdot 10^{-6} M$ ) with Porous Vycor glass (PVG) (PVG + cyclohexane). There is one broad emission band with maximum at  $\tilde{\nu}_{F, \max} = 20800 \text{ cm}^{-1}$ , which is the same value as for AC in water at  $\text{pH} \approx 1$ . Therefore, this broad emission band is assigned to the protonated form of AC on the surface. Also, in the excitation spectrum, the maximum of the  ${}^1\text{L}_b$ -band at  $\tilde{\nu}_{\max} = 28100 \text{ cm}^{-1}$  and the  ${}^1\text{L}_a$ -band at  $\tilde{\nu}_{\max} = 24500 \text{ cm}^{-1}$  are comparable to those observed in water at  $\text{pH} \approx 1$ . So, it is proposed that at PVG surfaces the major species of AC is the protonated form ( $\text{ACH}^+$ ). This is confirmed by the fluorescence decay time measurements. The fluorescence lifetime of adsorbed AC at the PVG surface has value of  $\tau_F \approx 28 \text{ ns}$  and it is slightly shorter than, but still comparable to the  $\tau_F$  of AC in water at  $\text{pH} \approx 1$  ( $\tau_F = 34.2$ , see Table 5). For this reason, this lifetime value is due to the protonated form of the adsorbed AC at PVG surface.

The fluorescence anisotropy of AC (PVG + cyclohexane), with loading  $l = 6.0 \cdot 10^{-8} \text{ mole/g}$  has a maximum value of  $r \approx 0.18$  at  $22800 \text{ cm}^{-1}$  which is approximately the same as in glycerol (see Table 8) and this means that the protonated species of AC are immobilized at the PVG surface. The fluorescence anisotropy spectrum of AC (PVG + cyclohexane) is positive over the  ${}^1\text{L}_a$  absorption band and negative over the  ${}^1\text{L}_b$  absorption band and comparable to the fluorescence anisotropy spectrum of AC in glycerol, see Fig. 33.

Table 9 lists the rotational correlation times  $\langle \tau_R \rangle$  of the adsorbed AC, 1-DBA and 3-DBA at PVG surfaces which are determined by inserting the fluorescence decay times  $\tau_F$ , fluorescence excitation anisotropies  $r$  and the fundamental anisotropies  $r_0$  (as measured in glycerol, see Table 8) of each probe into Eq. 16. From this Table, it is found that  $\tau_R \gg \tau_F$ .

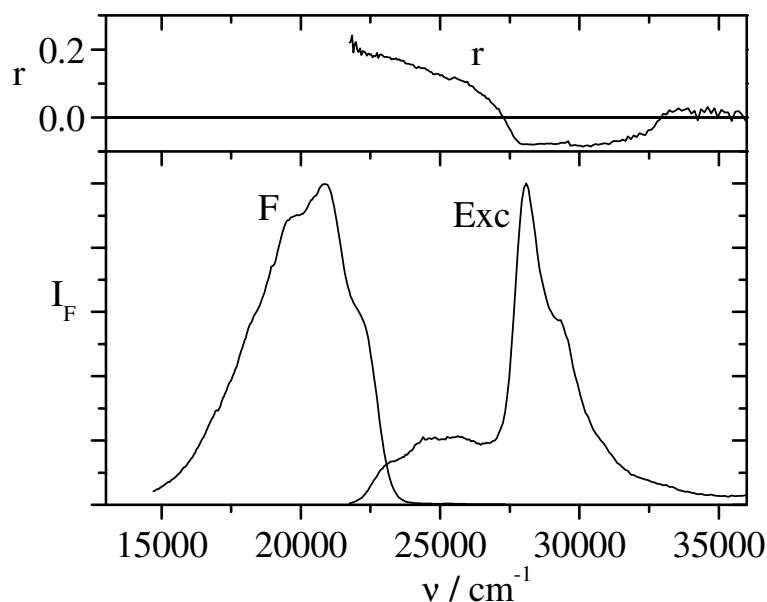


Fig. 33. Fluorescence (F), fluorescence excitation (Exc) and fluorescence anisotropy ( $r$ ) spectra of AC (PVG + cyclohexane),  $l = 6.0 \cdot 10^{-8} \text{ mole/g}$ ; the fluorescence spectrum is excited at  $\tilde{\nu}_{ex} = 25000 \text{ cm}^{-1}$ , the excitation and the anisotropy spectra are observed at  $\tilde{\nu}_{em} = 21000 \text{ cm}^{-1}$ .

Fig. 34 presents the emission fluorescence, fluorescence excitation and fluorescence anisotropy spectra of the adsorbed 1-DBA at PVG surface in presence of cyclohexane ( $c = 3.7 \cdot 10^{-6} \text{ M}$ ) (PVG + cyclohexane), the measurements are performed after 5h after the addition of PVG sheet to 3 ml of 1-DBA solution. There is an emission band at about  $\tilde{\nu}_{F, \max} = 22300 \text{ cm}^{-1}$  which is due to the protonated form of 1-DBA adsorbed at the PVG surface. The excitation spectrum observed at  $21300 \text{ cm}^{-1}$  has a broad  ${}^1L_b$ -band, and this band has a red-shift compared to the  ${}^1L_b$ -band of 1-DBA in neutral ethanol (see Fig. 23). Also, there is a decrease in the intensity of the  ${}^1L_a$ -band, and a red-shift of the  $B_b$ -band as is the same case for the absorption spectrum of 1-DBA in ethanol at  $\text{pH} \approx 2$  (see Fig. 23). This means that 1-DBA forms the protonated form, when it is adsorbed at the PVG surface. The fluorescence anisotropy excitation spectrum of protonated adsorbed 1-DBA reaches a maximum value of  $r \approx 0.25$  at  $22800 \text{ cm}^{-1}$ . This means the protonated species of 1-DBA are immobilized at the PVG surface.

The emission and excitation spectra of the adsorbed 1-DBA at PVG without solvent are given in Fig. 35. Only one broad band in the emission spectrum at about  $22000 \text{ cm}^{-1}$  is

found and no band due to the H- bonded species. The excitation spectrum observed at  $21300\text{ cm}^{-1}$  is due to the protonated form of 1-DBA, which is adsorbed at the PVG surface.

The fluorescence decay curve of 1-DBA (PVG + cyclohexane) is fitted single-exponentially. The lifetime  $\tau_F \approx 6.4\text{ ns}$ , (see Table 9) corresponds to the decay time of the adsorbed 1-DBA at PVG which is slightly shorter than, but still comparable to the  $\tau_F$  of 1-DBA in ethanol at pH 1, and this ensures that 1-DBA is adsorbed at PVG in its protonated form.

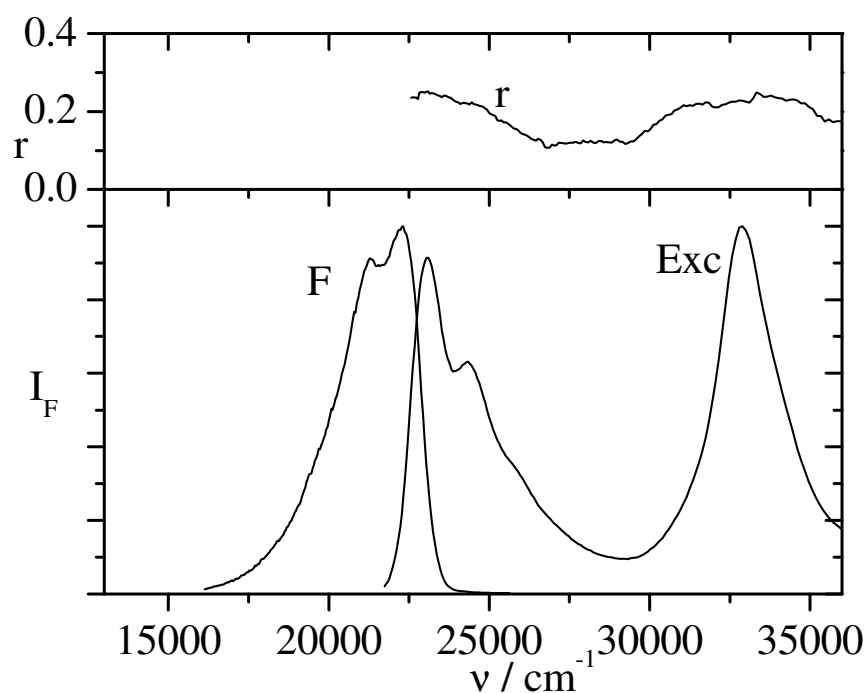


Fig. 34. Fluorescence (F), fluorescence excitation (Exc) and fluorescence anisotropy ( $r$ ) spectra of 1-DBA (PVG + cyclohexane),  $l = 1.0 \cdot 10^{-7}\text{ mole/g SiO}_2$  after 5h. The fluorescence spectrum is excited at  $\tilde{\nu}_{ex} = 26900\text{ cm}^{-1}$ ; the excitation and the anisotropy spectra are observed at  $\tilde{\nu}_{em} = 21300\text{ cm}^{-1}$ .

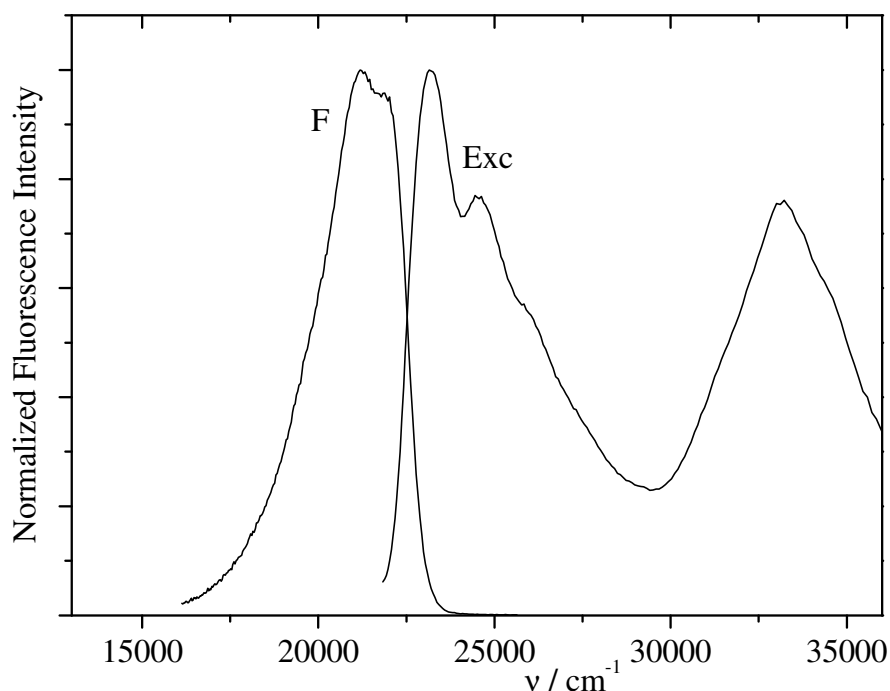


Fig. 35. Fluorescence (F) and fluorescence excitation (Exc) spectra of adsorbed 1-DBA at PVG surface without solvent,  $l = 3.7 \cdot 10^{-7} \text{ mole} / \text{g SiO}_2$ . The fluorescence spectrum is excited at  $\tilde{\nu}_{ex} = 26900 \text{ cm}^{-1}$  and the excitation spectrum is observed at  $\tilde{\nu}_{em} = 21300 \text{ cm}^{-1}$ .

The fluorescence emission, fluorescence excitation and fluorescence anisotropy spectra of 3-DBA (PVG + cyclohexane) 5 h after the addition of PVG sheet to 3 ml of 3-DBA solution are presented in Fig. 36. In this figure, the broad band (1) at  $20400 \text{ cm}^{-1}$  in the emission spectrum is due to the protonated 3-DBA, and the peaks (2) at  $25400$  and  $24000 \text{ cm}^{-1}$  are due to the neutral 3-DBA in solution. The excitation spectrum of the protonated species is very similar to that of 1-DBA (the spectra of 1-DBA and 3-DBA in acidic ethanol are more or less similar) in acidic ethanol. Thus, 3-DBA is adsorbed at PVG surface and formed its cation in the ground state. The maximum anisotropy for the protonated form has a value of  $r \approx 0.12$  at  $22600 \text{ cm}^{-1}$  and the measured anisotropy at  $25400 \text{ cm}^{-1}$  has a value of  $r \approx 0.0$  is due to the unprotonated 3-DBA in cyclohexane. The value of  $r$  at  $22600 \text{ cm}^{-1}$  is comparable to the  $r$  value of 3-DBA in glycerol (see table 8) and this value means that the protonated species of 3-DBA are immobilized at the surface.

The measurements of the adsorbed 3-DBA at the PVG surface in absence of cyclohexane (dry state) ensures the above results. Since in Fig. 37 the emission spectrum and the excitation spectra must be clearly assigned to the protonated form of 3-DBA at the PVG surface, the surface protonates 3-DBA in the ground state.

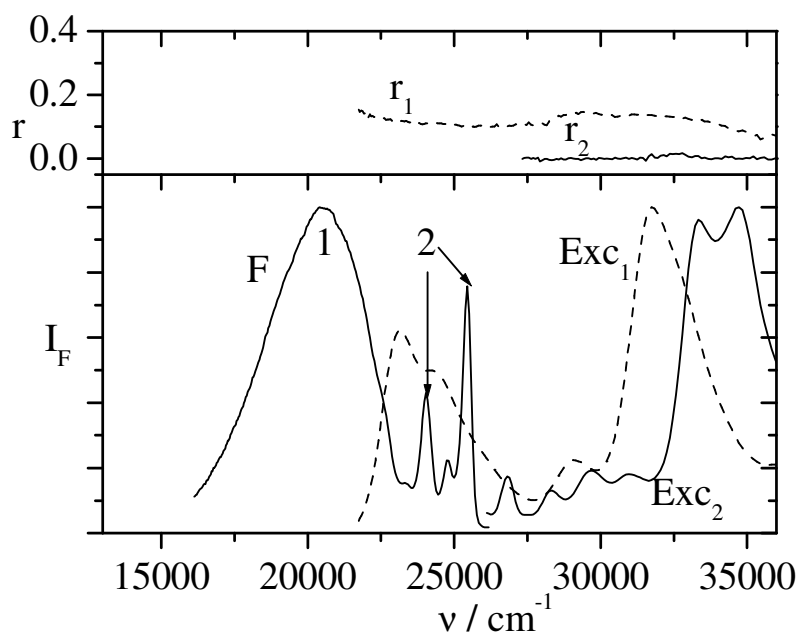


Fig. 36. Fluorescence (F), fluorescence excitation (Exc) and anisotropy ( $r$ ) spectra of 3-DBA (PVG + cyclohexane),  $l = 9.0 \cdot 10^{-8} \text{ mole/g SiO}_2$  after 5h. The fluorescence spectrum is excited at  $\tilde{\nu}_{ex} = 26800 \text{ cm}^{-1}$ ; the excitation (Exc<sub>1</sub>) and anisotropy ( $r_1$ ) spectra are observed at  $\tilde{\nu}_{em} = 20800 \text{ cm}^{-1}$  and the excitation (Exc<sub>2</sub>) and anisotropy ( $r_2$ ) spectra are observed at  $\tilde{\nu}_{em} = 25400 \text{ cm}^{-1}$ .

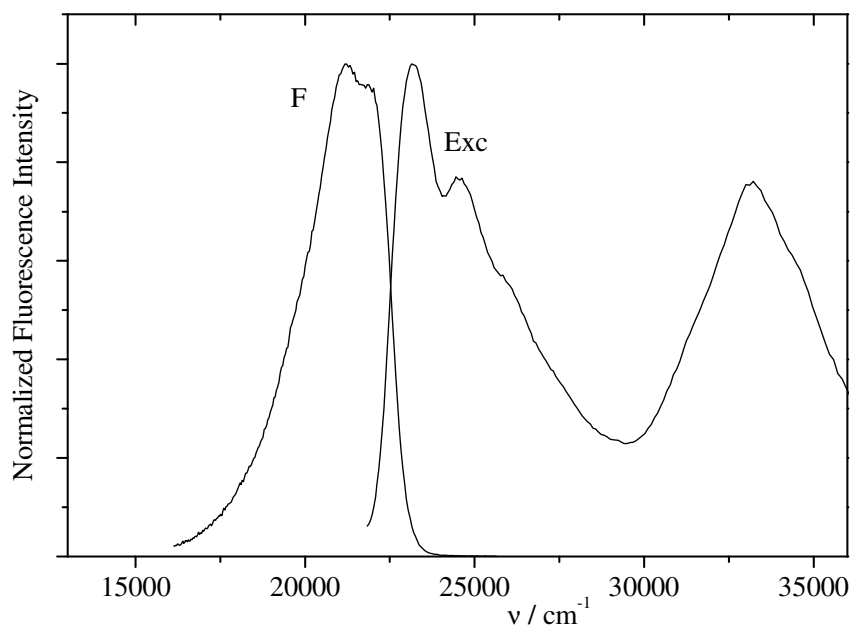


Fig. 37 Fluorescence (F) and fluorescence excitation (Exc) spectra of the adsorbed 3-DBA on PVG without solvent,  $l = 2.2 \cdot 10^{-7} \text{ mole/g SiO}_2$ . The fluorescence spectrum is excited at  $\tilde{\nu}_{ex} = 26800 \text{ cm}^{-1}$  and the excitation spectrum is observed at  $\tilde{\nu}_{em} = 20300 \text{ cm}^{-1}$ .

Also, the decay time measurements confirmed the above results. Since, adsorbed 3-DBA at the PVG surface exhibits a single-exponential fluorescence decay of  $\tau_F \approx 12.3$  ns and this value is comparable to the  $\tau_F$  of 3-DBA in acidic ethanol (20%  $H_2SO_4$ ). So, 3-DBA is protonated at PVG surface.  $\tau_F \approx 9.1$  ns is the lifetime of the neutral 3-DBA in cyclohexane.

The rotational correlation time  $\langle\tau_R\rangle$  of the protonated 3-DBA at the PVG surface calculated according to Eq. 16 by inserting the lifetime  $\tau_F$ , anisotropy value  $r$  and the fundamental anisotropy  $r_0$  (the value in glycerol, see Table 8) into this equation. The rotational correlation time  $\langle\tau_R\rangle$  of the protonated 3-DBA at the PVG surface is of the order of the fluorescence lifetime of the adsorbed 3-DBA at PVG surface, i.e., the adsorbed 3-DBA is immobilized at the PVG surfaces, see Table 9.

Table 9. Fluorescence decay times  $\tau_F$ , steady-state fluorescence anisotropies ( $r$ ), rotational correlation times  $\langle\tau_R\rangle$  of the adsorbed AC at PVG (PVG + cyclohexane) under air, ( $\tilde{\nu}_{ex} = 27000\text{ cm}^{-1}$ ).

Probe	$\tilde{\nu}_{em} / \text{cm}^{-1}$	$\tau_F / \text{ns}$	( $r$ )	$\langle\tau_R\rangle / \text{ns}$
AC	21000	28	0.18	252
1-DBA	21300	6.4	0.25	17.8
3-DBA	21000	12.3	0.12	21.1
	25400	9.1	0.0	0.0

#### 4.2.1.2 Porous Geltech glass as adsorbent

1-DBA is adsorbed at porous Geltech glass (PGG) from a cyclohexane solution ( $c = 1.21 \cdot 10^{-5} M$ ) and forms both protonated and H-bonded species on the surface, see Fig. 38. The emission spectrum consists of three peaks and by comparing it with the emission spectrum of 1-DBA in ethanol at  $\text{pH} \approx 2$  and  $\approx 6$ , it is concluded that: 1- The broad emission band (1) at about  $\tilde{\nu}_{F, \max} = 22100\text{ cm}^{-1}$  is due to the protonated form of 1-DBA at PGG surface. 2-The emission band (2) at  $\tilde{\nu}_{F, \max} = 24900\text{ cm}^{-1}$  is due to superposition of the spectra of the H-bond species of 1-DBA at the glass surface and the unprotonated form of 1-DBA in solution. 3-The two bands (3) at  $\tilde{\nu}_{F, \max} = 25400$  and  $24000\text{ cm}^{-1}$  are due to the unprotonated form of 1-DBA in solution. The excitation spectrum of the protonated 1-DBA at the surface exhibits less vibronic structure than that of the unprotonated 1-DBA and it is similar to the

absorption spectrum of the protonated 1-DBA in ethanol at  $\text{pH} \approx 5.2$ . Thus, some of the adsorbed 1-DBA at PGG surface is protonated in the ground state and the other is protonated in the excited state (see scheme 1, step 5). The fluorescence anisotropy excitation spectrum in Fig. 38 shows differences between the two species of 1-DBA at PGG surface. The polarisation spectrum which is observed at  $20000 \text{ cm}^{-1}$  is similar to that of 1-DBA in glycerol and it has maximum value of  $r \approx 0.29$  at  $22200 \text{ cm}^{-1}$ . This means that the corresponding excitation spectrum results from the protonated species of 1-DBA and these species are immobilized at the surface of the PGG. The excitation anisotropy spectrum which is observed at  $24700 \text{ cm}^{-1}$  is identical to that of 1-DBA in liquid paraffin but with higher value ( $r \approx 0.14$  at  $26800 \text{ cm}^{-1}$ ) due to the immobility of hydrogen-bonded 1-DBA at the surface. In this spectrum, the anisotropy ( $r_2$ ) has a value  $\approx 0$  when the excitation spectrum ( $\text{Exc}_2$ ) has the higher value which means that this lower value of  $r$  is due to the 3-DBA species in the solution. Whereas, the higher values of  $r \approx 0.14$  in this spectrum is due to the 3-DBA species at the surface.

Fig. 39 depicts the emission and excitation spectra of the adsorbed 1-DBA at PGG which are measured in absence of cyclohexane and after heating the glass disc for 30 min. at  $60^\circ\text{C}$ . In the this figure there is one broad band in the emission spectrum at about  $22100 \text{ cm}^{-1}$  which results from to the protonated form of the adsorbed 1-DBA at PGG surface. There is also a small shoulder in the emission spectrum at about  $24900 \text{ cm}^{-1}$  which is due to the H-bonded species of 1-DBA at the surface.

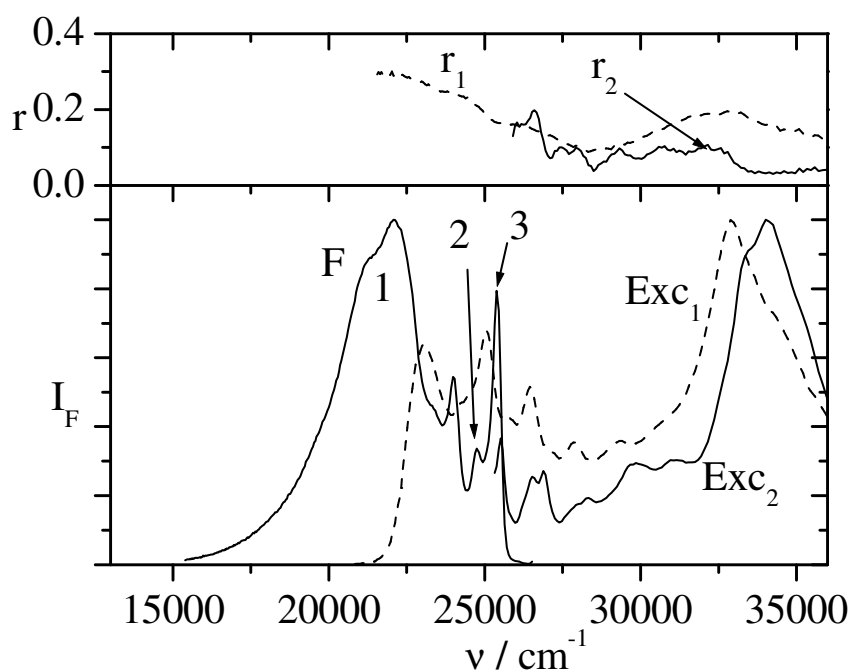


Fig. 38. Fluorescence (F), fluorescence excitation (Exc) and fluorescence anisotropy ( $r$ ) spectra of 1-DBA (PGG + cyclohexane),  $l = 5.6 \cdot 10^{-7} \text{ mole} / \text{g SiO}_2$ . The fluorescence spectrum is excited at  $\tilde{\nu}_{ex} = 26900 \text{ cm}^{-1}$ , the excitation (Exc<sub>1</sub>) and anisotropy ( $r_1$ ) spectra are observed at  $\tilde{\nu}_{em} = 20000 \text{ cm}^{-1}$  and the excitation (Exc<sub>2</sub>) and anisotropy ( $r_2$ ) spectra are observed at  $\tilde{\nu}_{em} = 24900 \text{ cm}^{-1}$ .

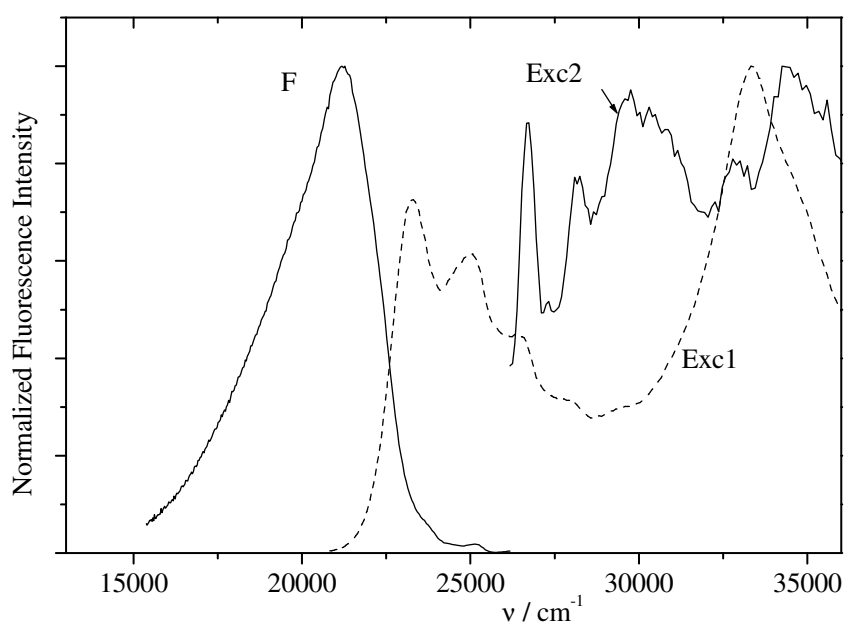


Fig. 39. Fluorescence (F) and fluorescence excitation (Exc) spectra of adsorbed 1-DBA on PGG without solvent,  $l = 5.6 \cdot 10^{-7} \text{ mole} / \text{g SiO}_2$ . The fluorescence spectrum is excited at  $\tilde{\nu}_{ex} = 26900 \text{ cm}^{-1}$ , the excitation spectrum (Exc<sub>1</sub>) is observed at  $\tilde{\nu}_{em} = 20000 \text{ cm}^{-1}$  and the excitation spectrum (Exc<sub>2</sub>) is observed at  $\tilde{\nu}_{em} = 24900 \text{ cm}^{-1}$ .



Upon pulsed laser excitation, the fluorescence decay curves of 1-DBA (PGG + cyclohexane) are observed. Comparing the fluorescence lifetimes to those of 1-DBA in acidic ethanol and in cyclohexane (see Table 6), it is found that the lifetime of  $\tau_F \approx 6.5$  ns corresponds to the protonated species of 1-DBA at the surface and the negative amplitude of the component of  $\tau_F \approx 3.7$  ns is due to the a rising component which is due to some of the adsorbed 1-DBA is protonated in the excited state. The decay curve which is observed at  $24900 \text{ cm}^{-1}$  is fit double-exponentially because of the superposition of the spectra of the H-bonded species of 1-DBA at the glass surface and the unprotonated form of 1-DBA in solution  $\tau_F \approx 7.6$  ns is the lifetime of the H-bonded species of 1-DBA at the surface, see Fig 40. The lifetime of  $\tau_F \approx 8.0$  ns corresponds to neutral 1-DBA in cyclohexane.

Table 10 lists the rotational correlation times  $\langle \tau_R \rangle$  of the adsorbed 1-DBA at PGG which are obtained by inserting mean fluorescence decay times  $\langle \tau_F \rangle$ , and fluorescence excitation anisotropies  $r$  and the fundamental anisotropies  $r_0$  (in glycerol for the protonated species and in glass at  $77^\circ\text{K}$  for the H-bonded species [89]) into Eq. 16. From this Table, the rotational correlation times  $\langle \tau_R \rangle$  of the adsorbed 1-DBA at PGG surface are of the order of the fluorescence lifetimes of the adsorbed 1-DBA at PGG surface.

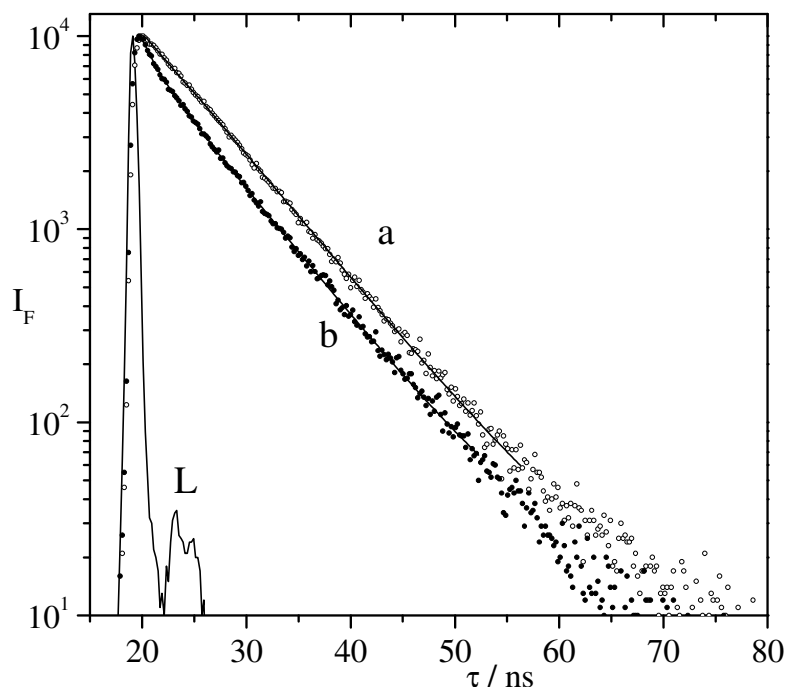


Fig. 40. Fluorescence decay curves of adsorbed 1-DBA (PGG + cyclohexane),  $l = 5.6 \cdot 10^{-7} \text{ mole / g SiO}_2$  under air; a)  $\tilde{\nu}_{em} = 21700 \text{ cm}^{-1}$  and b)  $\tilde{\nu}_{em} = 24900 \text{ cm}^{-1}$ ,  $\tilde{\nu}_{ex} = 27000 \text{ cm}^{-1}$ . L represents the profile of the exciting laser.

Table 10. Fluorescence decay times  $\tau_F$ , and their amplitudes B, steady-state fluorescence anisotropies r, mean Fluorescence decay times  $\langle\tau_F\rangle$ , rotational correlation times  $\langle\tau_R\rangle$  of 1-DBA (PGG + cyclohexane) under air, ( $\tilde{\nu}_{ex} = 27000 \text{ cm}^{-1}$ ).

Surface	$\tilde{\nu}_{em} / \text{cm}^{-1}$	$\tau_F / \text{ns}$	B	r	$\langle\tau_F\rangle / \text{ns}$	$\langle\tau_R\rangle / \text{ns}$
PGG	25400	1.7	0.40	$\approx 0$	7.9	0
		8.0	0.60			
	24900	1.6	0.24	$\approx 0.14$	7.3	25.6
		7.6	0.76			
	21700	3.7	-0.24	$\approx 0.29$		37.7
		6.5	0.76			

### 4.2.3. Non-modified silica beads as adsorbent

The fluorescence emission, fluorescence excitation spectra of the adsorbed AC at 6 mg bare silica in the presence of cyclohexane ( $c = 1.14 \cdot 10^{-5} \text{ M}$ ) (non-modified silica + cyclohexane), together with the corresponding fluorescence anisotropy spectrum are presented in Fig. 41. The species present at the surface are assigned by comparing the emission and the excitation spectra to those of AC in water at different pH values. It is found that the emission spectrum has a broad band at  $\tilde{\nu}_{F, \max} = 20900 \text{ cm}^{-1}$ , which is characteristic for the protonated form  $\text{ACH}^+$  with some small contribution from H-bonded species. The excitation spectrum is similar to that of hydrogen bonded species [99] and with a small shoulder at  $23000 \text{ cm}^{-1}$ , which is due to the protonated form of AC. These results suggest, that at bare silica surface most of AC forms a hydrogen-bonded complex, which undergoes an excited state proton transfer reaction (see scheme 1) [36], while some of adsorbed AC is protonated in the ground state.

These results are confirmed by the fluorescence decay time, which has a value of  $\tau_F \approx 19.4 \text{ ns}$ . This value is intermediate between the lifetime of AC in water at pH 12 and protonated AC in water at pH 1. This ensures that AC is adsorbed as hydrogen bonded species at bare silica surface in the ground state and that there is an equilibrium between the H-bonded and the protonated species in the excited state.

The fluorescence anisotropy excitation spectrum of the adsorbed AC at bare silica exhibits positive anisotropy in the region of the  ${}^1L_a$  band, which increases towards longer wavelengths, and reaches a maximum value of  $r \approx 0.19$  at  $\tilde{\nu} = 22800 \text{ cm}^{-1}$ . This means that the protonated AC is immobilized at the silica surface. In the  ${}^1L_b$  region, negative  $r$  values are observed (see Fig. 41), due to the  ${}^1L_b$  transition dipole moment being approximately perpendicular to the  ${}^1L_a$ -band.

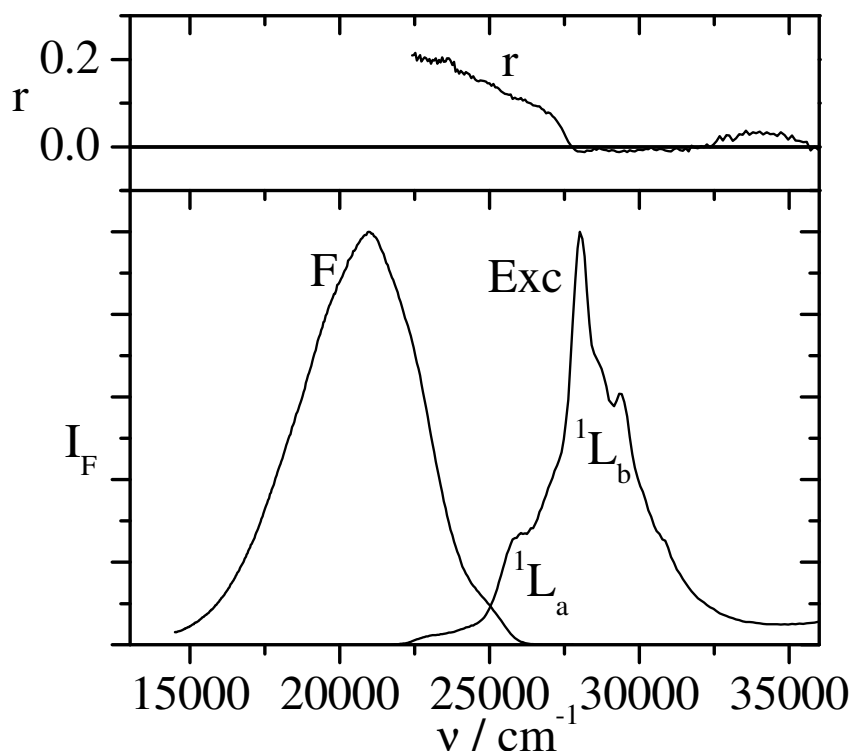


Fig. 41. Fluorescence (F), fluorescence excitation (Exc) and fluorescence anisotropy ( $r$ ) spectra of AC (bare silica + cyclohexane) of  $l = 4.4 \cdot 10^{-6} \text{ mole/g SiO}_2$ . The fluorescence spectrum is excited at  $\tilde{\nu}_{ex} = 28200 \text{ cm}^{-1}$ , the excitation and the anisotropy spectra are observed at  $\tilde{\nu}_{em} = 20800 \text{ cm}^{-1}$ .

The rotational correlation times  $\langle \tau_R \rangle$  of the adsorbed AC, 1-DBA and AO at non-modified silica surfaces are determined by inserting the fluorescence decay times  $\tau_F$  and fluorescence excitation anisotropies  $r$  and the fundamental anisotropy  $r_0$  (in glycerol for the protonated species, see Table 8 and  $r_0$  form [89] for the H-bonded species) of each probe, into Eq. 16, are given in Table 11.

Table 11. Fluorescence decay times  $\tau_F$ , steady-state fluorescence anisotropies ( $r$ ), mean Fluorescence decay times  $\langle\tau_F\rangle$ , rotational correlation times  $\langle\tau_R\rangle$  and the amplitudes B of AC, 1-DBA and AO (bare silica + cyclohexane) under air, ( $\tilde{\nu}_{ex} = 27000 \text{ cm}^{-1}$ ).

Probe	$\tilde{\nu}_{em} / \text{cm}^{-1}$	$\tau_F / \text{ns}$	B	( $r$ )	$\langle\tau_F\rangle / \text{ns}$	$\langle\tau_R\rangle / \text{ns}$
AC	20800	19.4	1.0	0.19		$\tau_R \gg \tau_F$
1-DBA	24900	4.3	0.07	0.18	8.2	$\tau_R \gg \tau_F$
		8.3	0.93			
	20800	2.4	-0.22	0.31		74
		7.2	0.60			
		9.5	0.18			
AO	17900	2.7	0.82	0.12	3.1	1.6
		4.4	0.18			

1,2,7,8-dibenzacridine (1-DBA) at silica surface exists in two forms, depending on the acidity of the medium. These species are the neutral (H-bonded species) and the protonated species. The fluorescence emission, fluorescence excitation anisotropy spectra of a solution of 1-DBA in cyclohexane ( $c = 0.87 \cdot 10^{-5} \text{ M}$ ) after addition of 6 mg of non-modified silica are appeared in Fig. 42. At least three different species contribute to the fluorescence spectrum and by comparing these spectra with those in ethanol at different pH values, it is concluded that: the broad emission band at  $\tilde{\nu}_{F, \max} = 22470 \text{ cm}^{-1}$  is due to the protonated form of 1-DBA at the silica surface. This protonated form is formed due to the interaction of 1-DBA with the surface silanol groups [100-104]. The emission band at  $\tilde{\nu}_{F, \max} = 24880 \text{ cm}^{-1}$  is due to the superposition of the spectra of the H-bonded species of 1-DBA at the silica surface and the neutral 1-DBA in solution. The third band  $\tilde{\nu}_{F, \max} = 25440 \text{ cm}^{-1}$  is due to the neutral form of 1-DBA in solution which is still nonadsorbed at the silica surface. The excitation spectrum, which is observed at  $\tilde{\nu}_{\max} = 20000 \text{ cm}^{-1}$ , is due to the contributions of the excitation spectra of both the H-bonded and the protonated 1-DBA adsorbed at the surface. The excitation spectrum, which is recorded at the excitation wavelength of  $24900 \text{ cm}^{-1}$  is that of the H-bonded 1-DBA at the surface. Thus, some of adsorbed 1-DBA is protonated in the ground state and the other is adsorbed as H-bonded species, which undergoes to protonation in the excited state.

The fluorescence intensity ratio between the peak of the protonated and the H-bonded species at the silica surface depends on the water content at the silica surface see (Fig. 43), where the experiment is performed without drying of cyclohexane. Here, the ratio of protonated and H-bonded species is shifted to the H-bonded, i.e., more H-bonded species are formed in the ground state and a small amount of adsorbed 1-DBA is protonated in the ground state. These results can be confirmed by the polarization measurements. Since the fluorescence anisotropy spectrum (Fig. 42) which is observed at  $20000\text{ cm}^{-1}$  is identical to that of the protonated 1-DBA in glycerol and it has a maximum value of  $r \approx 0.31$  at  $\tilde{\nu} = 23310\text{ cm}^{-1}$ . This means that the protonated species of 1-DBA are immobilized at the silica surface. The anisotropy spectrum which is observed at  $\tilde{\nu} = 24880\text{ cm}^{-1}$  can be compared to that of the neutral 1-DBA in paraffin liquid, but here it has higher value of  $r \approx 0.2$  and this is due to the immobility of the unprotonated 1-DBA at the silica surface. This value of  $r$  is agreed with the same value of 1-DBA in glass at low temperature [89].

The emission and fluorescence excitation spectra of a solution of 1-DBA in cyclohexane ( $c = 1.1 \cdot 10^{-6}\text{ M}$ ) after addition of 3 ml of this solution to 10 mg of bare silica are given in Fig. 44. The measurements are done for the silica particles adhere to the cell walls to avoid the noises which are in the emission spectrum (Fig. 42) due to the stirring and the adhesion of the silica particles on the cell walls. Two different species contribute to the fluorescence spectrum and by comparing these spectrum with those in ethanol at different pH values, it can be concluded that: the broad emission band (1) at  $\tilde{\nu}_{F,\text{max}} = 22300\text{ cm}^{-1}$  is due to the protonated form of 1-DBA at the silica surface. The emission band (2) at  $\tilde{\nu}_{F,\text{max}} = 24880\text{ cm}^{-1}$  is due to the H-bonded species of 1-DBA at the silica surface. The excitation spectrum, which is observed at  $\tilde{\nu}_{\text{max}} = 19200\text{ cm}^{-1}$ , is due to the contributions of the excitation spectra of both the H-bonded and the protonated 1-DBA adsorbed at the surface. The broad band at about  $23600\text{ cm}^{-1}$  ( $^1\text{L}_b$ -band) and the red-shift of this band is due to protonated 1-DBA at the non-modified silica surface. The band at  $25100\text{ cm}^{-1}$  and its pronounced vibronic replica are due to the H-bonded 1-DBA at the surface [100].

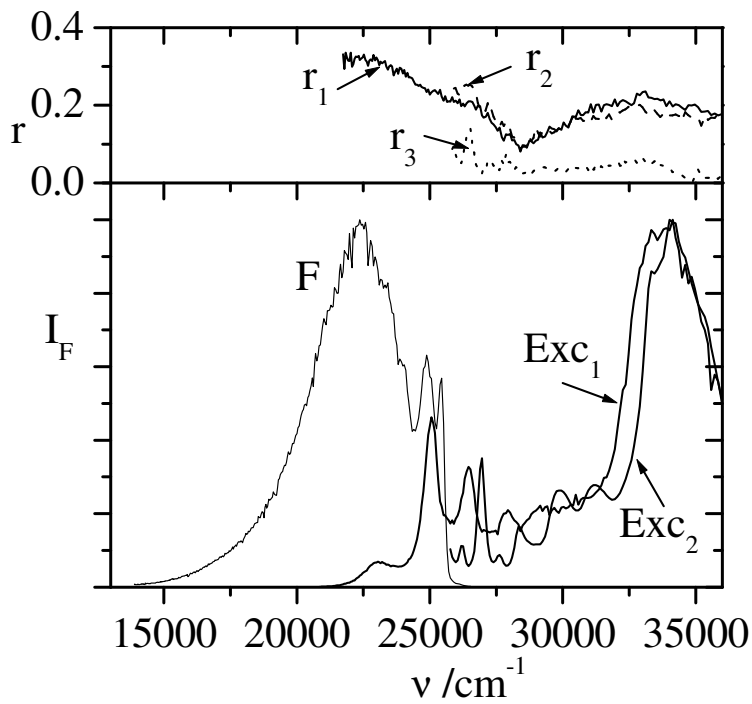


Fig. 42. Fluorescence (F), fluorescence excitation (Exc) and anisotropy spectra of 1-DBA (non-modified silica + cyclohexane),  $l=4.4 \cdot 10^{-6} \text{ mole} / \text{g SiO}_2$ . The fluorescence spectrum is excited at  $\tilde{\nu}_{ex} = 26880 \text{ cm}^{-1}$ . The excitation spectrum (Exc<sub>1</sub>) and the anisotropy ( $r_1$ ) are observed at  $\tilde{\nu}_{em} = 20000 \text{ cm}^{-1}$ . The excitation spectrum (Exc<sub>2</sub>) and the anisotropy ( $r_2$ ) are observed at  $\tilde{\nu}_{em} = 24880 \text{ cm}^{-1}$ . The anisotropy ( $r_3$ ) is observed at  $\tilde{\nu}_{em} = 25510 \text{ cm}^{-1}$ .

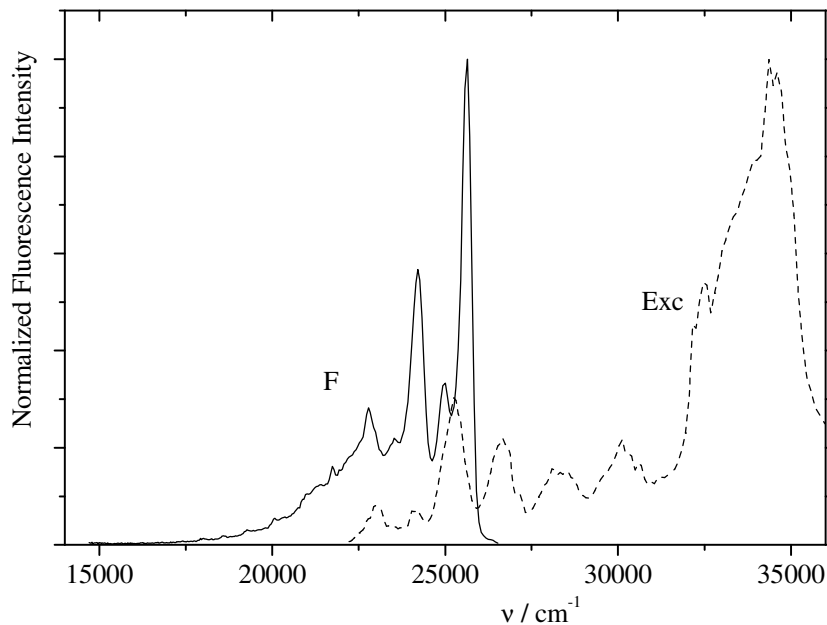


Fig. 43. Fluorescence (F) and fluorescence excitation (Exc) spectra of 1-DBA (non-modified silica + cyclohexane),  $l=4.4 \cdot 10^{-6} \text{ mole} / \text{g SiO}_2$ . The fluorescence spectrum is excited at  $\tilde{\nu}_{ex} = 26880 \text{ cm}^{-1}$ . The excitation spectrum (Exc) is observed at  $\tilde{\nu}_{em} = 21300 \text{ cm}^{-1}$ .

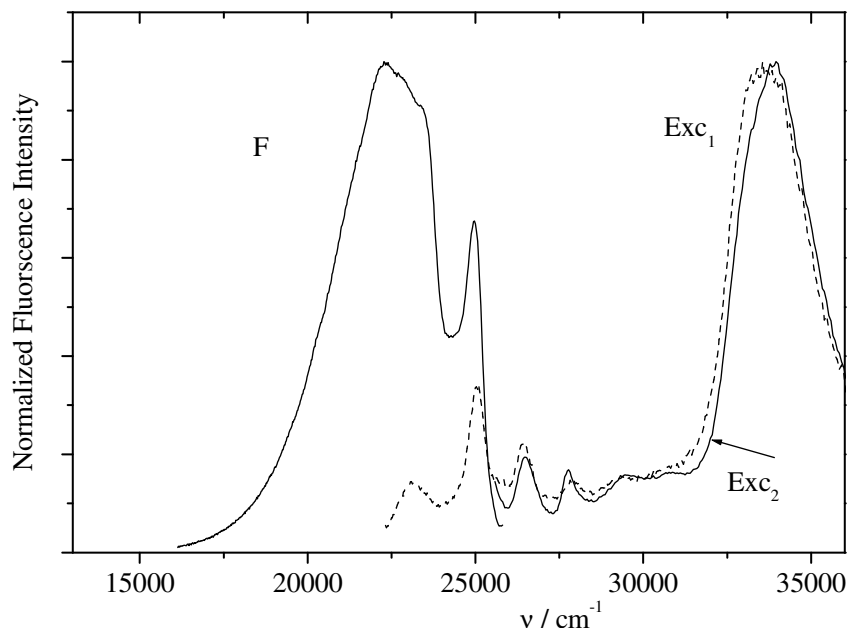


Fig. 44. Fluorescence (F) and fluorescence excitation (Exc) spectra of 1-DBA (non-modified silica + cyclohexane),  $l = 3.2 \cdot 10^{-7} \text{ mole / g SiO}_2$  for the particles on the cell walls. The fluorescence spectrum is excited at  $\tilde{\nu}_{ex} = 26500 \text{ cm}^{-1}$ . The excitation spectrum (Exc<sub>1</sub>) is observed at  $\tilde{\nu}_{em} = 19200 \text{ cm}^{-1}$  and the excitation spectrum (Exc<sub>2</sub>) is observed at  $\tilde{\nu}_{em} =$

The fluorescence decay time leads to the same results which are obtained from the steady state fluorescence and the fluorescence anisotropy measurements. By comparing the obtained values of  $\tau_F$  of the adsorbed 1-DBA at non-modified silica to those of 1-DBA in solutions, it is found that the component of  $\tau_F \approx 7.2 \text{ ns}$  is due to the protonated species of 1-DBA at the silica surface in the ground state. The component of  $\tau_F \approx 2.4$  with negative amplitude, see Table 11, is a rising component which means that some of the adsorbed 1-DBA is protonated in the excited state. The value of  $\tau_F \approx 8.3 \text{ ns}$  is due to the H-bonded 1-DBA on the surface. The life time of the protonated 1-DBA at the surface is slightly longer than, but still comparable to that observed in acidic polar solvent (acidic ethanol).

The effect of the variation of 1-DBA concentration (mol/l) on the emission fluorescence and fluorescence excitation spectra is studied at constant weight of bare silica (6 mg). The measurements are performed for the precipitate after centrifugation and evaporation the remaining solvent (dry state measurements). Two concentrations of 1-DBA are used; the first one is of low concentration in cyclohexane ( $c = 6.0 \cdot 10^{-8} \text{ M}$ ) and the other of high

concentration ( $c = 8.5 \cdot 10^{-5} M$ ). The Fluorescence and fluorescence excitation spectra of these two concentrations of 1-DBA in cyclohexane after addition of 6 mg of bare silica to 3 ml of these solutions are appeared in Fig. 45. In this figure the emission spectrum of the lower loading,  $l = 3.0 \cdot 10^{-8} \text{ mole} / \text{g SiO}_2$  is characterised by two bands. The first band (the broad band) at  $22300 \text{ cm}^{-1}$  is due to the protonated form of 1-DBA and the other one at  $25000 \text{ cm}^{-1}$  is due to the H-bonded 1-DBA at the silica surface. The emission spectrum of the higher loading,  $l = 4.3 \cdot 10^{-5} \text{ mole} / \text{g SiO}_2$  of 1-DBA, has a broad band characterized by a strong red shift (at  $18900 \text{ cm}^{-1}$ ) due to the aggregation of 1-DBA at the silica surface [75].

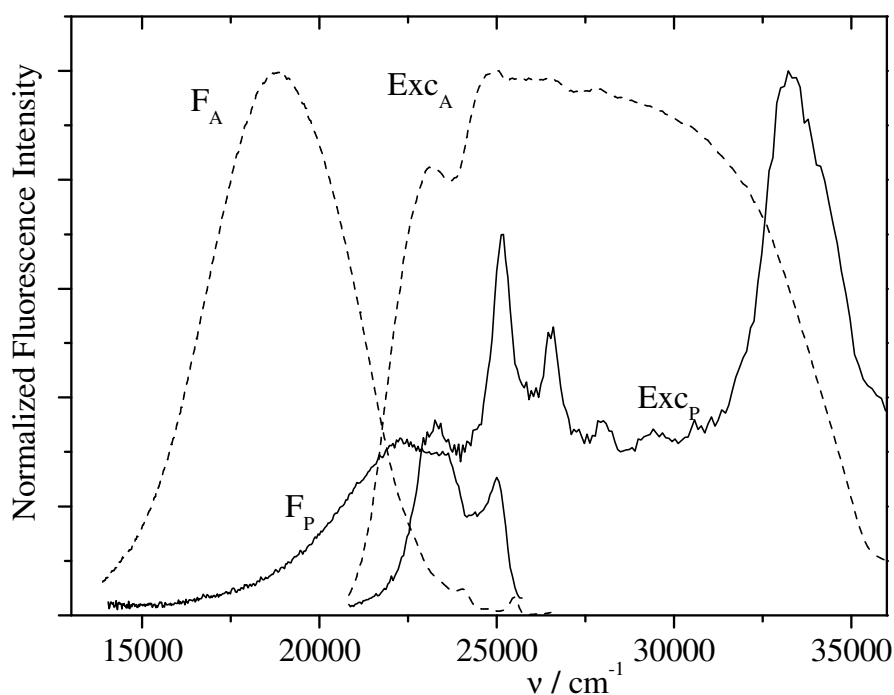


Fig. 45. Fluorescence (F) and fluorescence excitation (Exc) spectra of dry precipitate of 1-DBA at non-modified silica surface; A = for a higher loading,  $l = 4.3 \cdot 10^{-5} \text{ mole} / \text{g SiO}_2$  and P = for the lower loading,  $l = 3.0 \cdot 10^{-8} \text{ mole} / \text{g SiO}_2$ .

Fig. 46 shows the fluorescence emission and fluorescence excitation spectra of solution of 3-DBA in cyclohexane after addition 3 ml of this solution to 6 mg of non-modified silica. The emission and excitation spectra are almost identical to the emission and excitation spectra of 1-DBA solution in neutral ethanol (the spectra of 1-DBA and 3-DBA are more or



less identical). This means that, 3-DBA is not adsorbed at the non-modified silica surface and this is due to the fact that the free electron pair on the nitrogen is sterically shielded by the benzo groups [74].

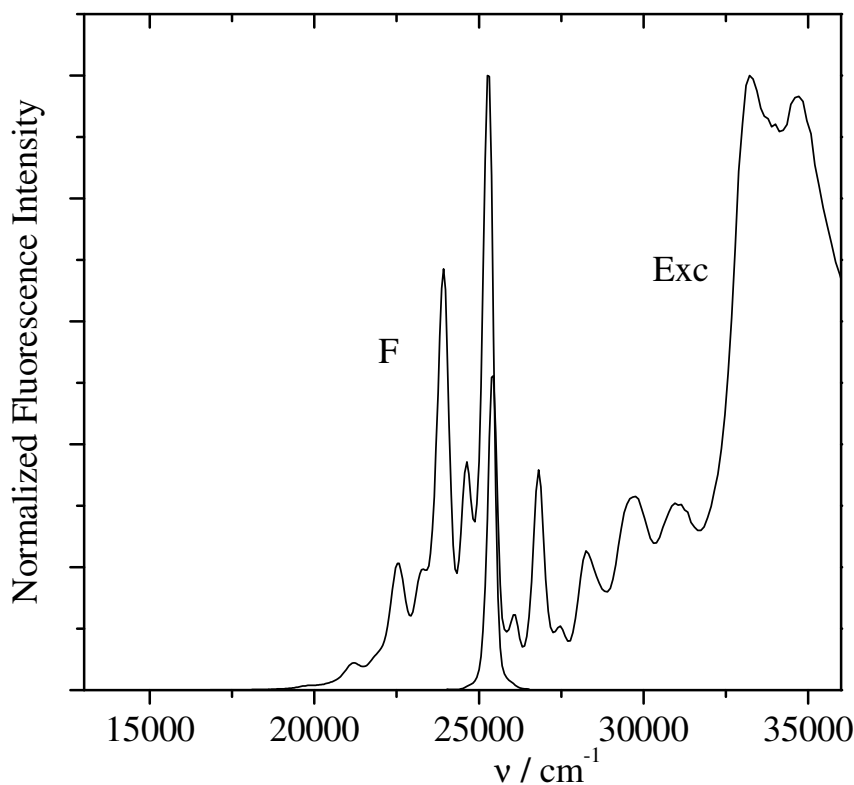


Fig. 46. Fluorescence (F) and fluorescence excitation (Exc) spectra of solution of 3-DBA in cyclohexane ( $c=1.43 \cdot 10^{-5} M$ ) after addition of 6 mg non-modified silica to 3 ml of 3-DBA solution. The fluorescence spectrum is excited at  $\tilde{\nu}_{ex} = 26800 \text{ cm}^{-1}$  and the excitation spectrum is observed at  $\tilde{\nu}_{em} = 21000 \text{ cm}^{-1}$ .

The fluorescence emission, fluorescence excitation and anisotropy spectra of adsorbed AO at bare silica surface in the presence of dichloromethane (non-modified silica + dichloromethane) are given in Fig. 47. There is one emission band at  $\tilde{\nu}_{F_{max}} = 18900 \text{ cm}^{-1}$  and the same fluorescence band is observed for AO in acidic ethanol. Therefore, this band is due to the protonated form of AO at the silica surface. Also, the excitation spectrum is similar to that obtained in acidic ethanol solution. This means, that neutral AO is adsorbed predominantly by Coulombic forces on the anionic silanol groups,  $[\text{SiO}^-]$  and formed the cationic AO [80]. The fluorescence anisotropy excitation measurements provided information about the rotational mobility of AO at the non-modified silica surface. The anisotropy has a

value of  $r \approx 0.12$  at  $21400 \text{ cm}^{-1}$ . This means that the protonated species of AO are immobilized at the silica surface.

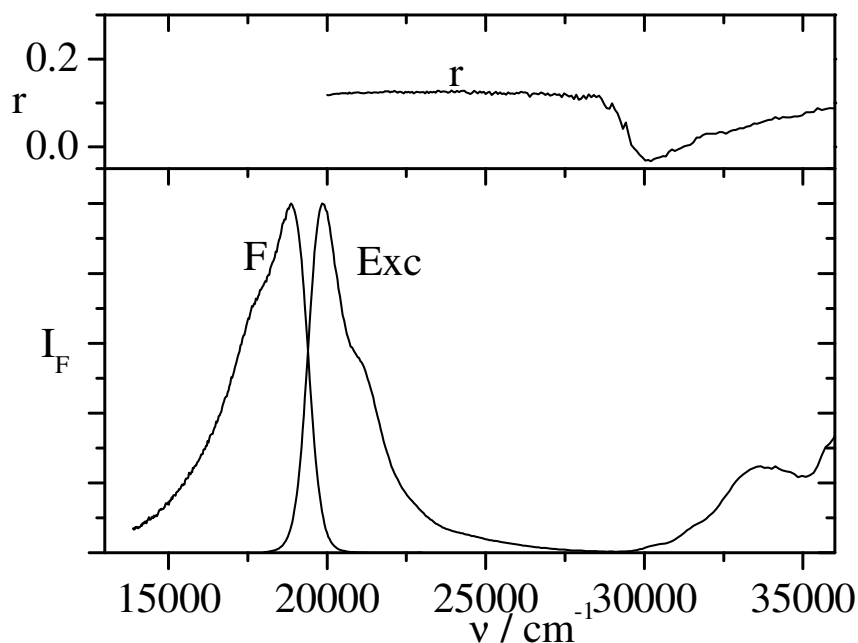


Fig. 47. Fluorescence (F), fluorescence excitation (Exc) and fluorescence anisotropy spectra of adsorbed AO (bare silica + dichloromethane),  $l = 1.30 \cdot 10^{-6} \text{ mole / g SiO}_2$ . The fluorescence spectrum is excited at  $\tilde{\nu}_{ex} = 23300 \text{ cm}^{-1}$  and the excitation and anisotropy spectra are observed at  $\tilde{\nu}_{em} = 17900 \text{ cm}^{-1}$ .

The decay time of the adsorbed AO at non-modified silica surface has amounts  $\tau_F = 2.7 \text{ ns}$  which is of the same order of the value of the lifetime of AO in acidic ethanol. This means that the protonated species of AO is formed at the silica surface, see Table 11. From this Table it is obvious, that the rotational correlation time  $\langle \tau_R \rangle$  is in the order of the fluorescence lifetime of the adsorbed AO at silica surface.

The measured value of fluorescence anisotropy in silica is reduced by multiple scattering effects [81]. The scattering depolarization spectrum of two different amounts of bare silica is presented in Fig. 48. The sample of silica and 1-DBA excited by a vertical polarized beam and the emission polarizer is oriented one time parallel ( $\parallel$ ) to the direction of the polarized excitation (vertical) and another time perpendicular ( $\perp$ ) to the polarized excitation (horizontal direction). Excitation and emission monochromators are scanning at the

same wavelength. The calculations are done by subtracting the values of  $I_{\parallel}$  and  $I_{\perp}$  for 1-DBA with silica from that of cyclohexane (back ground), correction of the  $I_{\perp}$  values by the  $G$ -factor and then introducing these data in Eq. 14. The fluorescence scattering anisotropy has a value of  $r \approx 0.9$ , independent of the amount of silica. This means, that the polarization values in this thesis are reduced by less than 10%.

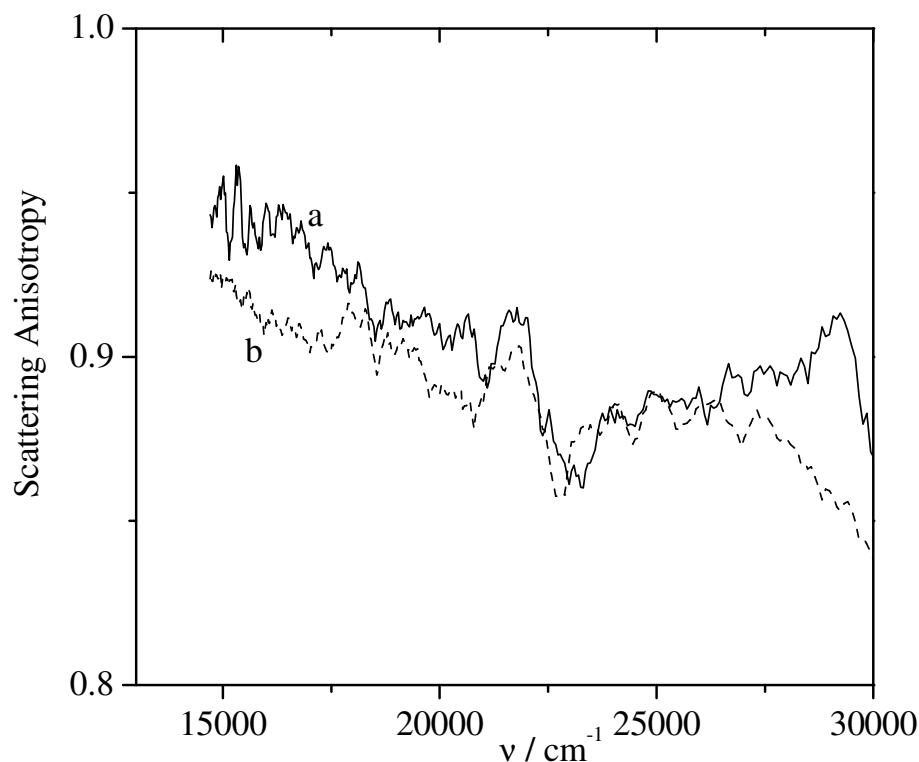


Fig. 48. Scattering anisotropy of a) 10 mg, b) 1 mg of non-modified silica in cyclohexane.

## 4.2.4. Modified silica as adsorbent

### 4.2.4.1. Silica modified with alkyl chains (silica C30)

1-DBA is adsorbed at a silica C30 surface from cyclohexane ( $c = 1.6 \cdot 10^{-6} M$ ) and formed both protonated and H-bonded species at the surface, see Fig. 49. The emission and excitation spectra are measured for the silica particles adherent to the cell walls. The emission spectrum is characterized by two different bands: The broad band (1) at  $\tilde{\nu}_{F, \max} = 22300 \text{ cm}^{-1}$  is due to the protonated form of 1-DBA at the silica surface. The emission band (2) at  $\tilde{\nu}_{F, \max} = 24880 \text{ cm}^{-1}$  is due to the H-bonded species of 1-DBA at the silica C30 surface. The

excitation spectrum of the protonated 1-DBA at the surface exhibits less vibronic structure than that of the H-bonded species of 1-DBA and it can be compared to the absorption spectrum of the protonated 1-DBA in ethanol at  $\text{pH} \approx 5.2$ . Thus most of the adsorbed 1-DBA at silica C30 surface is protonated in the ground state and some is adsorbed as H-bonded species which undergoes protonation in the excited state.

The fluorescence anisotropy excitation spectra of suspension of 1-DBA in cyclohexane with 6 mg silica C30 (silica C30 + cyclohexane) is depicted in Fig. 49. The anisotropy spectrum, which is observed at  $20800 \text{ cm}^{-1}$  is similar to that of protonated 1-DBA in glycerol and it has a maximum value of  $r \approx 0.32$  at  $\tilde{\nu} = 20800 \text{ cm}^{-1}$ . This means, that the protonated species of 1-DBA are immobilized on the silica surface. The anisotropy spectrum which is observed at  $\tilde{\nu} = 24880 \text{ cm}^{-1}$  is comparable to that of 1-DBA in paraffine liquid (neutral species) but with a much higher value. This means, that there is some of 1-DBA adsorbed at silica C30 surface as hydrogen bonded species. These results are confirmed by the fluorescence decay times, where the decay curve which is observed at  $20800 \text{ cm}^{-1}$  is fit three-exponentially. The lifetime of value  $\tau_F \approx 7.0 \text{ ns}$  is due to the protonated species of 1-DBA at the silica C30 surface in the ground state. The component of  $\tau_F \approx 0.2$  with negative amplitude is a rising component which means that some of the adsorbed 1-DBA is protonated in the excited state. The long lifetime of value  $\tau_F \approx 15.2 \text{ ns}$  may be due to the silica C30 itself. The value of  $\tau_F \approx 7.8 \text{ ns}$  is due to the H- bonded 1-DBA at the surface. The rotational correlation times of 1-DBA after adsorption at silica C30 surface are obtained by inserting mean fluorescence decay times and steady-state fluorescence anisotropies see Table 12 into Eq. 16.

Table 12. Fluorescence decay times  $\tau_F$ , steady-state fluorescence anisotropies ( $r$ ), mean Fluorescence decay times  $\langle\tau_F\rangle$ , rotational correlation times  $\langle\tau_R\rangle$  and the amplitudes B of 1-DBA (silica C30 + cyclohexane) under air, ( $\tilde{\nu}_{ex} = 27000 \text{ cm}^{-1}$ ).

Probe	$\tilde{\nu}_{em} / \text{cm}^{-1}$	$\tau_F / \text{ns}$	B	( $r$ )	$\langle\tau_F\rangle / \text{ns}$	$\langle\tau_R\rangle / \text{ns}$
1-DBA	24900	7.8	1.0	0.16		62.4
	20800	0.21	-0.20	0.32		112
		7.0	0.75			
		15.2	0.05			

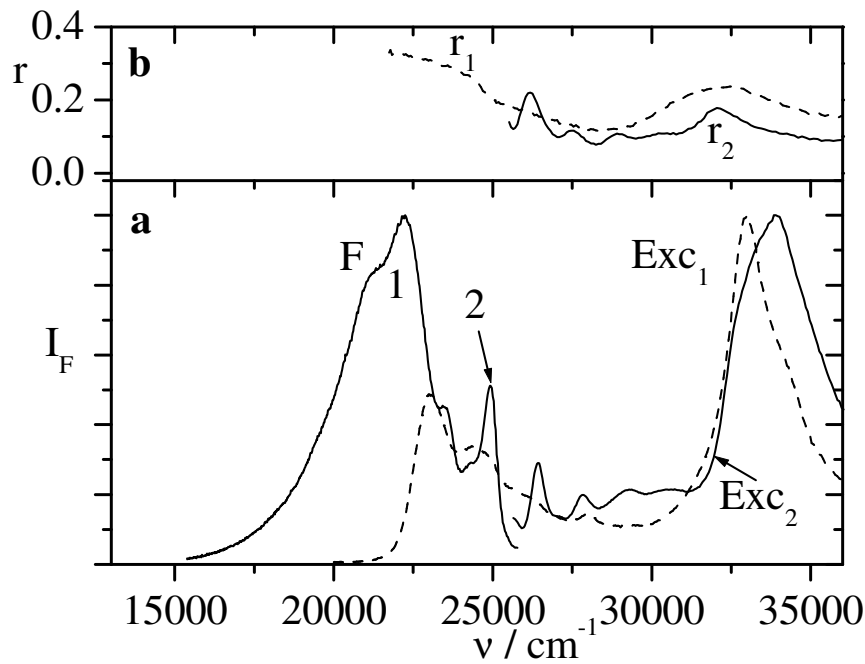


Fig. 49. a) Fluorescence (F) and fluorescence excitation (Exc) spectra of 1-DBA (silica C30 + cyclohexane),  $l=9.2 \cdot 10^{-7} \text{ mole/g SiO}_2$  for the particles on the cell walls. The fluorescence spectrum is excited at  $\tilde{\nu}_{ex} = 26500 \text{ cm}^{-1}$ . The excitation spectrum (Exc<sub>1</sub>) is observed at  $\tilde{\nu}_{em} = 18500 \text{ cm}^{-1}$  and the excitation spectrum (Exc<sub>2</sub>) is observed at  $\tilde{\nu}_{em} = 24900 \text{ cm}^{-1}$ . b) Anisotropy spectra of suspension of 1-DBA (silica C30 + cyclohexane),  $l=1.39 \cdot 10^{-6} \text{ mole/g SiO}_2$ . The anisotropy ( $r_1$ ) spectrum is observed at  $\tilde{\nu}_{em} = 20800 \text{ cm}^{-1}$  and ( $r_2$ ) the anisotropy spectrum is observed at  $\tilde{\nu}_{em} = 24900 \text{ cm}^{-1}$ .

Table 13 summarizes the position of the maximum emission peaks, the absorption transition energies and the maximum anisotropy of AC, 1-DBA, and AO respectively in different media. The 0-0 transition energies are given for the sharp bands, and for the broad bands their absolute maxima (M) are presented.

Table 13. Positions of the maximum emission  $\tilde{\nu}_{F, \max}$ , absorption transition energies (M = absolute maximum, 0-0 = zero-to-zero transition) and maximum anisotropy  $r$  of AC, 1-DBA and AO, respectively in different media.

Media	$\tilde{\nu}_{F, \max} / \text{cm}^{-1}$	${}^1L_a / \text{cm}^{-1}$	${}^1L_b / \text{cm}^{-1}$	$B_b / \text{cm}^{-1}$	$r$
Cyclohexane		26700 (M)	28000 (0-0)	40100 (0-0)	
Alkaline water	23200	26300 (M)	28300 (0-0)	40200 (0-0)	
Acidic water	20700	24800 (M)	28300 (0-0)	39100 (0-0)	
PVG	20900	24800 (M)	28100 (0-0)	38900 (0-0)	$\approx 0.18$
Non-modified silica	21000	25800 (M)	28000 (0-0)	39700 (0-0)	$\approx 0.2$

Media	$\tilde{\nu}_{F, \max} / \text{cm}^{-1}$	${}^1L_b / \text{cm}^{-1}$	${}^1L_a / \text{cm}^{-1}$	$B_b / \text{cm}^{-1}$	$r$
Cyclohexane	25400	25500 (0-0)	28300 (0-0)	34000 (M)	
Ethanol	25100	25300 (0-0)	28200 (0-0)	34200 (M)	
Acidic ethanol	22100	23500 (M)	28200 (0-0)	33400 (M)	
PVG	22300	23100 (M)		32900 (M)	0.25
PGG	22100	23000 (M)	27900 (0-0)	32900 (M)	0.29
Non-modified silica	22300	23100 (M)	27900 (0-0)	33600 (M)	0.31
Silica C30	22200	23000 (M)	27900 (0-0)	33000 (M)	0.32

Media	$\tilde{\nu}_{F, \max} / \text{cm}^{-1}$	${}^1L_b / \text{cm}^{-1}$	${}^1L_a / \text{cm}^{-1}$	$B_b / \text{cm}^{-1}$	$r$
Alkaline ethanol	18000	23000 (M)		32700 (M)	
Ethanol	18900	20400 (M)		32700 (M)	
Acidic ethanol	18900	20200 (M)		34300 (M)	
Non-modified silica	18900	19800 (M)		33700 (M)	3.1

#### 4.2.4.2. Silica modified with polymers

##### 4.2.4.2.1. TBB-coated silica

The fluorescence emission and fluorescence excitation spectra of a solution of 1-DBA in cyclohexane ( $c=1.26 \cdot 10^{-5} M$ ) after addition of 3 ml of 1-DBA solution to 6 mg of TBB-coated silica appear in Fig. 50. From this figure it becomes clear that there is no change in the emission or the excitation spectrum of 1-DBA, the emission and excitation spectra are similar to that observed for 1-DBA dissolved in neutral ethanol. The anisotropy has value of  $r \approx 0.003$  at  $\tilde{\nu} \approx 26880 \text{ cm}^{-1}$  which is approximately the same of that of neutral 1-DBA in cyclohexane and this means, that there is no adsorption of 1-DBA at the TBB-coated silica surface and the surface silanol groups are shielded by the TBB-coating.

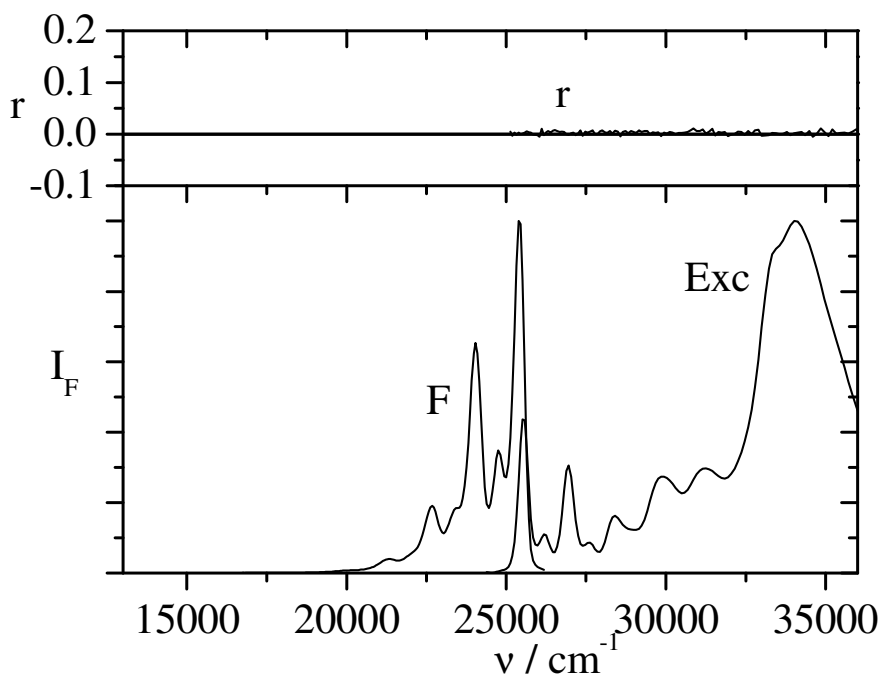


Fig. 50. Fluorescence (F), fluorescence excitation (Exc) and fluorescence anisotropy ( $r$ ) spectra of 1-DBA in cyclohexane ( $c=1.26 \cdot 10^{-5} M$ ) after addition of 6 mg of TBB-coated silica to 3 ml of 1-DBA solution. The fluorescence spectrum is excited at  $\tilde{\nu}_{ex} = 26900 \text{ cm}^{-1}$  and the excitation and anisotropy spectra are observed at  $\tilde{\nu}_{em} = 24100 \text{ cm}^{-1}$ .

Fig. 51 shows the emission, fluorescence excitation and fluorescence anisotropy spectra of AO with TBB-coated silica in the presence of dichloromethane. The emission and excitation spectra have the same peaks position as those of AO in acidic ethanol. The fluorescence excitation anisotropy of AO (DCM + TBB-coated silica) has maximum value of

$r \approx 0.018$  at  $21400 \text{ cm}^{-1}$ . This means, that there is a small amount of AO adsorbed on the TBB-coated silica surface and this is due to the high basicity of AO ( $\text{pK}_a = 10.5$ ).

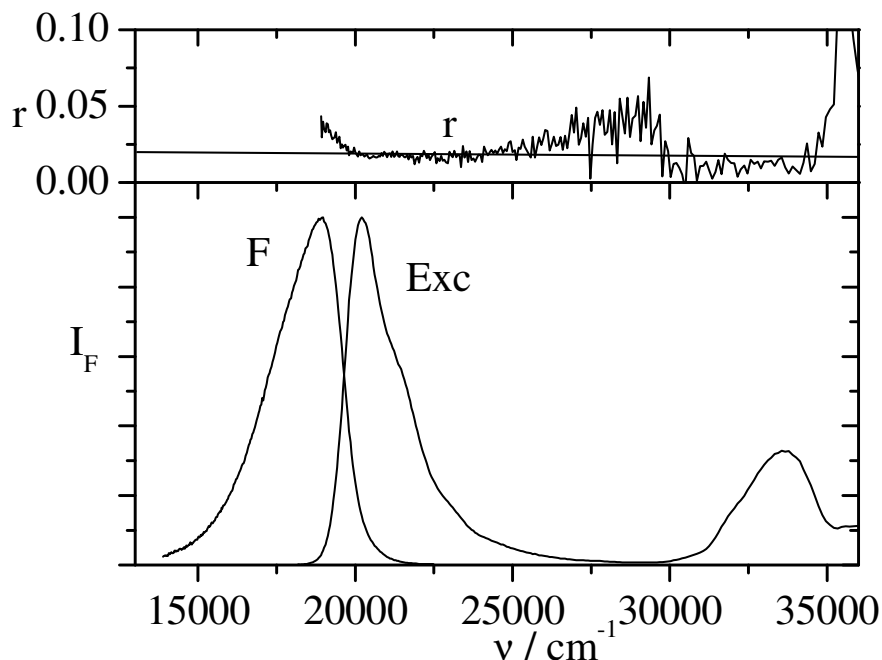


Fig. 51. Fluorescence (F), fluorescence excitation (Exc) and anisotropy ( $r$ ) spectra of solution of AO in dichloromethane ( $c = 1.7 \cdot 10^{-6} \text{ M}$ ) after addition of 3 ml to 6 mg of coated silica with TBB-coating. The fluorescence spectrum is excited at  $\tilde{\nu}_{ex} = 23300 \text{ cm}^{-1}$  and the excitation and anisotropy spectra are observed at  $\tilde{\nu}_{em} = 17900 \text{ cm}^{-1}$ .

#### 4.2.4.2.2. Polymerized divinylbenzene (DVB)-coated silica

Fig. 52 presents the emission, fluorescence excitation and fluorescence anisotropy spectra of the adsorbed AO at 6 mg of coated silica with 200 mg DVB. In the emission spectrum, there is a band at about  $18700 \text{ cm}^{-1}$ , which is still in the region of the protonated peak of AO, so this band is due to the protonated form of AO which is adsorbed at DVB-coated silica surface. This means, that some of the residual silanols are sufficiently acidic to protonate AO being adsorbed on these silanols. The fluorescence anisotropy spectrum of adsorbed AO on DVB-coated silica has a maximum value of  $r \approx 0.1$  at  $21400 \text{ cm}^{-1}$ . This means that there is some amount of AO adsorbed at DVB-coated silica. The fluorescence, fluorescence excitation and anisotropy spectra are measured at longer wavelength to avoid the fluorescence of the coating polymer DVB, since it fluoresces and emits at about  $\tilde{\nu}_F = 21600 \text{ cm}^{-1}$ .



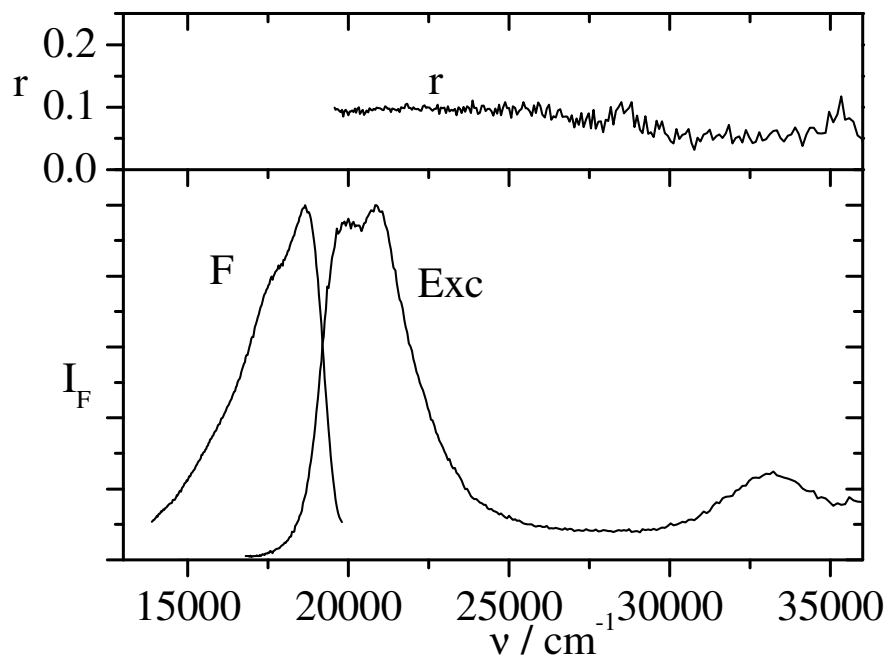


Fig. 52. Fluorescence (F), fluorescence excitation and anisotropy (Exc) spectra of AO (200 mg DVB-coated silica + dichloromethane),  $l = 1.30 \cdot 10^{-6} \text{ mole} / \text{g SiO}_2$ . The fluorescence spectrum is excited at  $\tilde{\nu}_{ex} = 20000 \text{ cm}^{-1}$  and the excitation and anisotropy spectra are observed at  $\tilde{\nu}_{em} = 14300 \text{ cm}^{-1}$ .

## Discussion

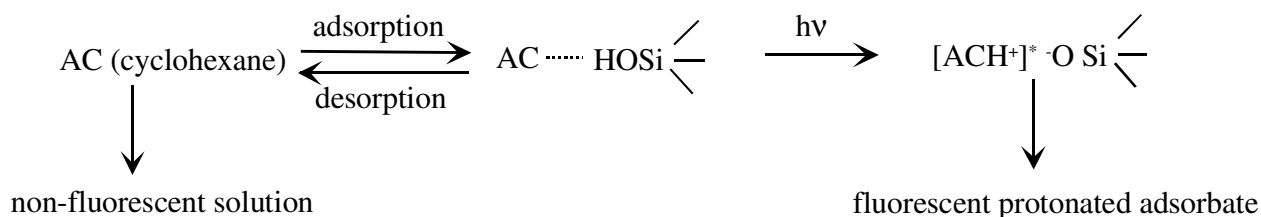
The adsorption of aza-aromatic compounds with different  $pK_a$  values (acridine, 1,2,7,8-dibenzacridine, 3,4,5,6-dibenzacridine and acridine orange) at controlled porous glasses, non-modified porous silica, modified silica with alkyl chains (silica C30) and modified silica with polymers is studied by fluorescence spectroscopy. In the case of acridine adsorbed at Porous Vycor glass surface, the excitation and emission spectra must be clearly assigned to the acridinium cation, i.e., the Vycor glass surface protonates acridine in the ground-state.

1-DBA is adsorbed at Vycor porous glass surfaces only in its protonated form as a result from the interaction between acidic surface silanol groups and free lone pair on the nitrogen ( $\text{Si-O}^- \text{HB}^+$ ). This is confirmed by the fluorescence spectra and fluorescence decays.

The steady state fluorescence and fluorescence decays reveal that 3-DBA is adsorbed at Vycor porous glass and forms the protonated species at the surface. The fluorescence anisotropy spectrum demonstrates that the protonated species of 3-DBA are immobilized at the Vycor glass surface.

Geltech porous glass is used as adsorbent for 1-DBA. The fluorescence spectra, fluorescence excitation anisotropy spectra and fluorescence decays establish that 1-DBA is adsorbed at the Geltech porous glass as protonated form ( $\tau_F \approx 6.5$  ns and  $r \approx 0.29$ ) and as H-bonded species ( $\tau_F \approx 7.6$  ns and  $r \approx 0.20$ ) which are immobilized at the surface. Upon excitation the H-bonded species are transformed to the protonated form. This is evident from the negative amplitude of the protonated form at the surface.

Non-modified silica is applied as adsorbent for acridine from solution in cyclohexane and the main surface product is H-bonded acridine (B.....H) which is protonated in the excited singlet state according to the following scheme [76-78, 96].



Scheme 2. Adsorption of AC at bare silica surface.

It has been reported that the  $pK_a$  of the singlet excited state of acridine is 10.7, much higher than for its ground state ( $pK_a = 5.5$ ). This facilitates the proton addition reaction of excited acridine [105]. This is in the contrast to our results for the PVG surface, since AC forms the protonated species at PVG surface in the ground state. The lifetime measurements differentiate between acridinium cation at the Vycor glass surface which is protonated in  $S_0$  and acridinium cation at non-modified silica surface which is protonated in  $S_1$ . This is because the adsorbent centres in Vycor glass are more acidic than those at the silica surface. This can be explained by the remainder  $B_2O_3$  during the preparation of PVG, which strongly enhances the acidity of the residual silanols and increase the silanol interactions with basic analytes.

Fluorescence anisotropy measurements reveal that the cationic acridine is immobilized at PVG and silica surface.

1-DBA is mainly assigned to protonated cations ( $Si-O^+ \dots (HB)$ ) and hydrogen-bonded complexes ( $Si-OH \dots B$ ) on bare silica surface. The ratio between the two species at silica surface depends on the water content. The hydrogen-bonded species undergo protonation upon excitation. The negative amplitude in the life time of the protonated species proves that some of adsorbed 1-DBA is protonated in the excited state. By increasing the loading of 1-DBA at the silica surface, a red-shift of the emission spectrum is observed. This suggests, that there is aggregation of adsorbed 1-DBA at the silica surface with increasing the concentration of 1-DBA [75]. The fluorescence excitation anisotropy spectra and the fluorescence life decays distinguished the two adsorbed species (protonated and hydrogen-bonded) of 1-DBA at the silica surface.

3-DBA is not adsorbed and not protonated at the silica bead surface, since the free electron pair on the nitrogen is sterically shielded by the benzo groups [74]. The bare silica used as the adsorbent for acridine orange from solution in dichloromethane. The cationic acridine orange was formed as a result of the interaction with anionic silanol groups on the silica surface. Fluorescence anisotropy measurements show that the cationic acridine orange is immobilized on the silica surface.

1-DBA is adsorbed at silica C30 from cyclohexane solution. There are two species formed at silica C30 surface; the main one is the protonated form of 1-DBA and the other is the hydrogen-bonded species. The decay time of the protonated species has a component with negative amplitude which means that there is some of the adsorbed 1-DBA is protonated in the excited state. The fluorescence excitation anisotropy distinguished the two adsorbed

species on silica C30 surface. Compared to bare silica, it is found that in case of silica C30 as adsorbent there is more protonation of the adsorbed 1-DBA in the ground state than on bare silica surface. This means that the surface silanols in silica C30 are more acidic than those on bare silica surface.

By comparing these results to those obtained for the non-modified silica surface, PGG and PVG, it is found, that at the bare silica, silica C30 and PGG surfaces, 1-DBA is adsorbed as protonated and H-bonded species with different ratios depending on the acidity of the surface silanol groups and the H-bonded species is protonated in the excited state. Where, in case of Vycor porous glass the protonated 1-DBA is the only adsorbed species which is observed and this due to change in the surface's acidic properties. The silanol groups on the glass surface act as acids with  $pK_{a(\text{SiOH})}$  values reported in the range from about 3 to 9.5 [106]. This means that the Vycor glass is more acidic than bare silica due to the fact that  $\text{B}_2\text{O}_3$  are not removed during the preparation process of PVG. Also, from the above results, it is found that the concentration of the acidic silanol groups at Vycor glass surface is larger more than that at the Geltech glass surface.

1-DBA is not adsorbed at TBB-coated silica and the fluorescence anisotropy spectrum demonstrates that, since it has value of  $r \approx 0$  which is exactly the value for 1-DBA in cyclohexane. This means that the TBB coating shields most of surface silanol groups from the fluorescence analysis.

Acridine organe is still adsorbed at 200 mg DVB-coated silica and formes the protonated molecule due to the interaction with residual silanol groups. This protonated form is immobilized on the surface. On the other hand, a very small amount of AO is adsorbed on TBB-coated silica less than 5%. This means that the TBB coating shields most of the acidic surface silanol groups from the fluorescence analysis, whereas the DVB- coating shields only some of the surface silanol groups.

### 4.3. Adsorption equilibria

A comparison of the surface acidity of different micro porous environments is investigated. Porous Vycor glass, porous Geltech glass, non-modified silica beads, silica C30, DVB- and TBB-coated silica are used as adsorbents. Probes of different  $pK_a$  values (AC, 1-DBA, 3-DBA and AO) are considered as adsorbates. The ratio of the adsorbed species at the surfaces to the nonadsorbed in solvent is taken as the reaction equilibrium according to Eq. 40. This equilibrium is measured by UV/vis absorption spectroscopy of the initial solution of probes in cyclohexane  $[B_o]$ . 3-6 mg of non-modified silica are suspended (a planar PVG sheet is immersed) into 2 ml of dry cyclohexane into a fluorescence cell and stirred for 2 min. Then 1 ml of the solutions in cyclohexane  $[B_o]$  is injected and the solution is stirred well. The concentration of nonadsorbed  $[B_o]_{\infty}$  is determined from the absorbance of the supernatant in cyclohexane after equilibration and centrifugation occurred. Thus, the concentration of adsorbed probes  $[BS]_{\infty}$  can be determined from  $[BS]_{\infty} = [B_o] - [B_o]_{\infty}$ . Then the equilibrium constant  $K$  of the adsorbed probes at surfaces is calculated from Eq. 40

#### 4.3.1. Controlled porous glass as adsorbent

##### 4.3.1.1. Porous Vycor glass (PVG)

AC, 1-DBA and 3-DBA are adsorbed at PVG surfaces with different loadings ( $l = 3 \cdot 10^{-7} - 6 \cdot 10^{-8} \text{ mole} / \text{g SiO}_2$ ) depending on the initial concentration of probes in cyclohexane. In the case of AC and 1-DBA, the reaction equilibrium could not be detected, since the absorption spectrum of the nonadsorbed AC and/or 1-DBA showed a value of  $[B_o]_{\infty} = 0$  after 5h of reaction time. In the case of 3-DBA as adsorbate the reaction equilibrium is detected, since there is still nonadsorbed 3-DBA in cyclohexane measured after 48 days of reaction time. This equilibrium is calculated according to Eq. 40,  $K = 470 \pm 40$ .

##### 4.3.1.2. Porous Geltech glass (PGG)

1-DBA is adsorbed at PGG surfaces from a solution in cyclohexane with loading in range of  $l = 10^{-6} \text{ mole} / \text{g SiO}_2$ . The equilibrium between the adsorbed and desorbed of 1-DBA is detected according to Eq.40,  $K = 560 \pm 40$ , since only about 65% of 1-DBA is adsorbed after 4h of the reaction time.

### 4.3.2. Non-modified silica beads as adsorbent

Acridine is adsorbed at non-modified silica surfaces from cyclohexane solution and the surface coverage of acridine had a value in range of  $\Gamma = 1 \cdot 10^{-6} - 4 \cdot 10^{-6} \text{ mole} / \text{g SiO}_2$ . Fig. 53 presents the absorption spectrum of a solution of acridine in cyclohexane ( $c = 1.14 \cdot 10^{-5} \text{ M}$ ) before and after addition of 6 mg bare silica beads.

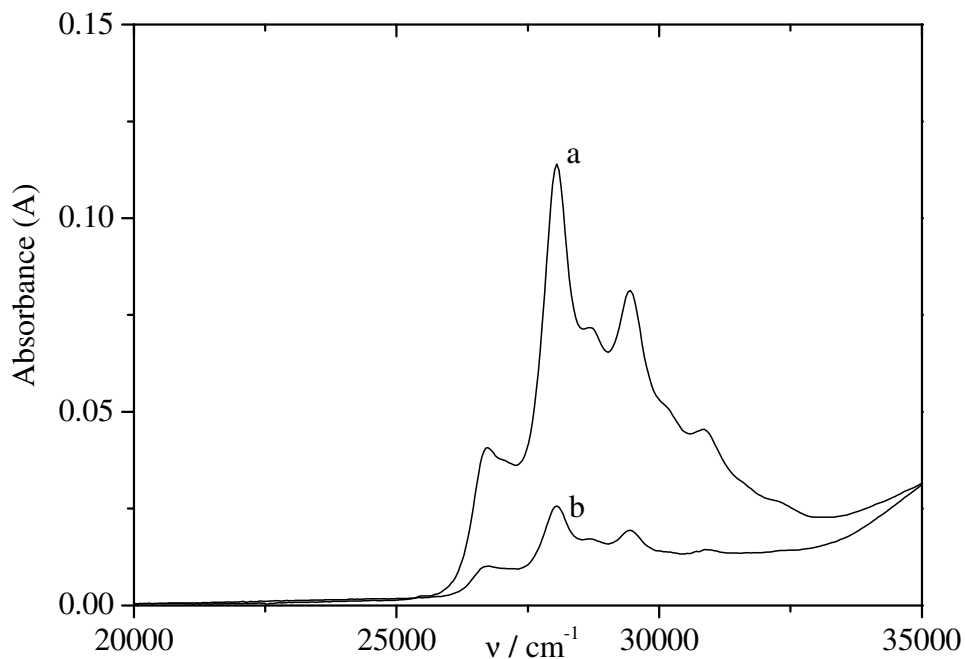


Fig. 53. Absorption spectra of AC in cyclohexane. ( $[B_o] = 1.14 \cdot 10^{-5} \text{ M}$ ) (a) before; and (b) after addition of 6 mg non-modified silica to 3 ml of AC solution.

The reaction equilibrium of adsorption of AC at non-modified silica surfaces could be determined as mentioned above and the values of the equilibrium constant are listed in Table 14. It is found that the equilibrium values are depend on the water coverage of the surface since a higher value of  $K$  is obtained when, cyclohexane is dried with heated zeolites and kept under nitrogen atmosphere.

Table 14. The ratio of adsorbed to nonadsorbed AC  $\left( \frac{[B]_o - [B]_\infty}{[B]_\infty} \cdot \frac{V_m}{V_r} \right)$  is calculated from Eq. 40 and taken as an equilibrium constant of adsorption of AC and at non-modified silica surfaces  $K$ , the initial concentrations of AC in cyclohexane  $[B_o]$  (dry = dry cyclohexane with preheated zeolites and not dry = without drying of cyclohexane), mass of silica  $m$  (not preheated), concentration of nonadsorbed AC  $[B]_\infty$ , concentration of adsorbed AC at non-modified silica surface  $[BS]_\infty$ .

Probe	$[B_o] \cdot 10^{-6}$ <i>mol/l</i>	$m_{SiO_2} / mg$	$[B]_\infty \cdot 10^{-6}$ <i>mol/l</i>	$[BS]_\infty \cdot 10^{-6}$ <i>mol/l</i>	$\frac{[B]_o - [B]_\infty}{[B]_\infty} \cdot \frac{V_m}{V_r} =$ $K$
AC	3.4 (not dry)	6.0	1.2	2.2	$1000 \pm 90$
	3.4 (dry)	6.0	0.33	3.05	$4600 \pm 800$
	3.4 (not dry)	3.0	2.3	1.1	$470 \pm 40$
	3.4 (dry)	3.0	0.70	2.7	$3800 \pm 300$

1-DBA is adsorbed at non-modified silica and silica C30 surfaces from a solution of cyclohexane. The surface coverage of 1-DBA is in range of  $l = 3 \cdot 10^{-7} - 4 \cdot 10^{-6} \text{ mole} / g \text{ SiO}_2$  depending on the initial concentration of 1-DBA in cyclohexane and on the amount of silica. The maximum loading of 1-DBA at 6 mg non-modified silica surface is of order of  $l = 8.5 \cdot 10^{-5} \text{ mole} / g \text{ SiO}_2$ . The absorption spectrum of 1-DBA in cyclohexane ( $[B_o] = 9.0 \cdot 10^{-6} \text{ M}$ ) before and after addition 6 mg bare silica to 3 ml of 1-DBA solution is shown in Fig. 54. While 3-DBA is not adsorbed any more at the non-modified silica surface, see Fig. 55.

AO is adsorbed at 6 mg of non-modified silica surfaces from a solution of dichloromethane by ratio  $\approx 95 \%$  and the surface coverage of AO has a value of,  $l = 1.2 \cdot 10^{-6} \text{ mole} / g \text{ SiO}_2$ .

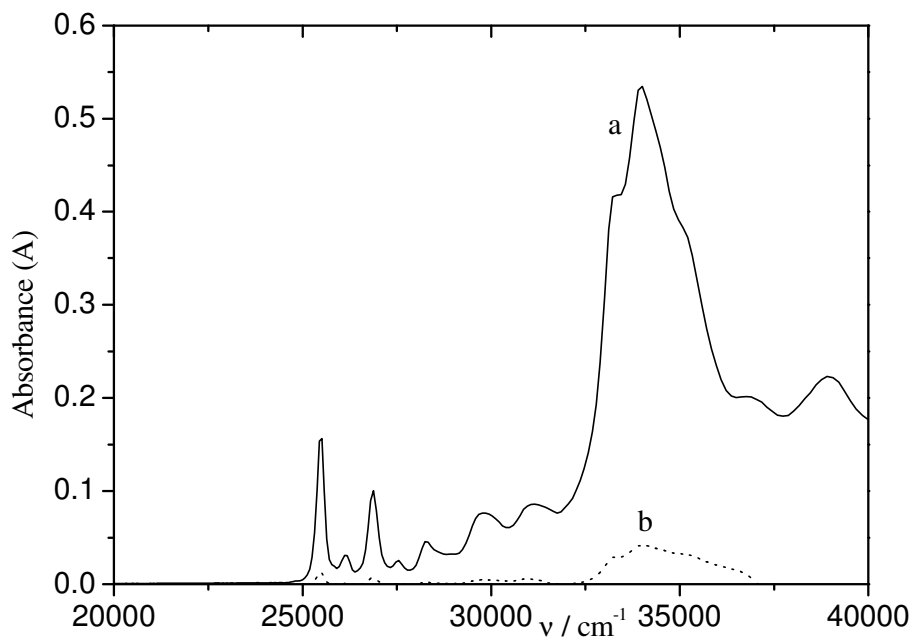


Fig. 54. Absorption spectra of 1-DBA in cyclohexane ( $[B_o] = 9.0 \cdot 10^{-6} M$ ). (a) Before; and (b) after addition of 6 mg non-modified silica to 3 ml of 1-DBA solution.

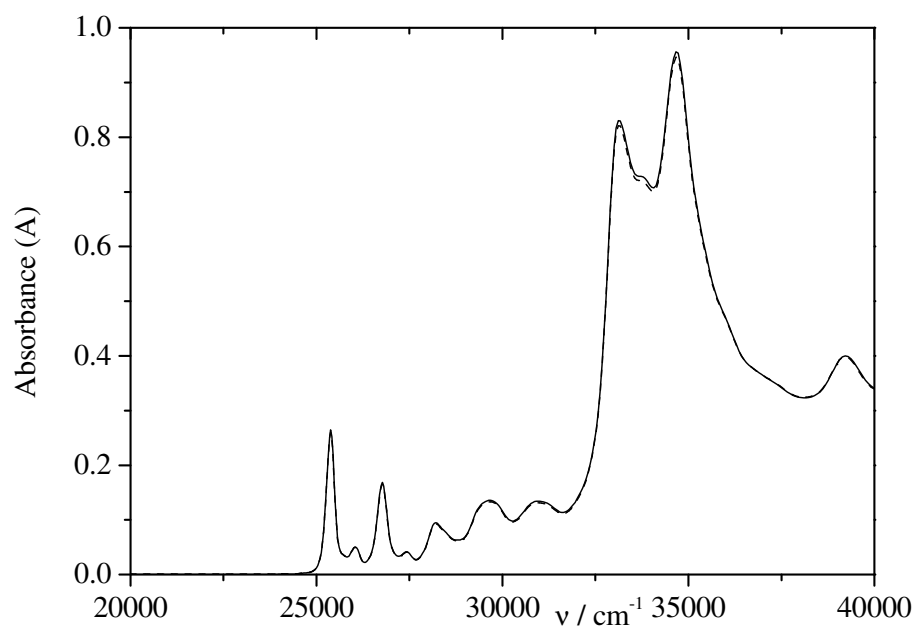


Fig. 55. Absorption spectra of 3-DBA in cyclohexane ( $[B_o] = 1.43 \cdot 10^{-5} M$ ) — before; and - - - - after addition of 6 mg non-modified silica to 3 ml of 3-DBA solution.



The reaction equilibrium of adsorption of 1-DBA at non-modified silica surfaces is determined and the values of the ratio of adsorbed to nonadsorbed 1-DBA are listed in Table 15. It is found that this ratio depends on the water content at silica surfaces, since the silica is not preheated. The value of this ratio increases strongly when, the silica sample is preheated at 120°C over night under vacuum and by using dry cyclohexane as a solvent. In this case the ratio of adsorbed to nonadsorbed 1-DBA at 6 mg non-modified silica surface has a value of  $\approx 11400 \pm 2500$  and this is due to the removal of the water from the silica surface then more concentration of the active silanol groups are available.

Table 15. The ratio of adsorbed to nonadsorbed 1-DBA  $\left( \frac{[B]_0 - [B]_\infty}{[B]_\infty} \cdot \frac{V_m}{V_r} \right)$  is calculated from Eq.

40 and taken as an equilibrium constant of adsorption of 1-DBA and at non-modified silica surfaces  $K$ , The initial concentrations of 1-DBA in cyclohexane  $[B]_0$  (dry = dry cyclohexane with preheated zeolites and not dry = without drying of cyclohexane), mass of silica  $m$  (preheated at 120°C and not preheated), concentration of nonadsorbed 1-DBA  $[B]_\infty$ , concentration of adsorbed 1-DBA at silica surface  $[BS]_\infty$ .

Probe	$[B]_0 \cdot 10^{-6}$ mol/l	$m_{SiO_2} / mg$	$[B]_\infty \cdot 10^{-6}$ mol/l	$[BS]_\infty \cdot 10^{-6}$ mol/l	$\frac{[B]_0 - [B]_\infty}{[B]_\infty} \cdot \frac{V_m}{V_r} =$ $K$
1-DBA	4.4 (not dry)	6.0 (not preheated)	0.90	3.50	$2000 \pm 100$
	4.6 (dry)	6.0 (not preheated)	0.37	4.20	$5700 \pm 1000$
	4.7 (dry)	6.0 (preheated)	0.20	4.50	$11400 \pm 2500$
	4.4 (not dry)	3.0 (not preheated)	2.20	2.20	$1100 \pm 50$
	4.6 (dry)	3.0 (not preheated)	1.20	3.40	$2900 \pm 260$

### 4.3.3. Modified silica beads as adsorbent

#### 4.3.3.1. Modified with polymer

##### 4.3.3.1.1. TBB-coated silica

Figs. 56 and 57 show the absorption spectra of AC in cyclohexane ( $[B_o]=7.4 \cdot 10^{-6} M$ ) and 1-DBA ( $[B_o]=1.26 \cdot 10^{-5} M$ ) before and after addition of 6 mg TBB-coated silica to 3 ml of these solutions. From these two figures, it is obvious that there is no adsorption of AC and/or 1-DBA at TBB-coated silica surfaces and this means that the TBB-coating (Fig. 17 in the experimental part) shields most of surface silanol groups from the reaction with AC and/or 1-DBA. Absorbance spectra of AO in dichloromethane ( $[B_o]=9.0 \cdot 10^{-7} M$ ) before and after addition of 6 mg of TBB-coated silica to 3 ml of this solution is shown in Fig. 58. It is noticed that, there is a very small amount of AO (less than 5 %) is adsorbed at TBB-coated silica and the surface coverage of AO is amounts to ( $l=0.04 \cdot 10^{-6} \text{ mole} / \text{g SiO}_2$ ).

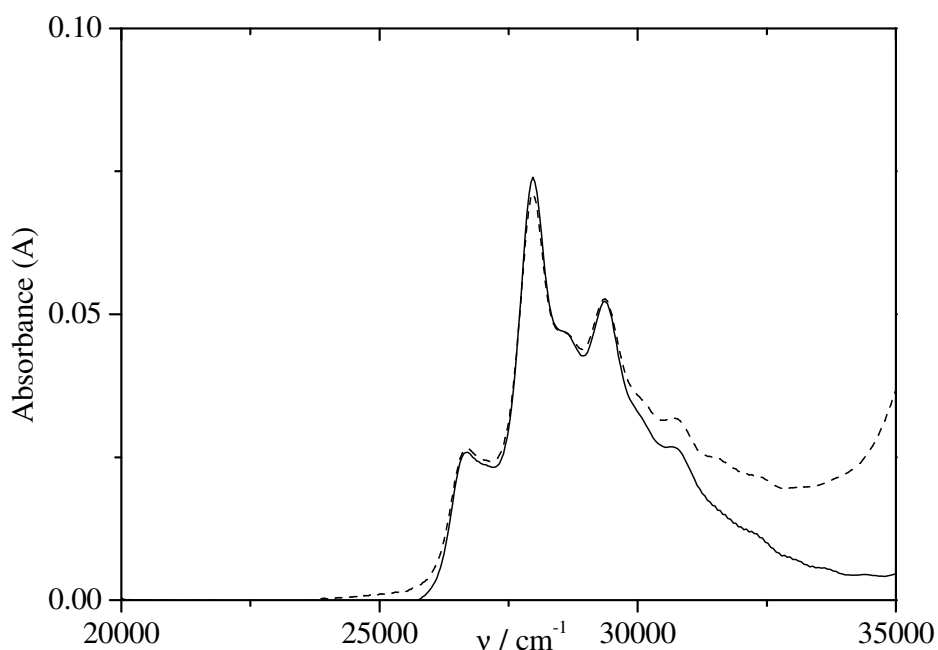


Fig. 56. Absorption spectra of AC in cyclohexane ( $[B_o]=7.4 \cdot 10^{-6} M$ ): — before; and - - - after addition of 6 mg of TBB-coated silica to 3 ml of AC solution.

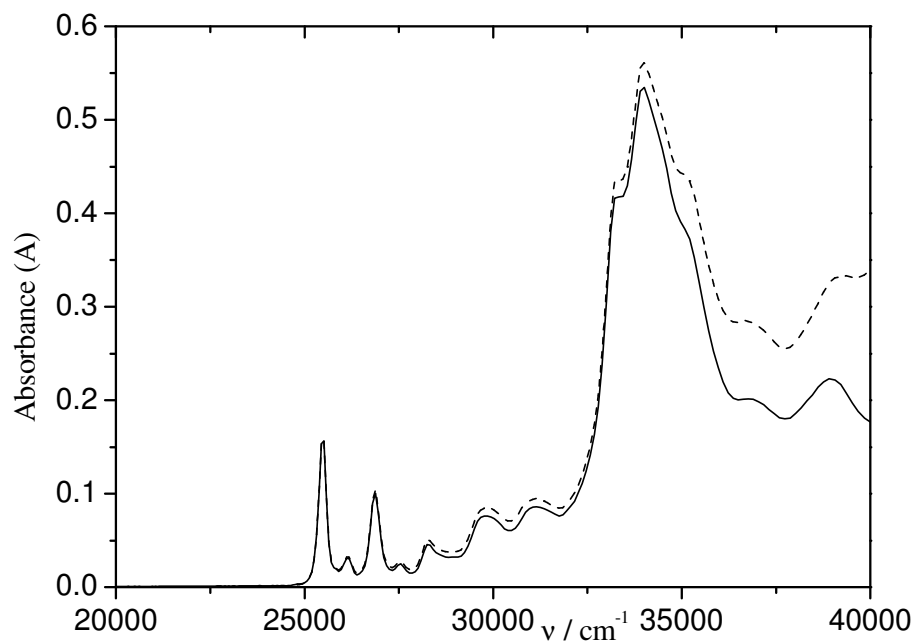


Fig. 57. Absorption spectra of 1-DBA in cyclohexane ( $[B_o]=1.26 \cdot 10^{-5} M$ ): — before, and - - - after addition of 6 mg of TBB-coated silica to 3 ml of 1-DBA solution.

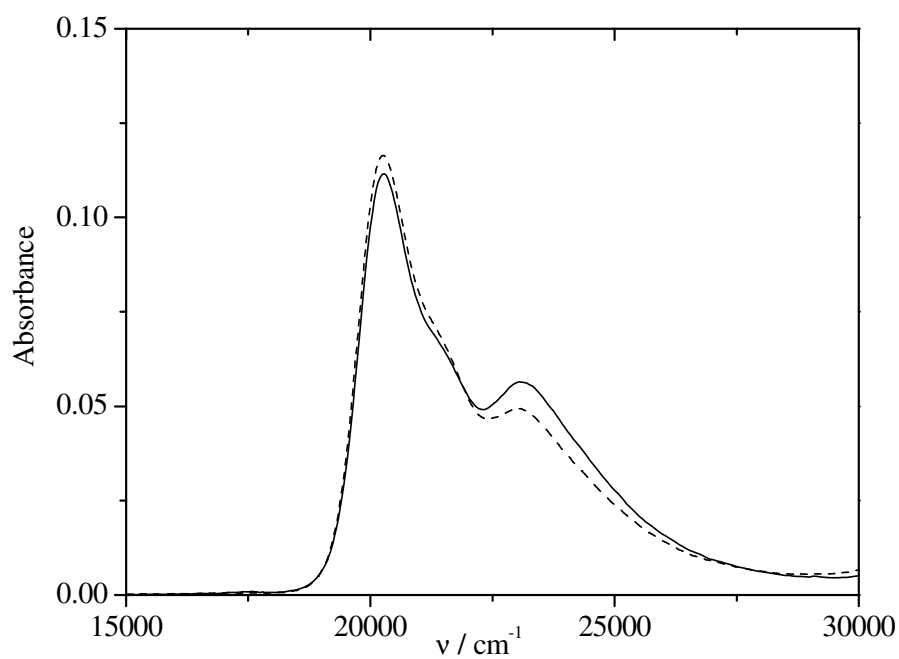


Fig. 58. Absorption spectra of solution of AO in dichloromethane ( $[B_o]=9.0 \cdot 10^{-7} M$ ): — before, and - - - after addition of 6 mg of TBB-coated silica to 3 ml of AO solution.

#### 4.3.3.1.2. Polymerized divinylbenzene (DVB)-coated silica as adsorbent

The absorption spectrum of AO in dichloromethane ( $[B_o] = 2.48 \cdot 10^{-6} M$ ) before and after addition of 6 mg of DVB-coated silica to 3 ml of AO solution is shown in Fig. 59. According to this figure, AO is adsorbed at the 200 mg DVB-coated silica surface with a ratio of about 70%, and this ratio decreased to 30% by increasing the thickness of the coating polymer to 500 mg. This means, that the coated silica with 500 mg DVB is more effective in shielding silanol groups and should be a better HPLC stationary phase than 200 mg DVB coated silica.

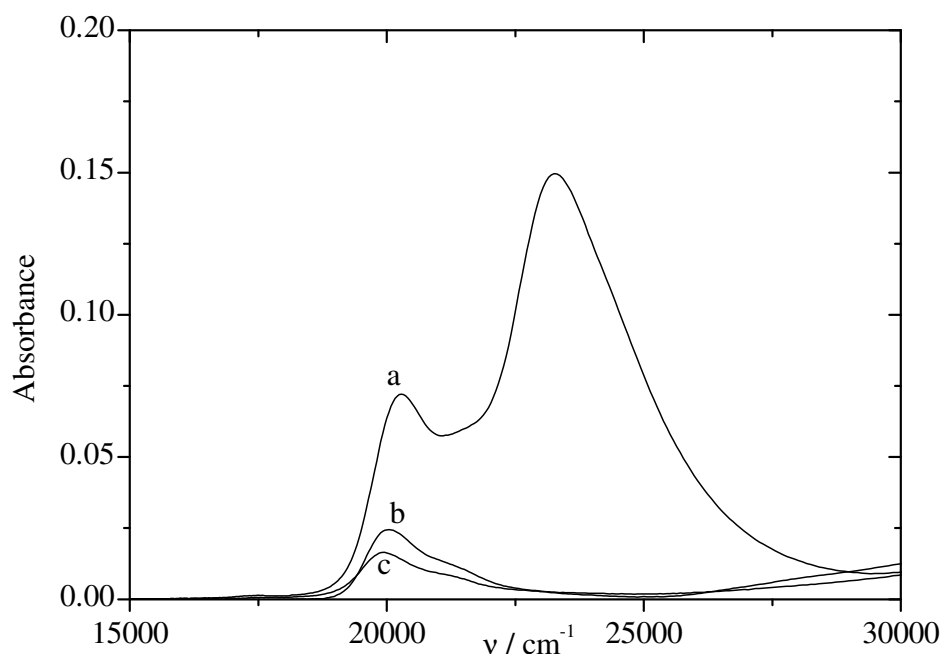


Fig. 59 Absorption spectra of AO in dichloromethane ( $[B_o] = 2.48 \cdot 10^{-6} M$ ): a) in solution, b) with 6 mg of 200 mg and c) with 6 mg of 500 mg of DVB-coated silica.

#### 4.3.4. HPLC measurements

Fig. 60 shows the chromatogram of separation of 3-DBA (I) and 1-DBA (II) by using TBB-coated silica as a stationary phase. From the chromatogram it is clear that (I) has a shorter retention time than (II). This is due to the smaller extent of adsorption of (I) than (II) on the stationary phase. Table 16 shows the dependence of the retention time  $\tau$  of 3-DBA (I) and 1-DBA (II) on the composition of the mobile phase

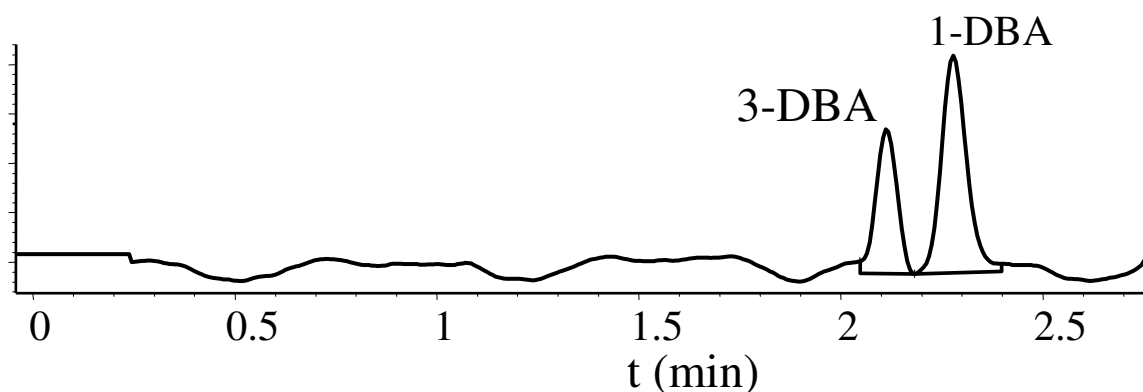


Fig. 60. Chromatogram of a mixture of 1-DBA and 3-DBA in cyclohexane using the stationary phase TBB-coated silica. The mobile phase composition of cyclohexane / isopropanol = 98.5/1.5 (V/V); flow rate 2 ml/min.

Table 16. Composition of the mobile phase, retention time of 3-DBA ( $\tau_I$ ) and retention time of 1-DBA ( $\tau_{II}$ ).

ratio of isopropanol % (V/V)	( $\tau_I$ )	( $\tau_{II}$ )
0	2.19	5.78
0.2	2.01	3.17
0.5	1.89	2.67
1.5	1.81	2.33
2.5	1.79	2.20

It can be seen from table 16 that the retention time of both DBA isomers is shifted to longer retention time by reducing the amount of isopropanol in the mobile phase. By introducing these retention times in Eq. 49, where  $t_m = 1.3$  min, the retention factors for both DBA isomers with different ratios of isopropanol in the mobile phase are obtained, see Fig. 61. The retention factor  $k'$  of 3-DBA (I) is always smaller than the retention factor  $k'$  of 1-DBA (II). The retention factors of both DBA isomers decrease with increasing ratio of isopropanol in the mobile phase. The selectivity factor  $\alpha$  is obtained by introducing the retention factors of (I) and (II) into Eq. 51. The selectivity factor decreases with increasing isopropanol ratio in the mobile phase as shown in Fig. 62.

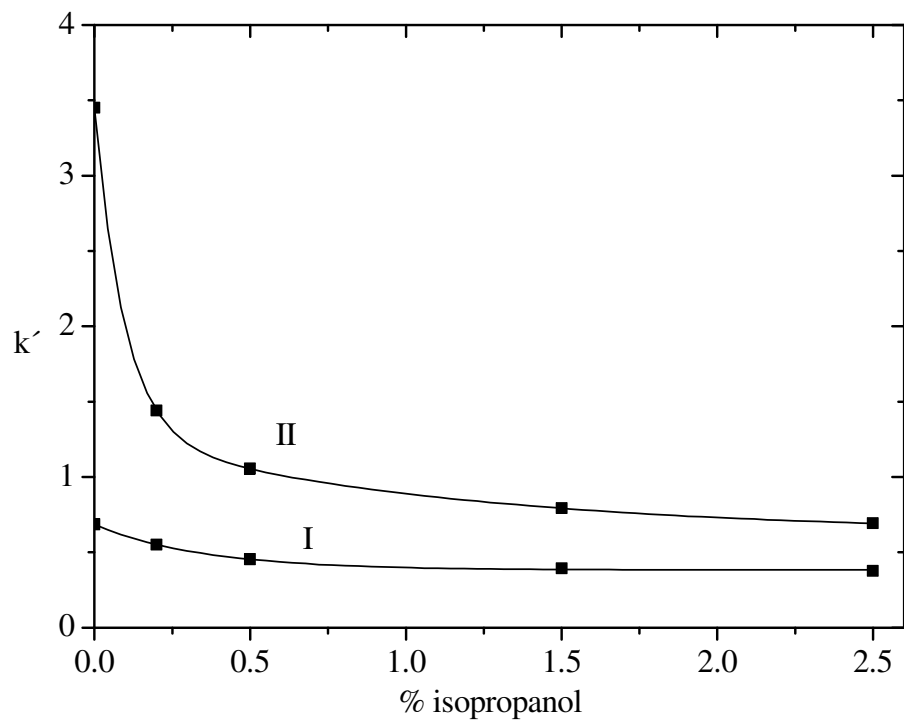


Fig. 61. Relationship between the retention factors of 3-DBA (I), 1-DBA (II) and the ratios of isopropanol / cyclohexane (V/V) in the mobile phase.

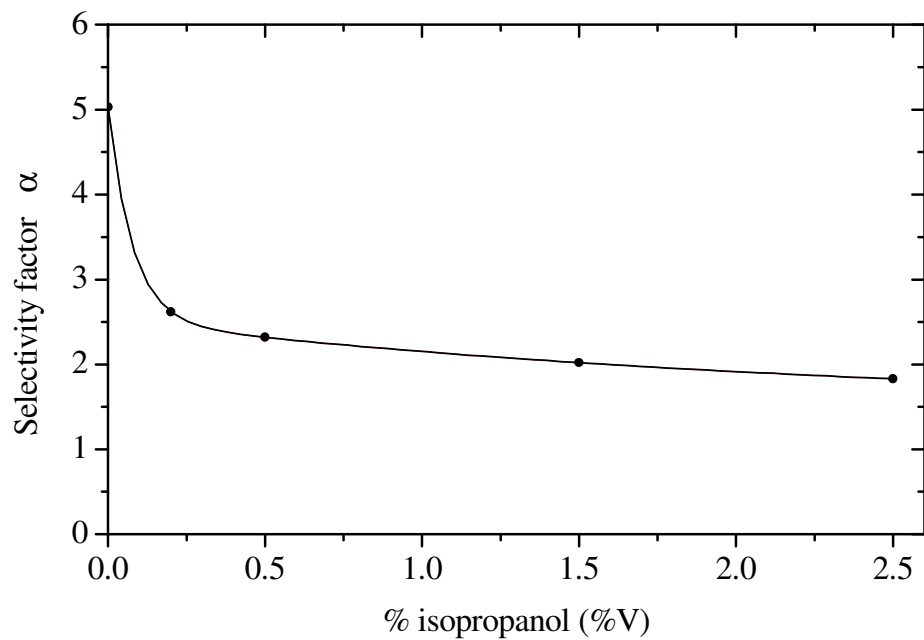


Fig. 62. Relationship between of the selectivity factor  $\alpha$  and the ratio of isopropanol / cyclohexane (V/V) in the mobile phase.

## Discussion

A series of different types of porous surfaces mainly porous Vycor glass, porous Geltech glass and silica beads (non-modified and modified) are investigated with respect to their surface acidity. This is carried out via determination of the adsorption equilibria of probes of different  $pK_a$ .

When PVG is used as adsorbent the reaction equilibrium can not be observed in case of AC and/or 1-DBA as adsorbates. On the other hand, the 3-DBA shows a clear equilibrium after 48 days, since the absorption spectrum of nonadsorbed 3-DBA is measured after 48 days. This is due to the low basicity of 3-DBA compared to that of AC and/or 1-DBA.

In case of non-modified silica beads used as adsorbent and AC and/or 1-DBA as adsorbates, there exists an equilibrium which is calculated according to Eq. 40. This reaction equilibrium depends on the water coverage of the non-modified silica surface (and thus on the humidity of air). The silica is not preheated because the aim of this study is to work with the same conditions like in the chromatographic measurements and to compare the results obtained by both techniques.

The results which were obtained in case of bare silica as adsorbent are in contrast to the results which are obtained from PVG as adsorbate, since the equilibrium could not be detected. This return to the higher amount of  $SiO_2$  in PVG sheet compared to bare silica (e.g. for PVG sheet the amount of  $SiO_2 \approx 100$  mg and for silica 6 mg).

The various types of silica (non-modified, silica C30, TBB-coated and DVB-coated silica) are different with respect to the concentration of surface silanol groups, thus the different return to the humidity do not seriously affect on the results of these different types. There is a clear decrease of accessible surface silanol groups in the series: non-modified silica  $\geq$  silica C30  $>$  DVB-coated silica  $>$  TBB-coated silica. For TBB-coated silica, AO is found to be the only probe which is adsorbed strongly enough to show a small effect in the fluorescence experiments.

The results demonstrate that AO still is adsorbed on coated silica with 200 mg DVB but less than on bare silica. The amount of adsorbed AO decreased when the thickness of the

coated polymer is increased to 500 mg DVB. This means, that the DVB-coated polymer shields some of the silanol groups and its ability for shielding is increased by increasing the thickness of the polymer

For the couple 1-DBA / 3-DBA, the effect of interaction of basic analytes on the selectivity of the separation was studied by using HPLC. It is used to separate 3-DBA (I) and 1-DBA (II) by applying TBB-coated silica as stationary phase. Both DBA isomers are interacted with the surface silanol groups at low isopropanol concentration in the mobile phase. This interaction of (I) and (II) is reduced with increasing isopropanol content in the mobile phase because silanol groups are blocked by isopropanol. The selectivity (separation) factor  $\alpha$  is reduced with increasing isopropanol content. The difference in the retention times of DBAs is due to the difference in the interactions of the basic analytes with the acidic surface silanol groups. As shown before (in part 1), the interaction of 3-DBA with acids is reduced due to the steric shielding of the nitrogen atom. As the interaction with silanol groups decreases with increasing isopropanol content, the separation factor decreases and approaches unity for large isopropanol contents. From Eq. 48 we can calculate the concentration of the protonated species, and by replacing from Eq. 47 then Eq. 48 one obtains.

$$k' = \frac{[c_r] \cdot V_r}{[c_m] \cdot V_m} = \frac{n_r}{n_m} \quad (1)$$

For 1-DBA and 0 % isopropanol in the mobile phase:  $k' = 3.5 \rightarrow \frac{n_r}{n_m} = 3.5 \rightarrow n_r = 3.5 n_m$ .

I.e., there is about three times more of 1-DBA inside the stationary phase than in the mobile phase. Thus, for 0% isopropanol the fluorescence spectra of 1-DBA at the surface should be clearly dominated by the protonated form. The fluorescence spectroscopy measurements of 3 ml of 1-DBA added to 6 mg of TBB-coated silica reveal that 1-DBA is not adsorbed at TBB-coated silica. The difference between the two results of fluorescence spectroscopy and HPLC

are returned to the ratio volume of  $\frac{V_m}{V_r}$  for the suspensions. This is much smaller in the

fluorescence experiments (by orders of magnitude  $\approx 270$ ) than in the HPLC measurements. In order to solve this problem, 20 $\mu$ l of 1-DBA solution into melting point tube packed with TBB-coated silica was injected and the fluorescence spectra of this system was measured. But this method was not successful because the TBB-coated silica is fluorescent at the same wavelength as 1-DBA.



## 4.4. Adsorption kinetics

### 4.4.1. Adsorption at porous Vycor glass (PVG)

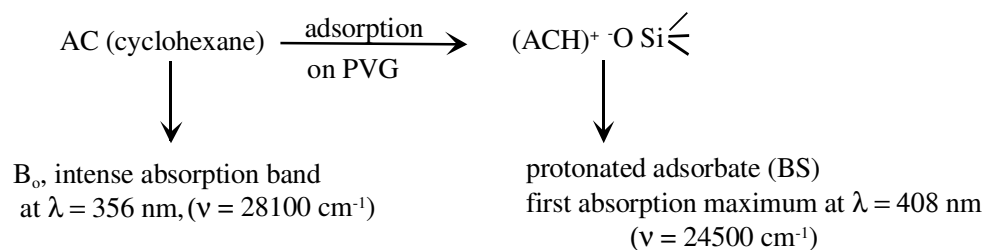
The kinetics of adsorption of AC, 1-DBA and 3-DBA at PVG are measured as described in the experimental part (section 3.3.2.3.). The experimental optical absorption  $A$  can be separated into three contributions: 1) base in solution, 2) base in the free volume of PVG and 3) adsorbate at the surface of PVG. Thus the absorbances are

$$A = \varepsilon_B \cdot c_B (l - d) + \varepsilon_B \alpha \cdot l \cdot c_B + \varepsilon_{BS} \cdot l \cdot c_{BS}$$

where  $l$  is the light path length = 1 cm,  $d$  is the sheet thickness = 0.1 cm,  $\alpha$  is the free volume ratio of PVG,  $c_B$  is the initial concentration of the base in solution and  $c_{BS}$  is the concentration of the adsorbate at the PVG surface.

#### 4.4.1.1. Adsorption of AC at PVG

The adsorption of AC in a sheet of PVG is illustrated by the following reaction scheme:



Scheme 3. The adsorption of AC in a sheet of PVG.

The change of the absorbance of the whole system (adsorbed AC at PVG surface, AC in solution) with time is shown in Fig. 63. The experiment was repeated for 3 times and always led in good approximation to the same results.

The absorbance values of the adsorbed AC at PVG at  $24500 \text{ cm}^{-1}$  (peak of protonated AC) and at  $28100 \text{ cm}^{-1}$  (mixture of both protonated and neutral AC) increases with time. This increase in absorbance is due to the progress of adsorption of AC and formation the protonated species [BS] at the PVG surface and it becomes slower after 60 min since there is no neutral AC species in the outer solution. This slow increasing may be due to diffusion of protonated AC

from the top and bottom of the glass sheet into the middle. The kinetics of adsorption is evaluated at  $\tilde{\nu} = 24500 \text{ cm}^{-1}$ , where only the protonated species  $\text{ACH}^+$  at PVG has absorption band.

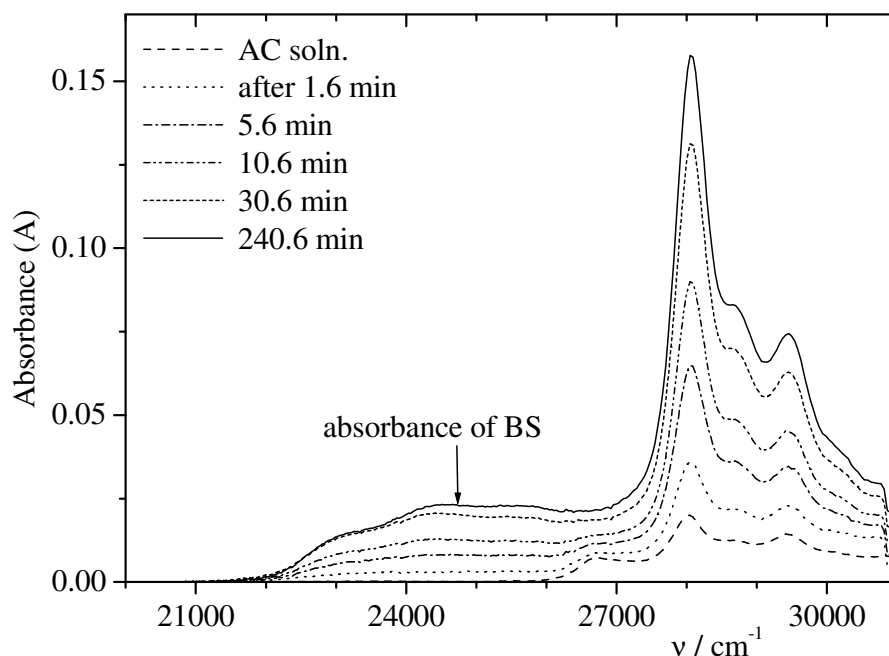


Fig. 63. Absorption spectra of AC (PVG + cyclohexane) as a function of time. Initial concentration of AC in cyclohexane,  $[B_o] = 2.2 \cdot 10^{-6} \text{ mole/l}$ .

The kinetics of adsorption is calculated by plotting  $\frac{(A_\infty - A_t)}{A_\infty}$  (see Eq. 35 in the theory part) of  $\text{ACH}^+$  at  $24500 \text{ cm}^{-1}$  in a semi-logarithmic graph vs. time. Here,  $A_t$  is the absorbance of  $\text{ACH}^+$  at time  $t$  after acridine injection and  $A_\infty$  is the equilibrium value at time  $t \rightarrow \infty$ , Fig. 64. In this figure the first 10 min. of the reaction can be evaluated by a first-order kinetics with a slope of  $k_{tot} = 1.28 \cdot 10^{-3} \text{ s}^{-1}$ . The rate constant  $k_{tot}$  is a mixture of diffusion and rate constant of the reaction.

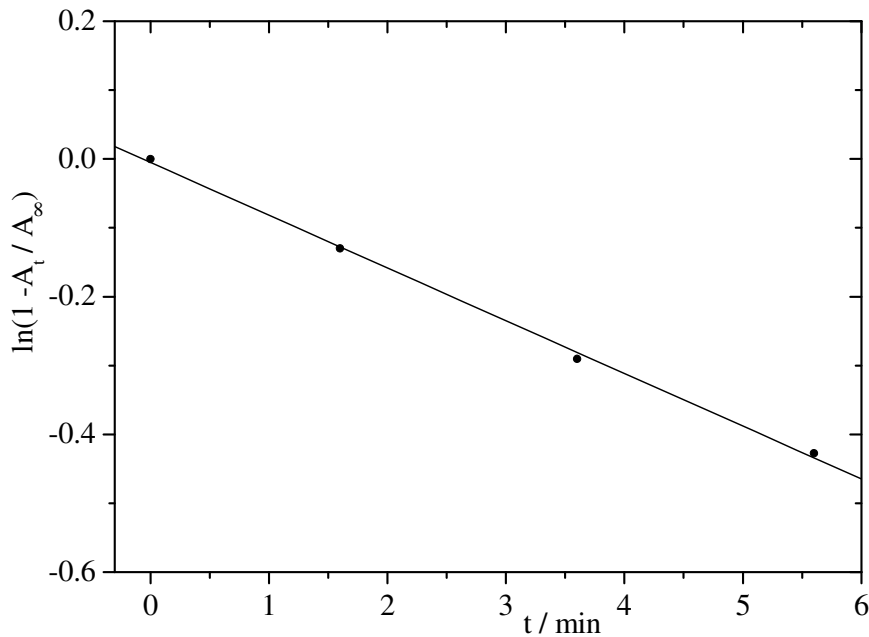


Fig. 64. semi-logarithmic plot at short time-scale of the adsorbed AC at PVG observed at  $\lambda = 408 \text{ nm}$ ,  $[B_o] = 2.2 \cdot 10^{-6} \text{ mole/l}$ .

Since the glass sheet is porous, AC will diffuse into the PVG sheet and react with the acidic centers  $S$  to form the protonated form  $ACH^+$ . A simulation programme of the diffusion and adsorption kinetics (see part 2.6. in the theory part) is used to get an idea about the value of  $D_{eff}$  and to determine the second-order rate constant of reaction,  $k_{ads}$  which is called in this algorithm  $k_1$ , see section 2.6. in the theory part. In this simulation programme, the inserted  $k_1$  and  $k_{-1}$  are obtained from the equilibrium and different values of the effective diffusion coefficients are used to get good agreement with the experimental data. Fig. 65 compares between the experimental data are obtained at  $\lambda = 408 \text{ nm}$  ( $\tilde{\nu} = 24500 \text{ cm}^{-1}$ ) with some simulated results with different values of the effective diffusion coefficient,  $D_{eff}$ . The experimental results are more or less close to the simulated data for  $D_{eff} = 2.0 \cdot 10^{-7} \text{ cm}^2 / \text{s}$ .

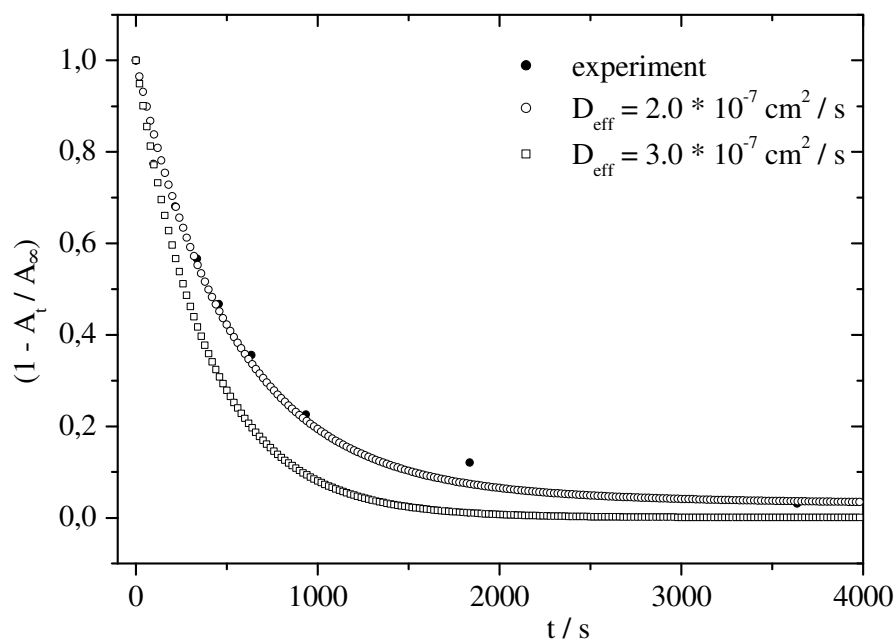
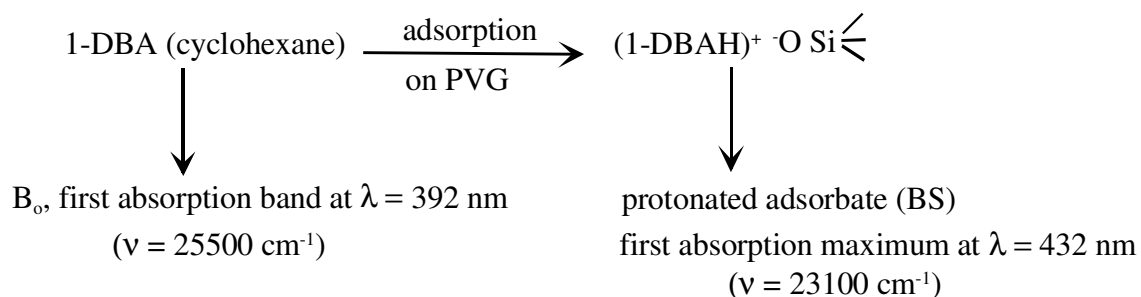


Fig. 65. Comparison between the experimental and simulated data of adsorbed AC  $[B_o] = 2.2 \cdot 10^{-6} \text{ mole/l}$  with different values of  $D_{\text{eff}}$ . Mass concentration of  $\text{SiO}_2$  in the glass sheet =  $35 \text{ g/l}$ , initial concentration of  $\text{SiO}_2 = 1 \cdot 10^{-4} \text{ mol/g}$ ,  $k_1 = 1.0 \cdot 10^4 \text{ M}^{-1} \text{ s}^{-1}$ ,  $k_{-1} = 5.0 \cdot 10^{-3} \text{ s}^{-1}$ .

#### 4.4.1.2. Adsorption of 1-DBA at PVG

The adsorption of 1-DBA at a sheet of PVG can be described by the reaction scheme 4:



Scheme 4. The adsorption of 1-DBA at a sheet of PVG.

The absorption spectra of the adsorbed 1-DBA at PVG  $[BS]$  at  $23100\text{ cm}^{-1}$ , increases with time, see Fig. 66. This is due to the progress of adsorption of 1-DBA and formation of the protonated species  $[BS]$  at the PVG surface. The reaction takes approximately 5 h, after injection of 1-DBA to reach the equilibrium.

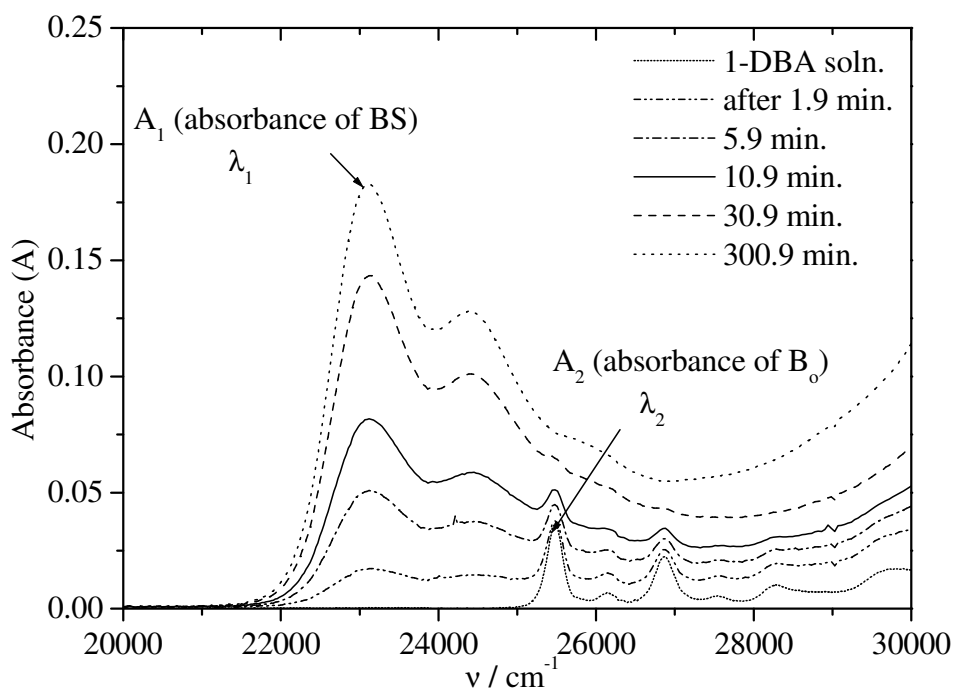


Fig. 66 Absorption spectra of 1-DBA (PVG + cyclohexane) as a function of time. Initial concentration of 1-DBA in cyclohexane,  $[B_o] = 2.0 \cdot 10^{-6} M$ .

The rate of disappearance of 1-DBA  $[B_o]$  can be determined from the decrease in the absorption peak of 1-DBA at  $25500\text{ cm}^{-1}$   $A_B (\lambda_2)$  with time according to Eq. 6 which is still in the solution. Therefore, the peak at  $25500\text{ cm}^{-1}$  is a mixture of the protonated form  $[BS]$  at the surface and nonadsorbed 1-DBA in solution. Table 17 summarizes the changes in the absorption values of the protonated 1-DBA at the surface and of the disappearing 1-DBA from solution with time as obtained from Fig. 66. The absorbance of the initial solution of 1-DBA in absence of the glass sheet is multiplied by 0.9 due to the change of light path length in presence of the sheet.

Table 17. The change of the absorption values  $A_{BS}$  of the protonated 1-DBA at PVG surface at  $\lambda_1$ , the absorbance  $A_2$  at  $\lambda_2$ , and the absorbance of disappearance 1-DBA in solution at  $A_B(\lambda_2)$  as calculated from Eq. 6 with time.

Time / min.	$A_{BS}$	$c \cdot A_{BS}$	$A_2$	$A_B(\lambda_2)$
0	0.0	0.0	0.0327	0.0327
1.89	0.0163	0.0067	0.0369	0.0302
3.89	0.0346	0.0143	0.0407	0.0264
5.89	0.0502	0.0207	0.0441	0.0234
7.89	0.0636	0.0262	0.0468	0.0206
10.89	0.0807	0.0332	0.0503	0.0171
20.89	0.1200	0.0458	0.0587	0.0129
30.89	0.1422	0.0586	0.0635	0.0049
60.89	0.1640	0.0676	0.0676	$\approx 0.00$
120.89	0.1737	0.0716	0.0705	$\approx 0.00$
180.89	0.1778	0.0733	0.0723	$\approx 0.00$
240.89	0.1801	0.0742	0.0738	$\approx 0.00$
300.89	0.1817	0.0749	0.0748	$\approx 0.00$

The rate of adsorption of 1-DBA at PVG can be calculated by plotting the absorbance of 1-DBAH<sup>+</sup> at 23100 cm<sup>-1</sup>,  $A_1$ , normalized to the absorbance at very long reaction times  $A_\infty$  vs. time in a semi-logarithmic graph, Fig. 67. The first 10 min. of the reaction can be evaluated by a first-order kinetics with a slope of  $k_{tot} = 0.92 \cdot 10^{-3} s^{-1}$ . The total rate constant is a mixture of diffusion and rate constant of the reaction. Also, the rate constant of disappearance of 1-DBA is calculated from the slope of semi-logarithmic plot of the calculated absorbance  $A_B(\lambda_2)$  normalized to the initial absorbance value of 1-DBA in cyclohexane without the glass sheet (see Eq. 34 in the theory part) against time, see Fig. 67. The rate constant of disappearance of 1-DBA,  $k_{tot} = 1.02 \cdot 10^{-3} s^{-1}$  from a first-order kinetics. This means, that the total rate of disappearance of 1-DBA in solution is approximately equal to the total rate of formation of 1-DBAH<sup>+</sup> at the PVG surface.

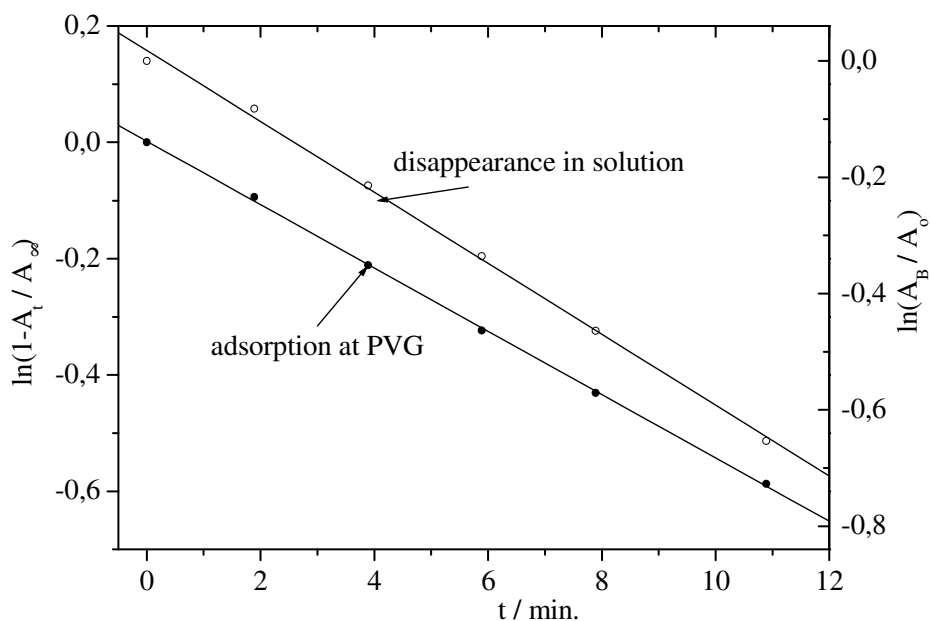


Fig. 67. semi-logarithmic plot at short time-scale of the adsorption and disappearance of 1-DBA observed at  $\lambda_1 = 432 \text{ nm}$  and  $\lambda_2 = 392 \text{ nm}$ , respectively,  $[B_o] = 2.0 \cdot 10^{-6} \text{ M}$ .

A simulation programme of the diffusion and adsorption kinetics is used to get an idea about the value of  $D_{eff}$  and to determine the second-order rate constant of reaction,  $k_{ads}$  which is called in this algorithm  $k_1$ , see section 2.6. in the theory part. A comparison between the experimental data of the disappearing 1-DBA which are obtained from Table 17 at  $\lambda_2 = 392 \text{ nm}$  ( $\tilde{\nu} = 25500 \text{ cm}^{-1}$ ) and some simulated results with various values of the effective diffusion coefficient,  $D_{eff}$  is given in Fig. 68. It is found, that the experimental results are near to the simulated data of  $D_{eff} = 1.20 \cdot 10^{-7} \text{ cm}^2 / \text{s}$ .

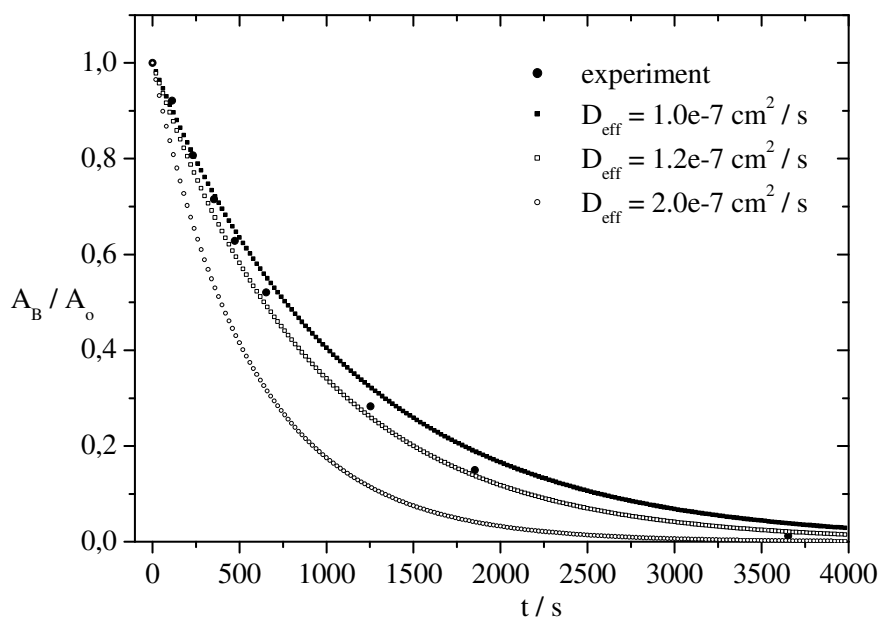
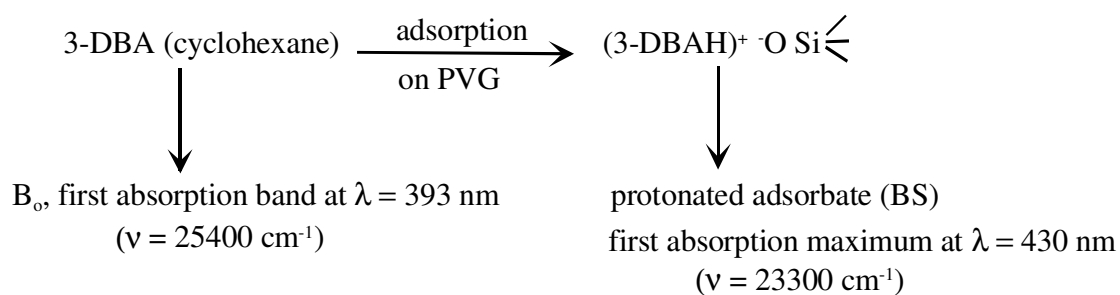


Fig. 68. Comparison between the experimental and simulated data of disappearance of 1-DBA  $[B_o] = 2.0 \cdot 10^{-6} M$  with different values of  $D_{eff}$ . Mass concentration of  $SiO_2$  in the glass sheet =  $35 g/l$ , initial concentration of  $SiO_2 = 1 \cdot 10^{-4} mol/g$ ,  $k_1 = 1.0 \cdot 10^4 M^{-1} s^{-1}$ ,  $k_{-1} = 1.0 \cdot 10^{-5} s^{-1}$ .

#### 4.4.1.3. Adsorption of 3-DBA at PVG

The adsorption of 3-DBA in a sheet of PVG is explained by scheme 5:



Scheme 5. The adsorption of 3-DBA in a sheet of PVG.



The change in the absorbance during adsorption of 3-DBA at PVG surfaces with time is shown in Fig. 69. The peak at  $23200\text{ cm}^{-1}$  raises with time due to the adsorption of 3-DBA and formation of its protonated form  $[BS]$  at the PVG surfaces. The absorption peak at  $25500\text{ cm}^{-1}$  of 3-DBA in solution  $[B_o]$  decreases with time. The reaction is not finished after 24 h and there is a clear equilibrium between adsorption and desorption of 3-DBA at PVG which is discussed in chapter 3 of the results and discussions part.

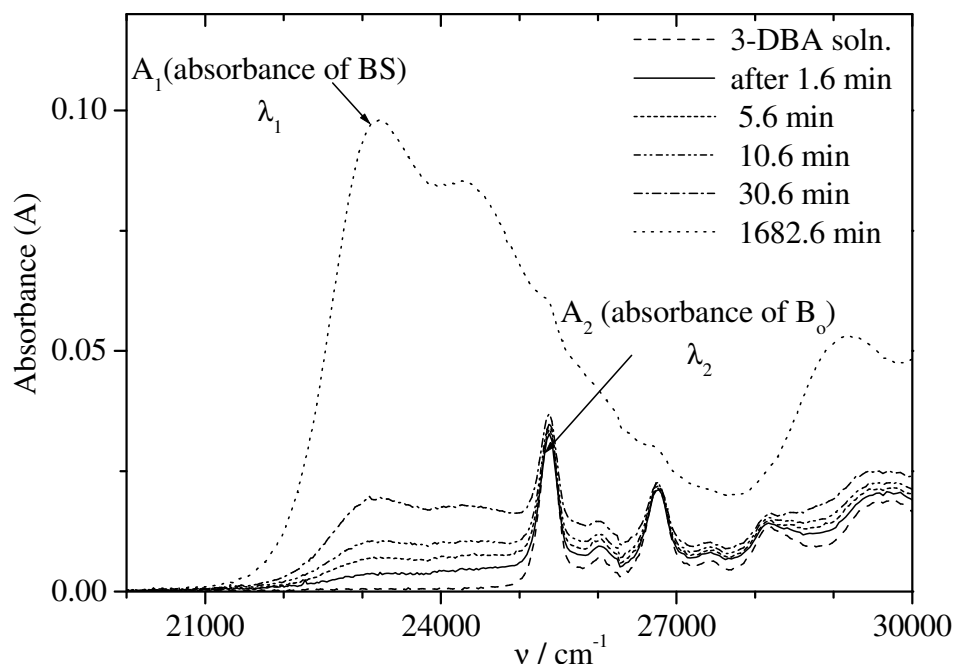


Fig. 69. Absorption spectra of 3-DBA (PVG + cyclohexane) as a function of time, concentration of 3-DBA in cyclohexane,  $[B_o] = 2.1 \cdot 10^{-6} M$ .

The absorption values of disappearance of 3-DBA in cyclohexane are determined from the decrease in the absorption peak of 3-DBA which is still in solution at  $25500\text{ cm}^{-1}$   $A_B (\lambda_2)$  with time according to Eq. 6. Table 18 shows the change in the absorption values of the protonated 3-DBA on the surface and of the disappearance of 3-DBA from solution with time which are obtained from Table 18. The absorbance of initial solution of 3-DBA in absence of the glass sheet is multiplied by 0.9 due to the change of light path length in presence of the sheet.

Table 18. The change in the absorption values  $A_{BS}$  of the protonated 3-DBA at PVG surface at  $\lambda_1$ , the absorbance  $A_2$  at  $\lambda_2$ , and the absorbance of disappearance 3-DBA in solution  $A_B(\lambda_2)$  as calculated according to Eq. 6 with time.

Time / min.	$A_1, [BS]$	$c \cdot A_1$	$A_2$	$A_B(\lambda_2)$
0	0.0	0.00	0.03096	0.03096
1.88	0.0036	0.0021	0.0324	0.0303
3.88	0.0053	0.0031	0.0332	0.0301
5.88	0.0068	0.0040	0.0335	0.0295
7.88	0.0082	0.0048	0.0337	0.0289
10.88	0.0102	0.0060	0.034	0.0283
20.88	0.0151	0.0089	0.0354	0.0265
30.88	0.0192	0.0113	0.0365	0.0252
60.88	0.0268	0.0158	0.0384	0.0226
120.88	0.0376	0.0221	0.0416	0.0195
180.88	0.0455	0.0268	0.0440	0.0173
240.88	0.0515	0.0303	0.0458	0.0155
300.88	0.0564	0.0332	0.0471	0.0139
1440.88	0.0935	0.0549	0.0583	0.0033
2880.88	0.0975	0.0573	0.0595	0.0022

Fig. 70 shows the kinetics of adsorption which is calculated by plotting  $\frac{(A_\infty - A_t)}{A_\infty}$  (see Eq. 35 in the theory part) of 3-DBAH<sup>+</sup> at 23200 cm<sup>-1</sup> in a semi-logarithmic graph vs. time. Here,  $A_t$  is the absorbance of 3-DBAH<sup>+</sup> at time  $t$  after 3-DBA injection and  $A_\infty$  is the equilibrium value at time  $t \rightarrow \infty$ . In this figure, the first 10 min. of the reaction can be evaluated by a first-order kinetics with a slope of  $k_{tot} = 1.28 \cdot 10^{-4} s^{-1}$ . The rate constant  $k_{tot}$  is a mixture of diffusion and the summation of the first-order rate constant of the reaction  $k_{eff}$  and the rate of desorption  $k_{des}$ .

Also, the rate constant of disappearance of 3-DBA in cyclohexane is calculated from the slope of the semi-logarithmic plot of the absorbance  $A_B(\lambda_2)$  normalized to the initial absorbance value of 3-DBA in cyclohexane in absence of a glass sheet,  $A_0$  vs. time, see Fig.

70. The rate constant of disappearance of 3-DBA,  $k_{tot} = 1.36 \cdot 10^{-4} s^{-1}$  is obtained from a first-order kinetics. This means, that the rate of disappearance of 3-DBA from solution is approximately equal to the rate of adsorption of 3-DBA at the PVG surface.

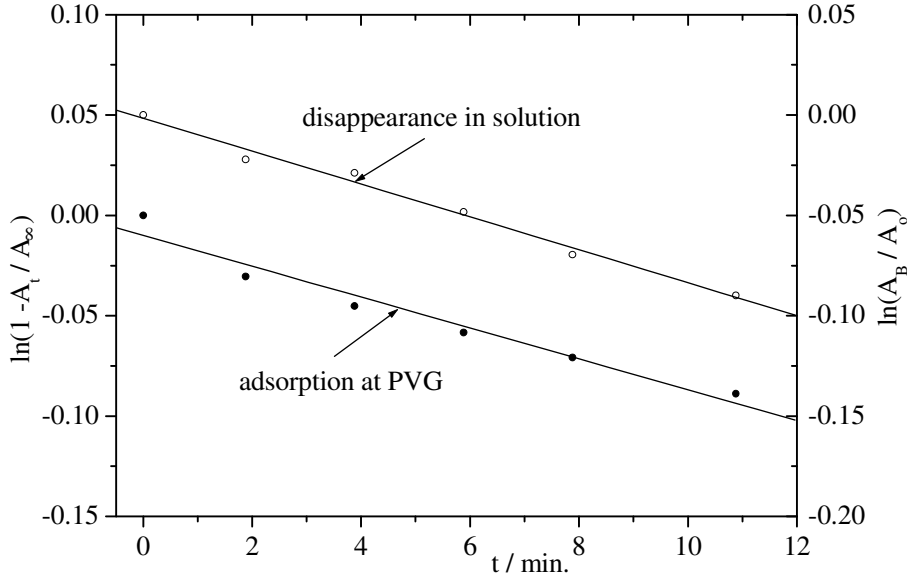


Fig. 70. semi-logarithmic plot at short time scale of the adsorption and disappearance of 3-DBA observed at  $\lambda_1 = 430.5$  nm and  $\lambda_2 = 393$  nm respectively, concentration of 1-DBA in cyclohexane,  $[B_o] = 2.1 \cdot 10^{-6} M$ .

From Fig. 70, the adsorption of 3-DBA at the PVG surfaces is not good exponential. This is due to the strong diffusion of 3-DBA in the glass sheet to find the strong acidic centres. With comparison to the rate of adsorption of AC and 1-DBA at PVG, it is found that, the total rate,  $k_{tot}$  of adsorption of 3-DBA is much slower than  $k_{tot}$  of 1-DBA and that of AC at PVG.

Fig. 71 compares the experimental data obtained from Table 18 at  $\lambda_2 = 392$  nm ( $\tilde{\nu} = 25500 cm^{-1}$ ) to some simulated results with different values of the effect diffusion coefficient  $D_{eff}$  which are obtained from the simulation programme according to the algorithm in section 2.6 (theory part). From Fig. 71, it is obvious that the simulated data with  $D_{eff} = 6.0 \cdot 10^{-8} cm^2 / s$  are close to the experimental at short time of the reaction.

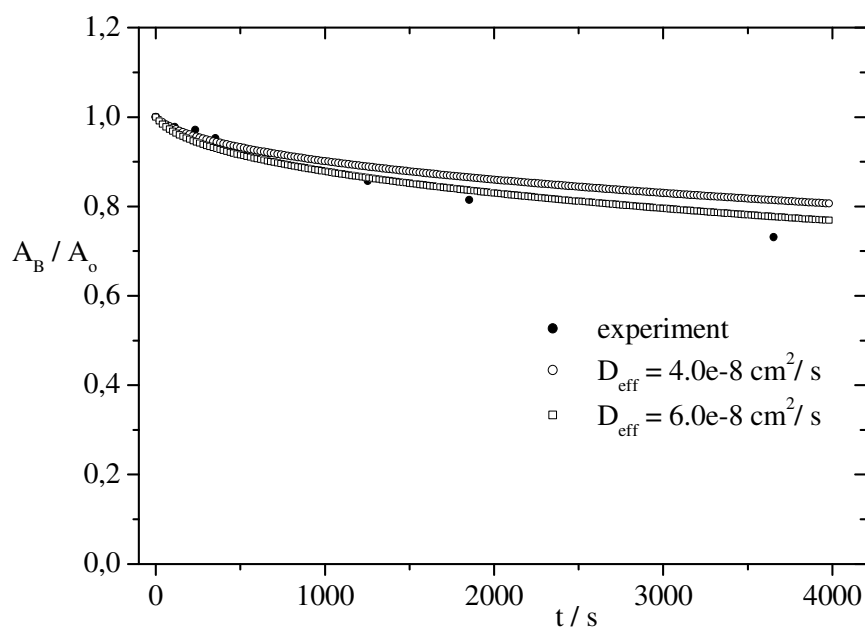
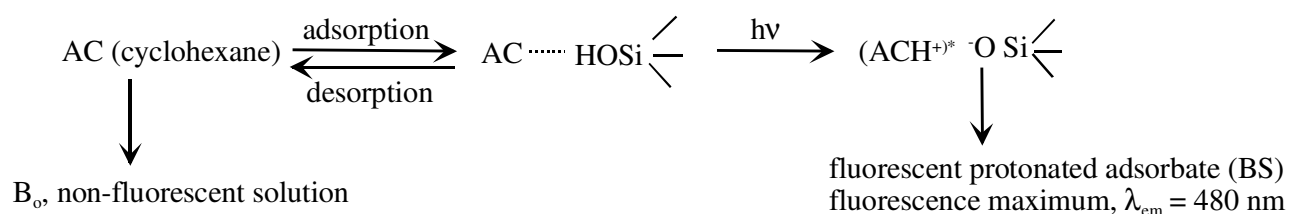


Fig. 71. Comparison between the experimental and simulated data of disappearance of 3-DBA  $[B_0] = 2.1 \cdot 10^{-6} M$  with different values of  $D_{eff}$ . Mass concentration of  $SiO_2$  in the glass sheet =  $35 g/l$ , initial concentration of  $SiO_2 = 1 \cdot 10^{-5} mol/g$   $k_1 = 1.00e4 M^{-1}s^{-1}$ ,  $k_{-1} = 0.1 s^{-1}$ .

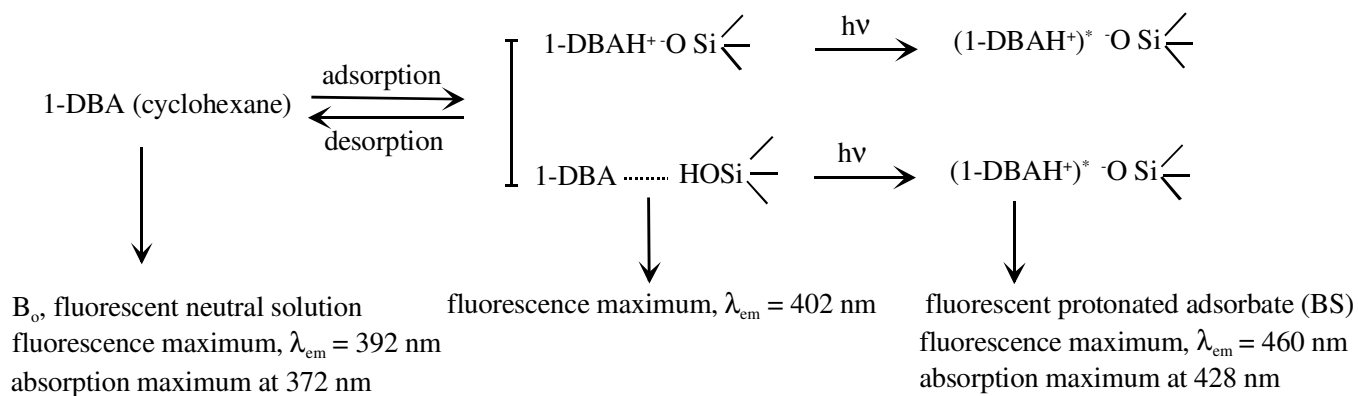
#### 4.4.2. Adsorption at non-modified silica beads

The kinetics of adsorption of AC and 1-DBA at non-modified silica are measured as described in (3.3.2.1) in the experimental part. The uptake of AC into silica is monitored by fluorescence spectroscopy of the protonated AC at the silica surface  $[BS]$  according to the following reaction scheme:



Scheme 6. The adsorption of AC at non-modified silica surface.

Also, the uptake of 1-DBA into silica is monitored by fluorescence spectroscopy in a similar way as AC. However, care is taken that only the protonated species is analysed, since 1-DBA also fluoresces strongly in cyclohexane.



Scheme 7. Adsorption of 1-DBA at non-modified silica.

Fig. 72 shows the increase in the fluorescence intensity of the protonated AC and 1-DBA species at silica surface [BS] as a function of time (curve a and b, respectively). The fluorescence intensity increases due to the progress of adsorption of AC or 1-DBA and formation the protonated species at the silica beads surface and then its reaches a maximum value.

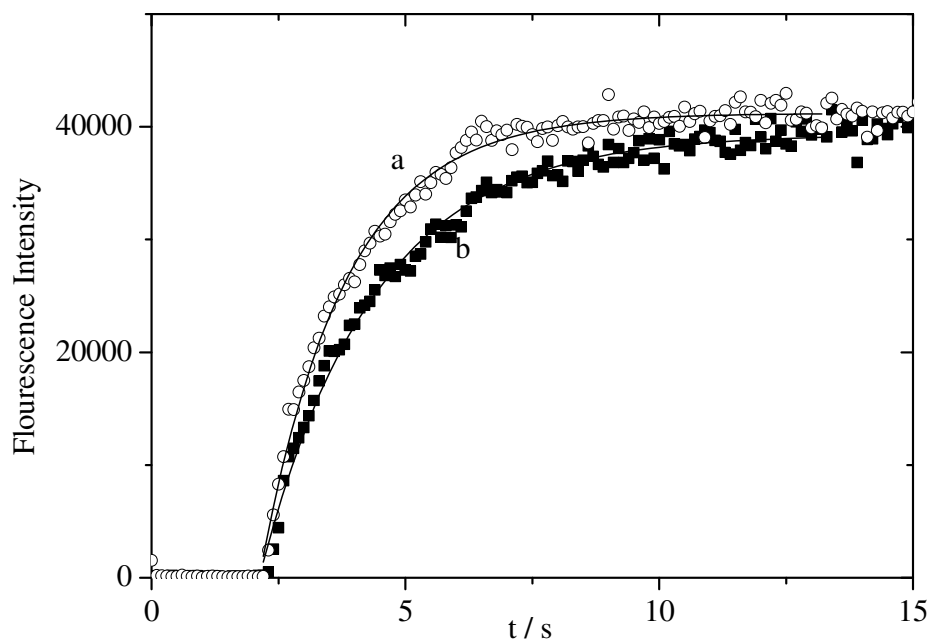


Fig. 72. Increase of fluorescence intensity of the adsorbed species with time of a stirred solution of: a) AC (3 ml cyclohexane + 6 mg non-modified silica),  $\lambda_{ex} = 355 \text{ nm}$ ,  $\lambda_{em} = 480 \text{ nm}$ ,  $[B_o] = 3.6 \cdot 10^{-6} \text{ mole/l}$ ; b) 1-DBA (3 ml cyclohexane + 6 mg bare silica),  $\lambda_{ex} = 377 \text{ nm}$ ,  $\lambda_{em} = 460 \text{ nm}$ ,  $[B_o] = 3.7 \cdot 10^{-6} \text{ mole/l}$ . Points are measured at time intervals of  $\Delta t = 0.1 \text{ s}$ , full lines are fitted according to 1<sup>st</sup>-order.

The data obtained from Fig. 72 are fitted exponentially to obtain the total rate constant of adsorption of AC and 1-DBA at non-modified silica surface according to Eq. 35, respectively. Fig. 73 shows a semi-logarithmic plot of  $\frac{(I_{F\infty} - I_{Ft})}{I_{F\infty}}$  against time. Since,  $I_{Ft}$  is the fluorescence intensity of adsorbed AC and/or 1-DBA at time  $t$  after AC and/or 1-DBA injection and  $I_{F\infty}$  is the infinity value. From figure 73, it is found that the total rate of adsorption of AC at 6 mg silica,  $k_{tot} = 0.73 \text{ s}^{-1}$  is faster than that of 1-DBA,  $k_{tot} = 0.54 \text{ s}^{-1}$ . This is may be due to the difference in diffusion of AC and 1-DBA in the silica beads, i.e. the adsorption of AC and 1-DBA at the silica surface may be controlled by the diffusion mechanism. Also this is clear from Fig. 73, since the adsorption of AC and 1-DBA at non-modified silica is not good exponential due to diffusion of probes in silica beads.

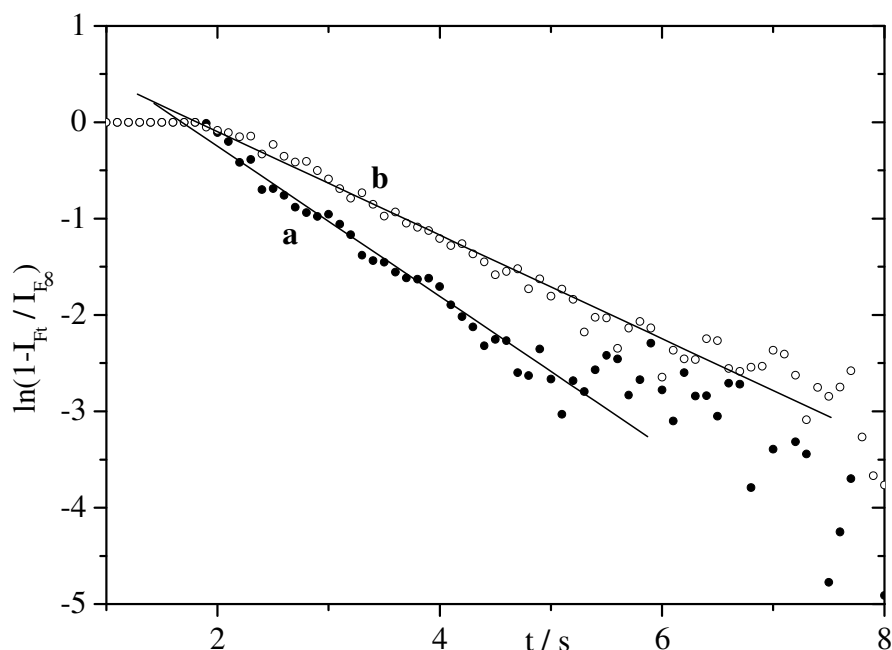


Fig. 73. semi-logarithmic plot at short time-scale of adsorbed species with time of a stirred solution of: a) AC (3 ml cyclohexane + 6 mg non-modified silica),  $\lambda_{ex} = 355 \text{ nm}$ ,  $\lambda_{em} = 480 \text{ nm}$ ,  $[B_o] = 3.6 \cdot 10^{-6} \text{ mole/l}$ ; b) 1-DBA (3 ml cyclohexane + 6 mg bare silica),  $\lambda_{ex} = 377 \text{ nm}$ ,  $\lambda_{em} = 460 \text{ nm}$ ,  $[B_o] = 3.7 \cdot 10^{-6} \text{ mole/l}$ .

The rate of disappearance of 1-DBA in cyclohexane due to the adsorption at 6 mg non-modified silica is given in Fig. 74. It is easier to measure the rate of nonadsorbed species than the adsorbed one. In case of the AC the rate of disappearance can not be measured because its solution in cyclohexane is not fluorescent. The rate constant of disappearance of 1-DBA is calculated from the slope of a semi-logarithmic plot of the fluorescence intensity of 1-DBA in solution  $I_{F_t}$  which is measured at  $\lambda_{ex} = 372 \text{ nm}$ ,  $\lambda_{em} = 391 \text{ nm}$  after subtraction of  $I_{F_\infty}$  and normalized to the initial value of 1-DBA in cyclohexane  $I_{F_0}$  (see Eq. 34 in the theory part) vs. time. The normalization is done to the value of  $I_{F_t}$  at time  $t = 0.3 \text{ s}$  from 1-DBA injection. This is because the first three points are not in a good order with the other points, which this is may be due to the dilution of the injected 1-DBA by cyclohexane takes approximately this time ( $\approx 0.3 \text{ s}$ ) until the concentration of 1-DBA becomes equal in the 3 ml cell. It is also found that the reaction is not finished until 120 s and there is still a slow decrease in the measured intensity after 120 s. So, in the calculation, the value of  $I_{F_\infty}$  is taken lower than the measured

end value at 120 s. The rate constant of the disappearance of 1-DBA is calculated from the slope of has a value,  $k_{tot} = 0.21 \text{ s}^{-1}$ .

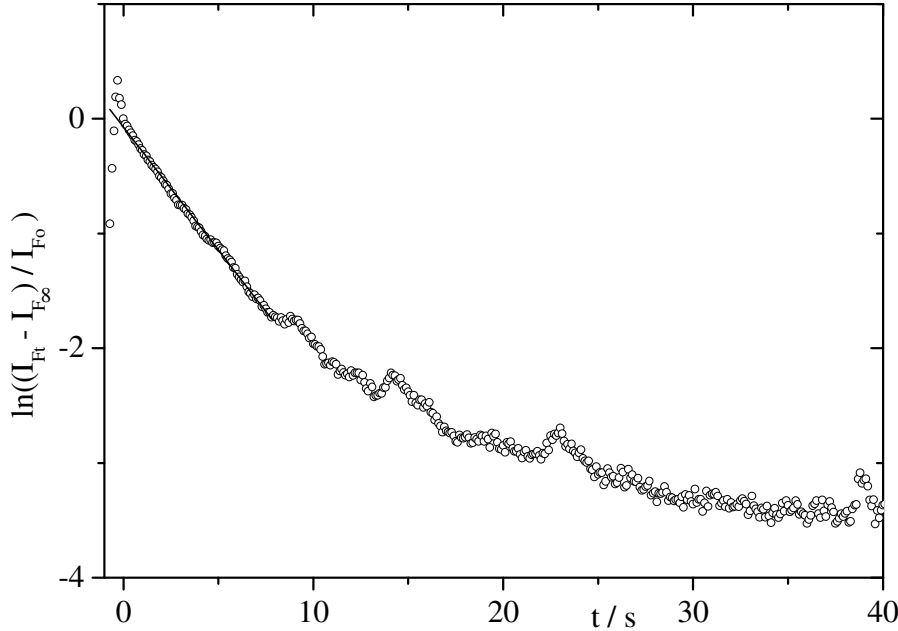


Fig. 74. semi-logarithmic plot at short time-scale of the disappearance 1-DBA  $[B_o] = 4.2 \cdot 10^{-6} \text{ mole/l}$ ,  $\lambda_{ex} = 372 \text{ nm}$ ,  $\lambda_{em} = 391 \text{ nm}$ . Points are measured at time intervals of  $\Delta t = 0.1 \text{ s}$ , full lines are fitted according to 1<sup>st</sup>-order.

The simulation for the disappearance 1-DBA in cyclohexane is performed and the adsorption AC at 6 mg non-modified silica is investigated to get an idea about the value of effective diffusion coefficient. Fig. 75 shows comparison between the data for adsorbed AC obtained at  $\lambda_{ex} = 355 \text{ nm}$ ,  $\lambda_{em} = 480 \text{ nm}$  and some simulated results with different values of the effective diffusion coefficient  $D_{eff}$ . From figure 75 it is found that the experimental data are in agreement with simulated data for  $D_{eff} = 3.0 \cdot 10^{-6} \text{ cm}^2 / \text{s}$ .

Fig. 76 demonstrates that the simulated data for  $D_{eff} = 4.0 \cdot 10^{-7} \text{ cm}^2 / \text{s}$  are in agreement with the experimental data of disappearance 1-DBA in solution at  $\lambda_{ex} = 372 \text{ nm}$ ,  $\lambda_{em} = 391 \text{ nm}$ . This means that the diffusion of AC is faster than 1-DBA inside the silica beads.



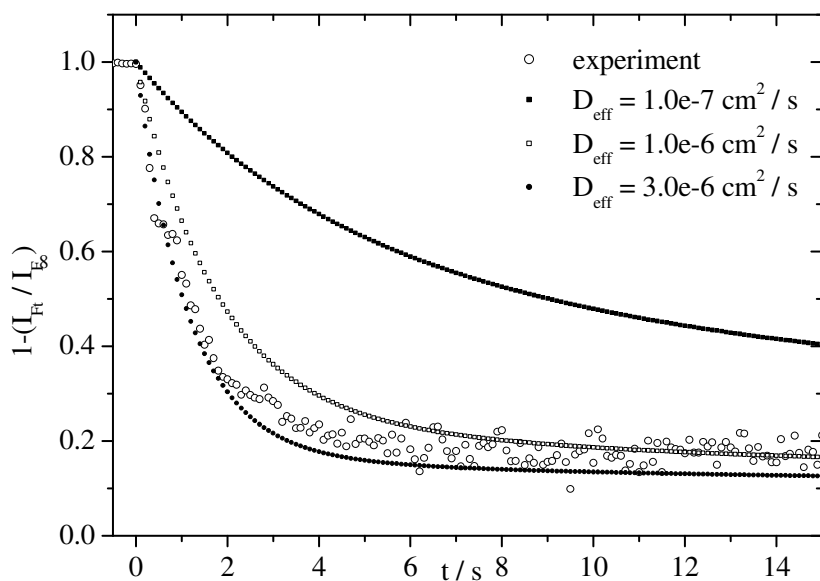


Fig. 75. Comparison between the experimental and simulated data of adsorbed AC  $[B_o] = 3.6 \cdot 10^{-6} \text{ mole/l}$  with different values for  $D_{eff}$ . Mass concentration of  $\text{SiO}_2$  in non-modified silica =  $2 \text{ g/l}$ ,  $\text{SiO}_2 = 1 \cdot 10^{-4} \text{ mol/g}$ ,  $k_1 = 1.0 \cdot 10^4 \text{ M}^{-1} \text{ s}^{-1}$ ,  $k_{-1} = 0.25 \text{ s}^{-1}$ .

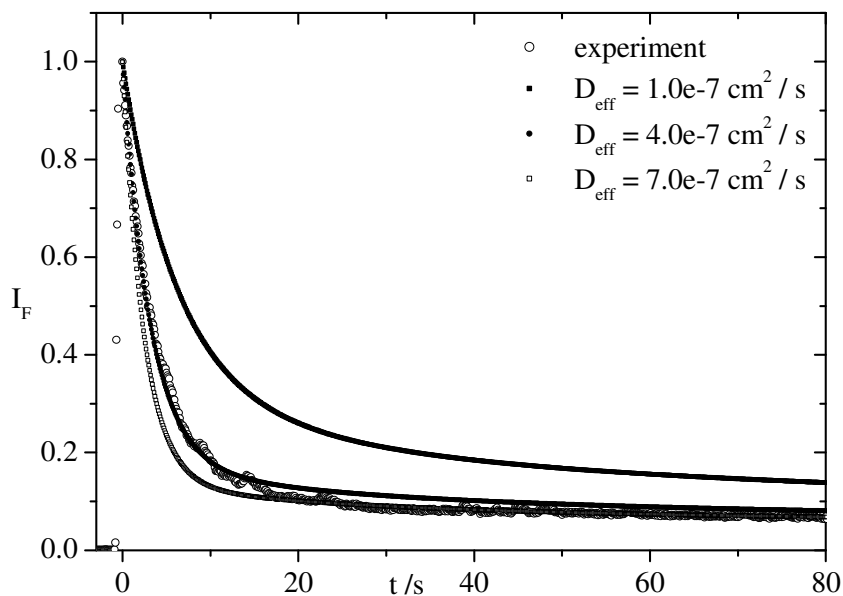


Fig. 76. Comparison between the experimental and simulated data of disappearance of 1-DBA  $[B_o] = 4.2 \cdot 10^{-6} \text{ mole/l}$  with different values for  $D_{eff}$ . Mass concentration of  $\text{SiO}_2$  in non-modified silica =  $2 \text{ g/l}$ ,  $\text{SiO}_2 = 1 \cdot 10^{-4} \text{ mol/g}$ ,  $k_{ads} = 1.0 \cdot 10^4 \text{ M}^{-1} \text{ s}^{-1}$ ,  $k_{des} = 0.10 \text{ s}^{-1}$ .

Table 19 shows the total rate constants of adsorption  $k_{tot}$  as calculated according to Eq. 35, the effective rate constant, the rate of desorption as calculated by using the equilibrium ratio (Eq. 40) and Eq. 36 together with the effective diffusion coefficients  $D_{eff}$  of AC, 1-DBA and 3-DBA at non-modified silica and PVG surfaces and the total rate constant divided by the outer surface area of silica and PVG.

Table 19. The total rate constants of adsorption  $k_{tot}$  as calculated from Eq. 35, the effective rate constant  $k_{eff}$ , the rate of desorption  $k_{des}$  (as calculated by using the equilibrium ratio  $K$  and Eqs. 36, 40), the effective diffusion coefficient  $D_{eff}$  of AC, 1-DBA and 3-DBA at nonmodified silica and PVG surfaces as known from the algorithm in section 2.6. (theory part) and the total rate by surface area.

System	$k_{tot}$ / $10^{-3} s^{-1}$	$k_{eff}$ / $10^{-3} s^{-1}$	$k_{des}$ / $10^{-3} s^{-1}$	$\frac{[B]_o - [B]_\infty}{[B]_\infty} \cdot \frac{V_m}{V_r}$ $= \frac{k_{eff}}{k_{des}} = K$	$k_{tot}$ / $10^{-3} s^{-1} cm^{-2}$	$D_{eff}$ / $10^{-7} cm^2 / s$
AC + 6 mg silica	$730 \pm 60$	729	0.007	$1000 \pm 90$	8.98	30.0
1-DBA + 6 mg silica	$540 \pm 30$	539	0.003	$2000 \pm 100$	6.64	4.0
AC + PVG	$1.28 \pm 0.03$	128	0.0		0.74	2.0
1-DBA + PVG	$0.92 \pm 0.03$	92.0	0.0		0.53	1.2
3-DBA + PVG	$0.13 \pm 0.03$	13.0	$\approx 0.0$	$470 \pm 40$	0.075	0.6

## Discussion

The kinetics of adsorption of AC, 1-DBA and 3-DBA at PVG are studied by measuring the absorbance of the adsorbed protonated species at PVG surfaces. By comparing the values of total rate constant of adsorption  $k_{tot}$ , which is calculated according to Eq. 37, it is noticed that the rate of the adsorption of the three compounds on PVG is decreased in the following order; AC > 1-DBA >> 3-DBA. This is due to the difference in the effective diffusion coefficient  $D_{eff}$  of the three compounds in the glass sheet. Since the effective diffusion coefficient which obtained from the algorithm in section 2.6. (theory part) shows that  $D_{eff}$  of the three compounds is decreases according to the following order: AC > 1-DBA >> 3-DBA. This means that the adsorption of the three probes at PVG surfaces is diffusion controlled. The rate of adsorption of 3-DBA at PVG is much slower than that of 1-DBA, since, 3-DBA diffuses more than 1-DBA in the glass sheet to find strong acidic centres.

The rate of disappearance of 1-DBA and 3-DBA from cyclohexane due to adsorption at PVG surface is calculated from Eq. 6. The rate constant of the disappearance of 1-DBA and/or 3-DBA is approximately equal to that of adsorbed 1-DBA and/or 3-DBA at PVG.

The kinetic studies for the adsorption of AC and 1-DBA at silica beads surface from cyclohexane solution show that, the rate of adsorption of AC at 6 mg silica is faster than the rate of adsorption of 1-DBA at the same amount of silica. This is may be due to the difference in the diffusion coefficient of AC and 1-DBA to silica particles. The effective diffusion coefficient of AC which obtained from the algorithm in section 2.6. (theory part) is faster than that of 1-DBA inside the silica beads, see Table 19. This means that the reaction is controlled by diffusion of the probe into silica particles.

In general, it is simpler to measure the rate of nonadsorbed prob than that of adsorbed. The rate of nonadsorbed 1-DBA can be measured, since 1-DBA is fluorescent in cyclohexane but it could not measured for AC which is nonflurescent in cyclohexane. By comparing between the values of the rate constants of the nonadsorbed 1-DBA and that of adsorbed 1-DBA, it is found that, the rate constant of adsorbed 1-DBA at silica surface has higher value than that of nonadsorbed 1-DBA. This is because a few of silica particles are accumulated

together and these big particles adhere to the cell walls, so only the small particles which are in light bath and only the rate of adsorption on these particles which is measured.

By comparing the kinetics of the adsorption of AC and 1-DBA at the PVG to that at the non-modified silica beads it is found that, the rate of adsorption of AC and 1-DBA at non-modified silica is much faster than that of AC and 1-DBA at PVG. At non-modified silica, the reaction is very fast and it is finished after approximately 15 s. At PVG, the reaction takes about 1 h until there is no dissolved AC and/or 1-DBA in solution. The adsorption is faster at silica surfaces than at PVG due to the diffusion length for glass sheet is longer than that of silica particles (small particle size, 6  $\mu\text{m}$ ). So, it can be concluded that, the interaction of AC, 1-DBA and 3-DBA with silica and PVG are consists of two processes: one is the diffusion into the glass sheet and the other one is the reaction of the base with the acidic silanol groups to form the protonated species on the surfaces and this interaction is diffusion controlled.

## 4.5. Accessibility of probes attached to silica surfaces

Bimolecular quenching of adsorbed fluorescence probes by oxygen is of considerable practical interest because it has been used for development of optical oxygen sensors [107-109]. It was found that the fluorescence quenching efficiencies of adsorbed anthracene on silica gel vary with pore size of the silica gel but not the oxygen quenching rate [110]. The adsorbed  $\text{Ru}(\text{bpy})_3^{2+}$  on PVG is quenched by  $\text{O}_2$  which is also adsorbed onto the glass [111]. Here, the accessibility of the adsorbed fluorescence probes on porous silica and PVG surface to  $\text{O}_2$  is studied. The quenching efficiencies of these adsorbed molecules by  $\text{O}_2$  are compared to those of these molecules in solutions.

### 4.5.1. Influence of $\text{O}_2$ on the fluorescence intensity and lifetime of adsorbates

#### 4.5.1.1. Acridine

AC is adsorbed at PVG surface and the protonated species is formed in the ground state. The lifetime of adsorbed AC at PVG surface decreases with increasing oxygen partial pressure. AC is adsorbed at bare silica surfaces as H-bonded species which are protonated upon excitation. The fluorescence of the adsorbed AC at non-modified silica is quenched by oxygen. Figs. 77 and 78 show the decay curves of the adsorbed AC at PVG and bare silica surfaces under oxygen and nitrogen atmosphere, respectively.

The decay times of adsorbed AC at PVG and non-modified silica surfaces are listed in Table 20. Figs. 79 and 80 present the corresponding Stern-Volmer plots (Eq. 21) which show that the quenching rate depends linearly on the oxygen concentration.

The quenching rate constants as obtained from the Stern-Volmer plots are given in Table 20.

Table 20. Fluorescence decay times  $\tau_F$ , and their amplitudes, and the quenching rate constants  $k_q$  as obtained from Eq. 21 of adsorbed AC at non-modified silica and at PVG under nitrogen and oxygen atmospheres respectively,  $\tilde{\nu}_{ex} = 27000 \text{ cm}^{-1}$ .

Surface	$\tilde{\nu}_{em} / \text{cm}^{-1}$	$\text{N}_2$			$\text{O}_2$			$k_q / 10^9 \text{ M}^{-1} \text{sec}^{-1}$
		$\tau_F / \text{ns}$	B	$\langle \tau_F \rangle / \text{ns}$	$\tau_F / \text{ns}$	B	$\langle \tau_F \rangle / \text{ns}$	
Silica	20800	19.9	1.0		6.7	0.67	16.2	9.45
					18.4	0.33		0.35
PVG	20800	7.3	0.16	29.6	3.7	0.43	18.5	0.81
		30.4	0.84		19.7	0.57		

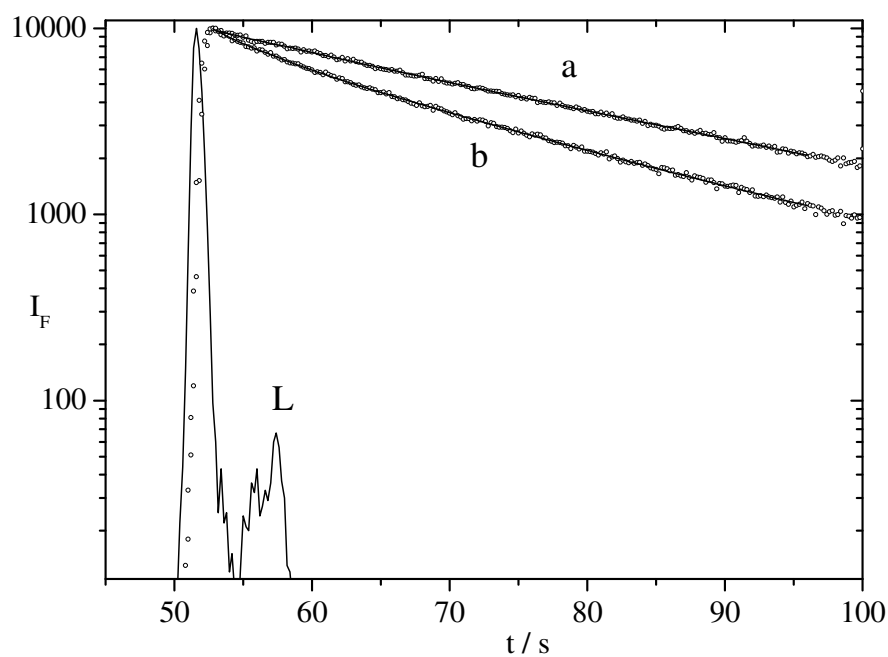


Fig. 77. Fluorescence decay curves of adsorbed AC (PVG + cyclohexane),  $l = 0.35 \cdot 10^{-6} \text{ mole / g SiO}_2$  under a)  $\text{N}_2$  and b)  $\text{O}_2$  atmosphere;  $\tilde{\nu}_{ex} = 27000 \text{ cm}^{-1}$  and  $\tilde{\nu}_{em} = 20800 \text{ cm}^{-1}$ . L represents the profile of the exciting laser pulse.

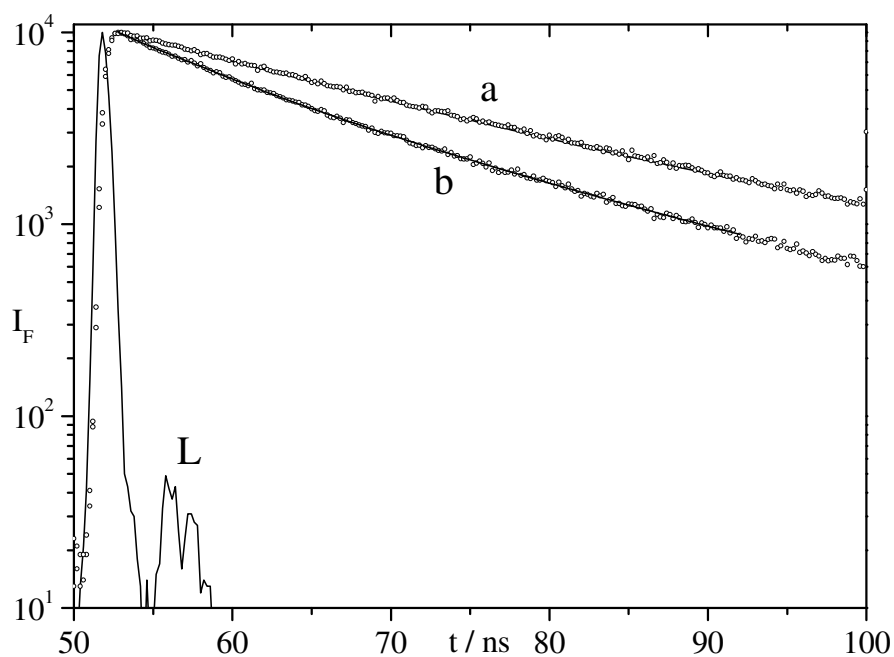


Fig. 78. Fluorescence decay curves of adsorbed AC (non-modified silica + cyclohexane),  $l = 4.4 \cdot 10^{-6} \text{ mole} / \text{gSiO}_2$  under a)  $N_2$  and b)  $O_2$  atmosphere;  $\tilde{\nu}_{ex} = 27000 \text{ cm}^{-1}$  and  $\tilde{\nu}_{em} = 20800 \text{ cm}^{-1}$ . L represents the profile of the exciting laser pulse.

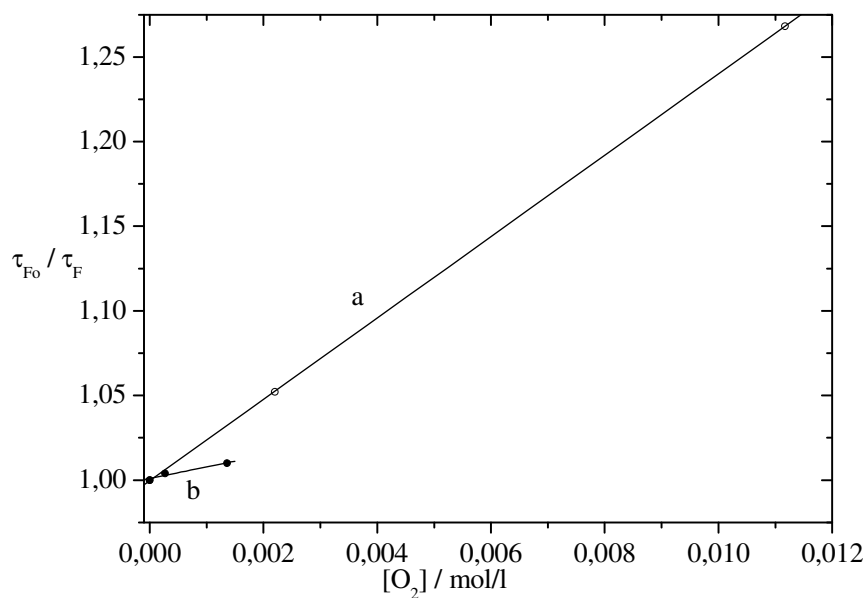


Fig. 79. Stern-Volmer plot of the fluorescence lifetime measurements of a) adsorbed AC at PVG from cyclohexane,  $l = 0.35 \cdot 10^{-6} \text{ mole} / \text{g SiO}_2$ ; b) AC in water at  $\text{pH} \approx 1$ ,  $\tilde{\nu}_{ex} = 27000 \text{ cm}^{-1}$  and  $\tilde{\nu}_{em} = 20800 \text{ cm}^{-1}$ .

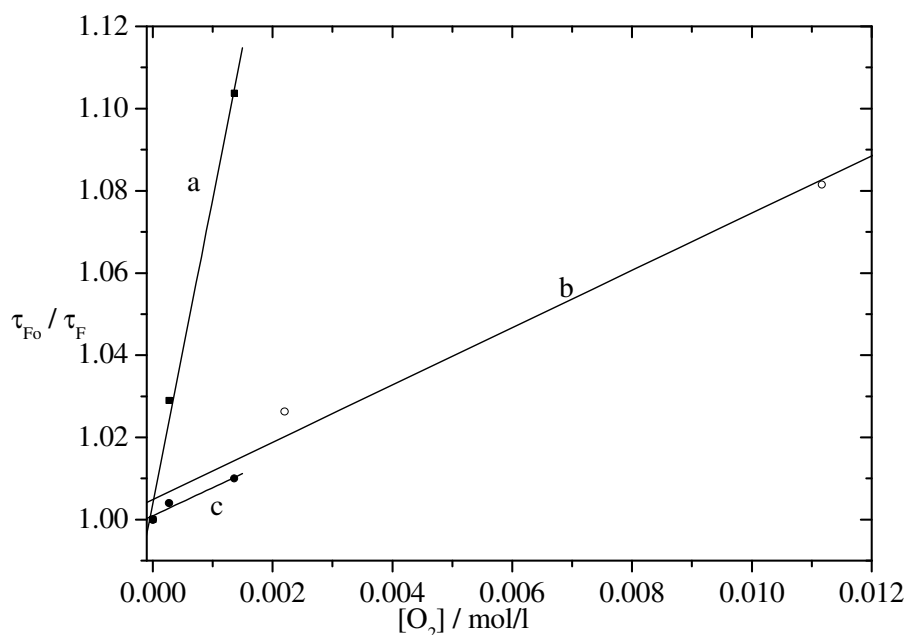


Fig. 80. Stern-Volmer plot of the fluorescence lifetime measurements of a) AC in water at pH  $\approx$  12 b) adsorbed AC at non-modified silica from cyclohexane,  $l = 4.4 \cdot 10^{-6} \text{ mole} / \text{gSiO}_2$ ; c) AC in water at pH  $\approx$  1,  $\tilde{\nu}_{ex} = 27000 \text{ cm}^{-1}$ ,  $\tilde{\nu}_{em} = 23400 \text{ cm}^{-1}$  (for alkaline water) and  $\tilde{\nu}_{em} = 20800 \text{ cm}^{-1}$

From Figs. 79 and 80, it is obvious, that the adsorbed AC at the surfaces (PVG and/or non-modified silica) is more quenched by oxygen than the protonated AC in water at pH  $\approx$  1. On the other hand, adsorbed AC at non-modified silica surfaces is less quenched by oxygen than neutral AC in water at pH  $\approx$  12.

#### 4.5.1.2. Dibenzacridines

##### 4.5.1.2.1. 1,2,7,8-Dibenzacridine

At PVG surfaces 1-DBA is adsorbed only as protonated species in the ground state. The fluorescence of these adsorbed species is quenched by oxygen. 1-DBA is adsorbed at bare silica and silica C30 surfaces and forms the protonated and the H-bonded species in the ground state. The H-bonded species is protonated in the excited state. The fluorescence of the adsorbed protonated species at non-modified silica and silica C30 is also quenched by oxygen. Figs. 81, 82 and 83 show the decay curves of adsorbed 1-DBA on PVG, non-modified silica and silica C30 under oxygen and nitrogen atmosphere, respectively.



The decay times of adsorbed 1-DBA at PVG, non-modified silica and silica C30 surfaces are listed in Table 21. Figs. 84 and 85 show the corresponding Stern-Volmer (Eq. 21) plots which show that the quenching rate depends linearly on the oxygen concentration. The quenching rate constants as obtained from the Stern-Volmer plots are given in Table 21.

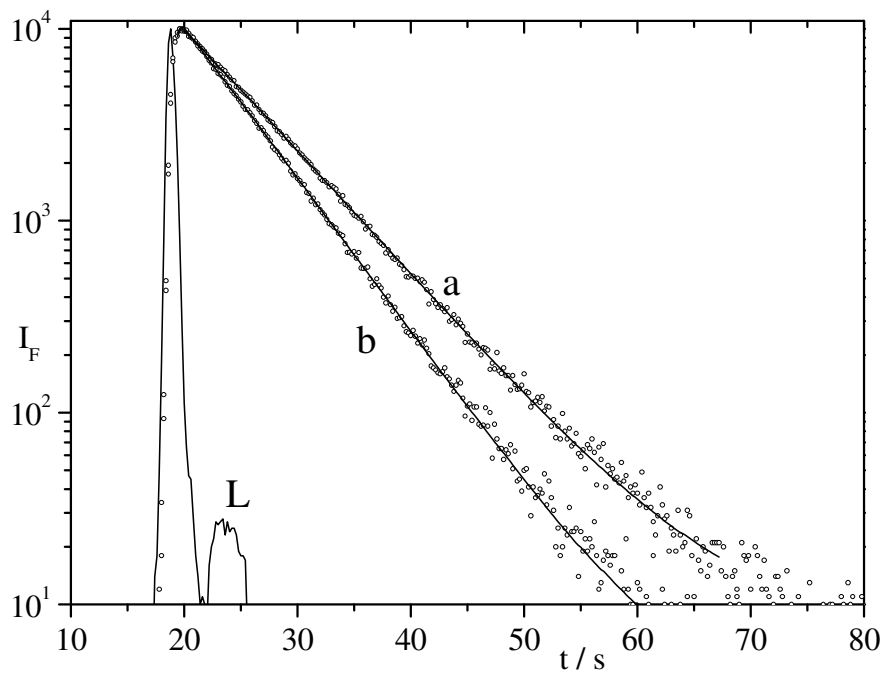


Fig. 81. Fluorescence decay curves of adsorbed 1-DBA (PVG + cyclohexane),  $l = 0.07 \cdot 10^{-6} \text{ mole / g SiO}_2$  under; a)  $\text{N}_2$  and b)  $\text{O}_2$  atmosphere;  $\tilde{\nu}_{ex} = 27000 \text{ cm}^{-1}$  and  $\tilde{\nu}_{em} = 21700 \text{ cm}^{-1}$ . L represents the profile of the exciting laser pulse.

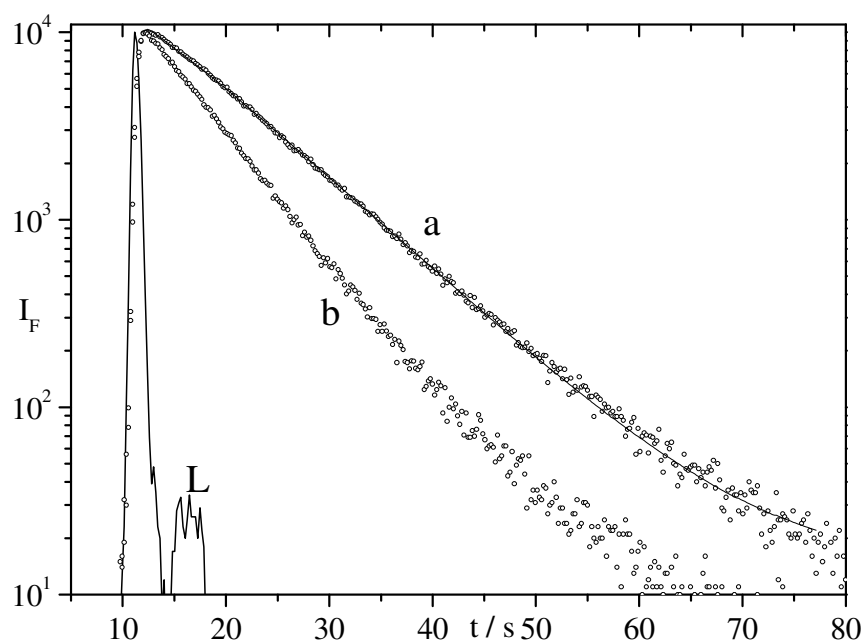


Fig. 82. Fluorescence decay curves of adsorbed 1-DBA (non-modified silica + cyclohexane),  $l = 2.9 \cdot 10^{-6} \text{ mole / g SiO}_2$  under; a)  $N_2$  and b)  $O_2$  atmosphere;  $\tilde{\nu}_{ex} = 27000 \text{ cm}^{-1}$  and  $\tilde{\nu}_{em} = 20800 \text{ cm}^{-1}$ . L represents the profile of the exciting laser pulse.

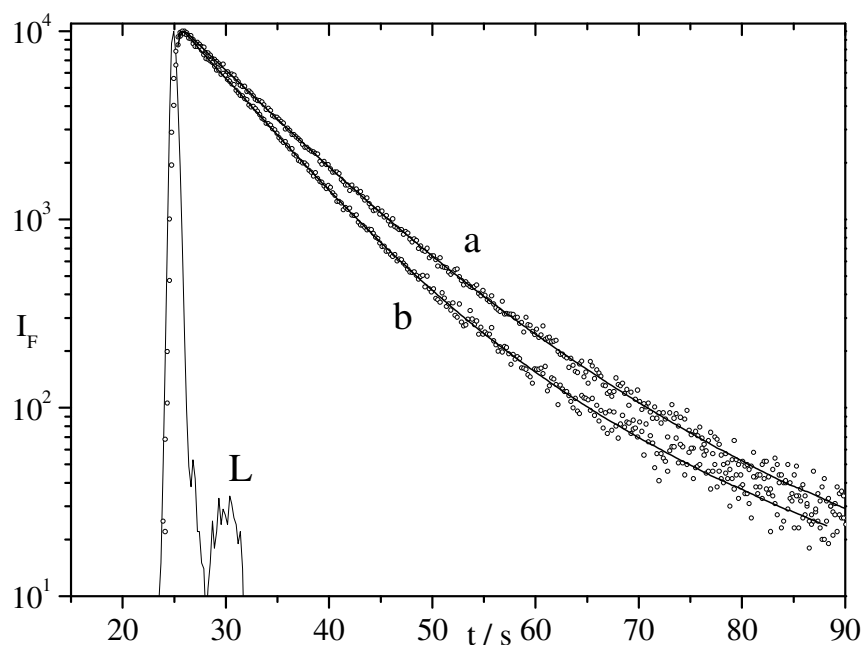


Fig. 83. Fluorescence decay curves of adsorbed 1-DBA (silica C30 + cyclohexane),  $l = 1.9 \cdot 10^{-6} \text{ mole / g SiO}_2$  under; a)  $N_2$  and b)  $O_2$  atmosphere;  $\tilde{\nu}_{ex} = 27000 \text{ cm}^{-1}$  and  $\tilde{\nu}_{em} = 20800 \text{ cm}^{-1}$ . L represents the profile of the exciting laser pulse.

Table 21. Fluorescence decay times  $\tau_F$ , the amplitudes and the quenching rate constants of 1-DBA (non-modified silica + cyclohexane), 1-DBA (silica C30 + cyclohexane) and 1-DBA (PVG + cyclohexane) after bubbling nitrogen and oxygen, respectively,  $\tilde{\nu}_{ex} = 27000 \text{ cm}^{-1}$ .

Surface	$\tilde{\nu}_{em} / \text{cm}^{-1}$	N <sub>2</sub>			O <sub>2</sub>			k <sub>q</sub> / 10 <sup>9</sup> M <sup>-1</sup> sec <sup>-1</sup>
		$\tau_F / \text{ns}$	$\langle \tau \rangle / \text{ns}$	B	$\tau_F / \text{ns}$	$\langle \tau \rangle / \text{ns}$	B	
Bare silica	25700	9.7		1.0	3.2		0.94	19.6
					11.1		0.06	
	24900	9.3		1.0	2.9	5.08	0.43	6.4
					5.6		0.57	
	20800	4.9		-0.21	6.1		1.0	4.4
		8.7		0.79				
Silica C30	25600	2.1		0.02	3.1		0.87	20.2
		9.5		0.80	6.8		0.13	
	24900	5.5		0.34	3.5		0.32	1.5
		9.3		0.66	7.8		0.68	
	20800	0.3		-0.30	6.6		0.70	1.1
		7.2		0.60	0.2		-0.24	
		14.4		0.10	18.0		0.06	
PVG	20800	6.7		1.0	5.4		1.0	3.2

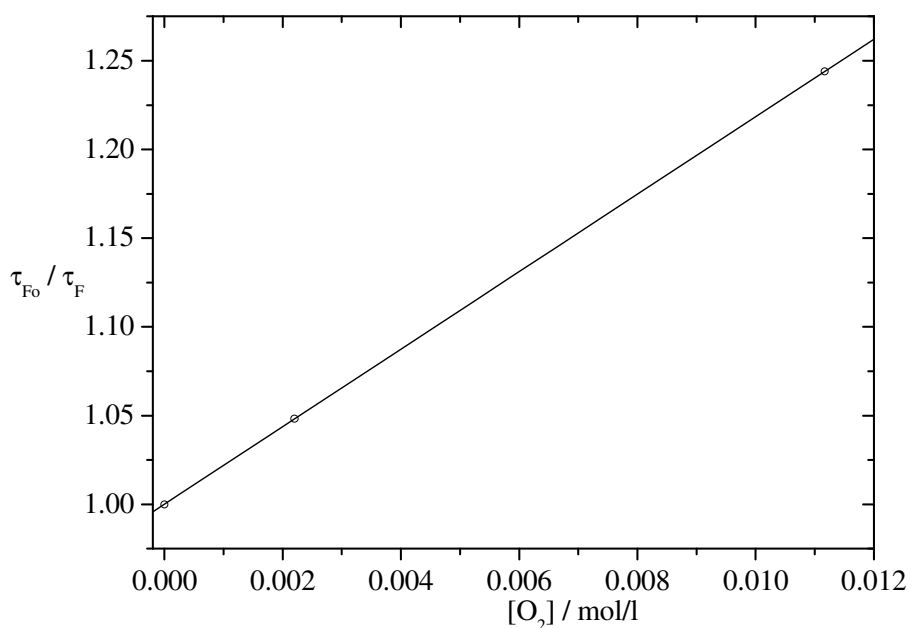


Fig. 84. Stern-Volmer plot of the fluorescence lifetime measurements of adsorbed 1-DBA on PVG from cyclohexane,  $l = 0.07 \cdot 10^{-6} \text{ mole} / \text{g SiO}_2$ ;  $\tilde{\nu}_{ex} = 27000 \text{ cm}^{-1}$  and  $\tilde{\nu}_{em} = 21700 \text{ cm}^{-1}$ .

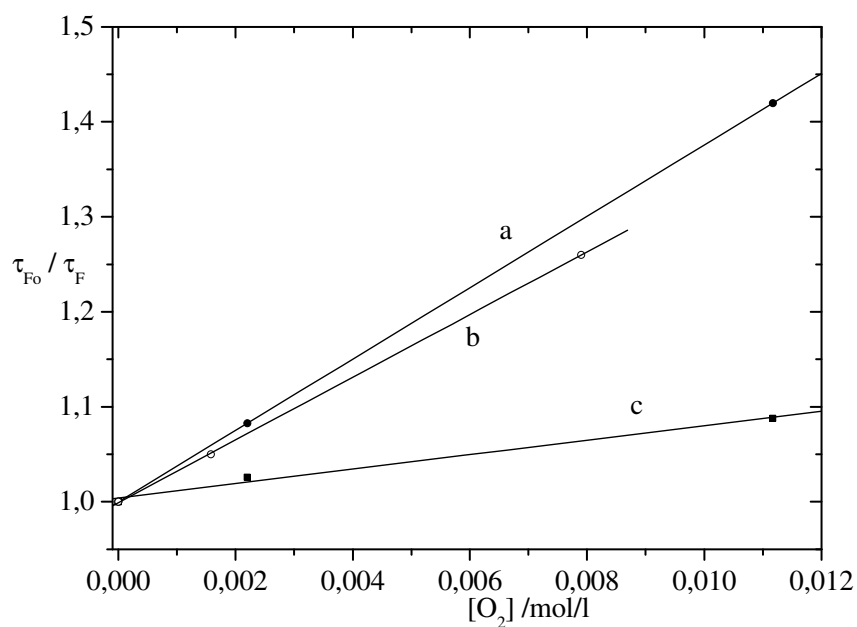


Fig. 85. Stern-Volmer plot of the fluorescence lifetime measurements of a) adsorbed 1-DBA on bare silica from cyclohexane,  $l = 2.9 \cdot 10^{-6} \text{ mole} / \text{g SiO}_2$ ; b) 1-DBA in acidic ethanol, c) 1-DBA adsorbed at silica C30 from cyclohexane,  $l = 1.9 \cdot 10^{-6} \text{ mole} / \text{g SiO}_2$   $\tilde{\nu}_{ex} = 27000 \text{ cm}^{-1}$  and  $\tilde{\nu}_{em} = 20800 \text{ cm}^{-1}$ .

From Figs. 84 and 85, it is found that the lifetime of the adsorbed protonated 1-DBA at PVG is quenched by  $O_2$  in the same order of 1-DBA in acidic ethanol. While the lifetime of the adsorbed protonated 1-DBA at non-modified silica are quenched strongly by  $O_2$  than that of 1-DBA in acidic ethanol. The decay time of the protonated 1-DBA on silica C30 is less quenched by oxygen than that in acidic ethanol. This is due to the effect of the alkyl chains on the surface, since oxygen is not capable of penetrating between the alkyl chains to reach the protonated 1-DBA at the surface.

#### 4.5.1.2.2. 3,4,5,6-Dibenzacridine

When 3-DBA is adsorbed at PVG, the protonated species is formed in the ground state. Fig. 86 shows the decay curves of protonated 3-DBA at PVG in oxygen and nitrogen atmosphere. The corresponding decay times are listed in Table 22 for the adsorbed 3-DBA at  $\tilde{\nu}_{em} = 2100 \text{ cm}^{-1}$  and nonadsorbed 3-DBA at  $\tilde{\nu}_{em} = 25300 \text{ cm}^{-1}$ . Fig. 87 presents the corresponding Stern-Volmer (Eq. 21) plot. The quenching rate constants obtained from the Stern-Volmer plots are also given in Table 22.

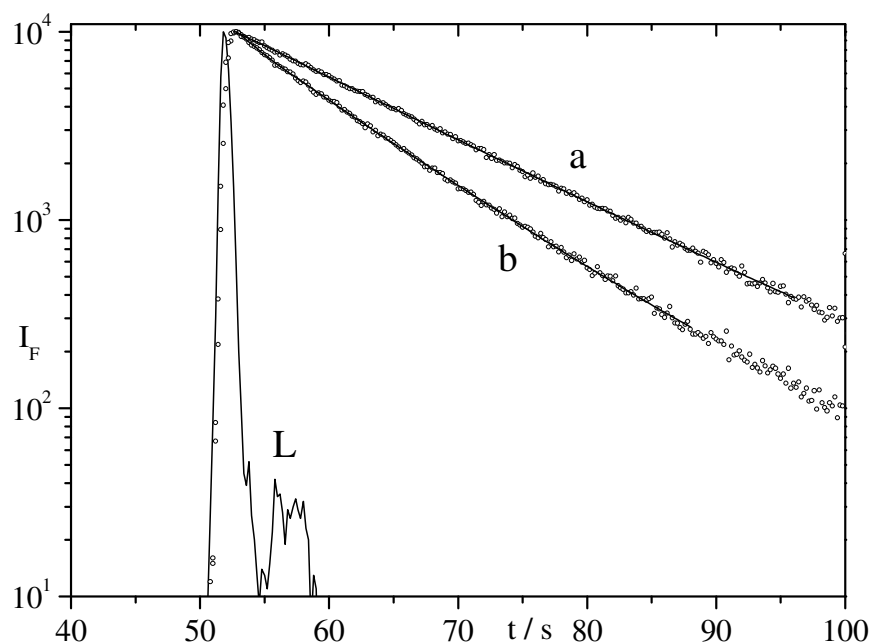


Fig. 86. Fluorescence decay curves of adsorbed 3-DBA (PVG + cyclohexane),  $l = 0.29 \cdot 10^{-6} \text{ mole/g SiO}_2$  under; a)  $N_2$  and b)  $O_2$  atmosphere;  $\tilde{\nu}_{ex} = 27000 \text{ cm}^{-1}$  and  $\tilde{\nu}_{em} = 21000 \text{ cm}^{-1}$ . L represents the profile of the exciting laser pulse.

Table 22. Fluorescence decay times  $\tau_F$ , and their amplitudes B, mean fluorescence decay times  $\langle\tau_F\rangle$  and the quenching rate constant  $K_q$  of 3-DBA (PVG + cyclohexane) after bubbling with nitrogen and oxygen, respectively,  $\tilde{\nu}_{ex} = 27000\text{ cm}^{-1}$ .

$\tilde{\nu}_{em} / \text{cm}^{-1}$	$\text{N}_2$			$\text{O}_2$			$k_q / 10^9 \text{ M}^{-1} \text{sec}^{-1}$
	$\tau_F / \text{ns}$	$\langle\tau_F\rangle / \text{ns}$	B	$\tau_F / \text{ns}$	$\langle\tau_F\rangle / \text{ns}$	B	
25300	4.46	9.1	0.20	0.37	3.2	0.48	18.1
	9.55		0.80	3.38		0.52	
21000	12.9		1.0	2.5	9.2	0.25	2.8
				9.61		0.75	

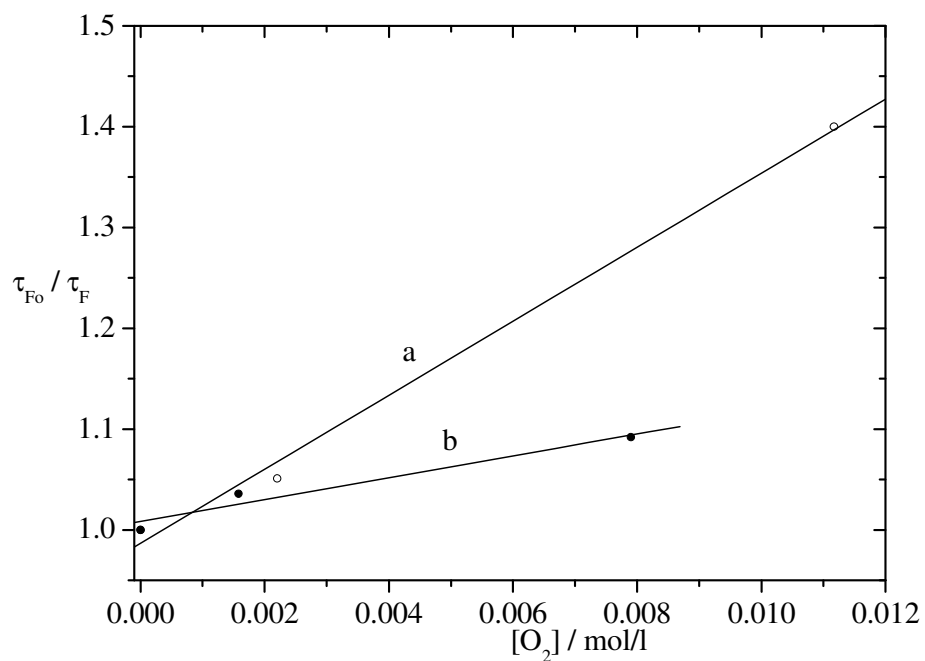


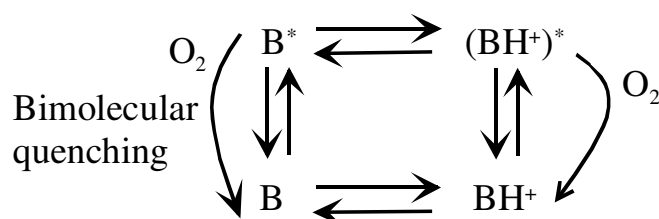
Fig. 87. Stern-Volmer plot of the fluorescence lifetime measurements of a) adsorbed 3-DBA on PVG from cyclohexane,  $l = 0.29 \cdot 10^{-6} \text{ mole} / \text{g SiO}_2$ ; b) 3-DBA in acidic ethanol,  $\tilde{\nu}_{ex} = 27000\text{ cm}^{-1}$  and  $\tilde{\nu}_{em} = 21000\text{ cm}^{-1}$ .

From Fig. 87 it is clear that the fluorescence lifetime of adsorbed 3-DBA at PVG is more strongly quenched by oxygen than that of 3-DBA in acidic ethanol.

## Discussion

The fluorescence lifetime of adsorbed acridine and 3-DBA at Vycor glass and at non-modified silica (all in their protonated state) is more strongly quenched by oxygen than the respective species in solution (in water at  $\text{pH} \approx 1$  for AC and acidic ethanol for the 3-DBA). Also the lifetime of adsorbed protonated 1-DBA at non-modified silica is more quenched by oxygen than that of 1-DBA in acidic ethanol. While the lifetime of the adsorbed 1-DBA at PVG is quenched by  $\text{O}_2$  in the same order of protonated 1-DBA in acidic ethanol. This means that the nitrogen heterocycles at the solid/air interface are more exposed to oxygen than in solution [76]. This is due to the adsorption of oxygen onto the PVG and/or silica and its surfaces diffusion. In this way, the interaction time of the adsorbed probe and oxygen is extended and excess translational, vibrational, and rotational energy of the oxygen is dissipated by the adsorption process. The adsorption process, thus, increases the quenching probability [106,111].

The following reaction scheme will be considered for the mechanism of quenching:



Scheme 7. Reaction scheme of the fluorescence quenching of the adsorbed base on silica and PVG by oxygen.

where B is the symbol for base in ground state,  $\text{B}^*$  is the base in excited state,  $\text{BH}^+$  is the protonated form of the base in ground state and  $(\text{BH}^+)^*$  is the protonated form of the base in the excited state.

The quenching rate constant for protonated 1-DBA at silica C30 surface is slightly decreased with respect to the non-modified surface and also with respect to the acidic solution. This is due to the lower mobility of oxygen in the interphase since oxygen is not capable of penetrating between the alkyl chains [112].

## 4.5.2. Chemical reactivity at silica surfaces

### 4.5.2.1. Introduction

Many modifications of silica surfaces have been performed with different lengths of alkyl chains, e.g. C<sub>2</sub>, C<sub>8</sub> and C<sub>18</sub> to improve the separation selectivity of silica in RP-HPLC [113-117]. Other modifications was done by using polar functional groups (NO<sub>2</sub>, NH<sub>2</sub>, CN or/and OH) bonded to short alkyl chains (C<sub>3</sub>, C<sub>4</sub>) [114-116].

In the last section (4.5.1.) the effect of surface modification (silica modified with alkyl chains, silica C30) on quenching reactions was investigated. Quenching reactions afford no or very little activation energy – they are more or less diffusion controlled. This was used to quantify the mobility of the quencher in the vicinity of the silica supported group. In this chapter the effect of surface modification on a "real" chemical reaction is investigated. Thus the effect of the surface modification on the transition complex of the reaction can be assessed. The reaction under consideration is an S<sub>N</sub>2 reaction with a moderately polar transition state (no free charges are to be expected where the effect of stabilization by polar environments would be much stronger). Nevertheless, modifying the surface with nonpolar groups might – in addition to steric effects due to crowding of the silica surface - change the stability of the transition complex and might thus change the reaction rate.

To this end modification is carried out for the silica surfaces by bonding different active groups (mainly amino groups with alkyl chain, phenyl ring and aliphatic acid) to the surface silanol groups. The aim of this modification is to compare between the reactivities of silica supported functional groups (in this case represented by amino groups). To this end, amino groups are bound to the silica surface (see section 3.1.3.1.2.2. in the experimental part). In addition the surface properties are varied by covering the silica surface with C8 alkyl chain, phenyl groups and butyric acid (the structures of these silicas are presented in Figs. 10-13 in the experimental part). The accessibility of the active groups is studied by the reaction of fluorescent probe (DANSyl chloride) with the modified silica by using the technique of fluorescence.

The reaction of the modified silica surface with DANSyl chloride in dry DCM as a solvent appears in the following scheme:





#### 4.5.2.2. Binding and mobility

The fluorescence emission, fluorescence excitation and fluorescence excitation anisotropy spectra of suspensions of 6 mg of four different silicas (3-aminopropyl, 3-aminopropyl and octyl, 3-aminopropyl and phenyl, and 3-aminopropyl and butyric silica) after the completion of the reaction with DANSyl chloride in dry dichloromethane ( $c=0.17 \cdot 10^{-5} M$ ) are presented in Figs. 88-91. There is a broad emission band at  $\approx 19200 \text{ cm}^{-1}$ , which is the same wave number region as DANSyl amide in dichloromethane. Also, the excitation spectrum possesses one band at the positions shown in Table 24, which are similar to that of DANSyl amide in dichloromethane. This means that DANSyl chloride has reacted with the amino groups of the four silica surfaces to form DANSyl amide.

The fluorescence anisotropy spectra reveal the mobility of surface-supported DANSyl amide. At the four silica surfaces, the anisotropy of the formed DANSyl amide has a value of  $r \approx 0.2$  at  $25000 \text{ cm}^{-1}$  which is smaller than that in glycerol (see Table 8). This is due to the fact that DANSyl amide is anchored at the surface but solvated by dichloromethane. The well solvation of DANSyl amide by dichloromethane is evident from: the low anisotropy values, which indicates a high mobility and the independence of the emission wavelengths on the type of silica (see Table 24).

Table 24. Positions of the excitation,  $\tilde{\nu}_{obs, \max}$  and the emission  $\tilde{\nu}_{F, \max}$  peaks of the formed DANSyl amide on the modified silica surfaces.

Type of silica	$\tilde{\nu}_{obs, \max} / \text{cm}^{-1}$	$\tilde{\nu}_{F, \max} / \text{cm}^{-1}$
1	29500	19200
2	29800	19200
3	29400	19200
4	29400	19300

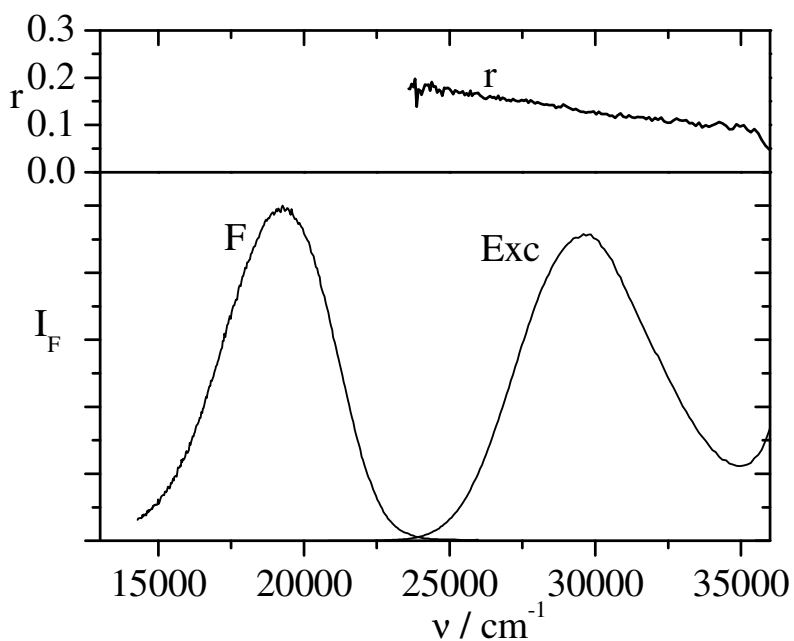


Fig. 88. Fluorescence, fluorescence excitation and fluorescence anisotropy spectra of the covalently bound DANSyl amide on silica 1. The fluorescence spectrum is excited at  $26700 \text{ cm}^{-1}$ ; the excitation and the anisotropy spectra are observed at  $20000 \text{ cm}^{-1}$ .

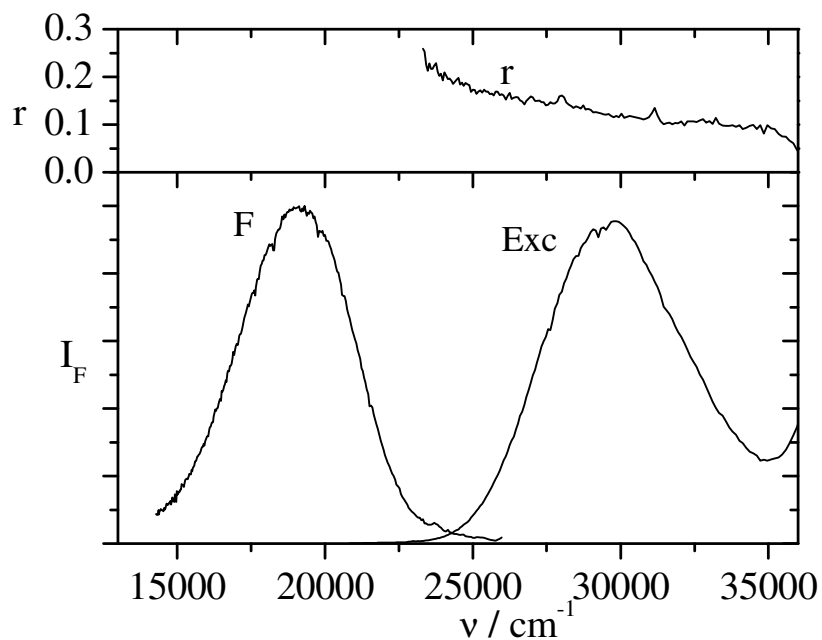


Fig. 89. Fluorescence, fluorescence excitation and fluorescence anisotropy spectra of the covalently bound DANSyl amide on silica 2. The fluorescence spectrum is excited at  $26700 \text{ cm}^{-1}$ ; the excitation and the anisotropy spectra are observed at  $20000 \text{ cm}^{-1}$ .

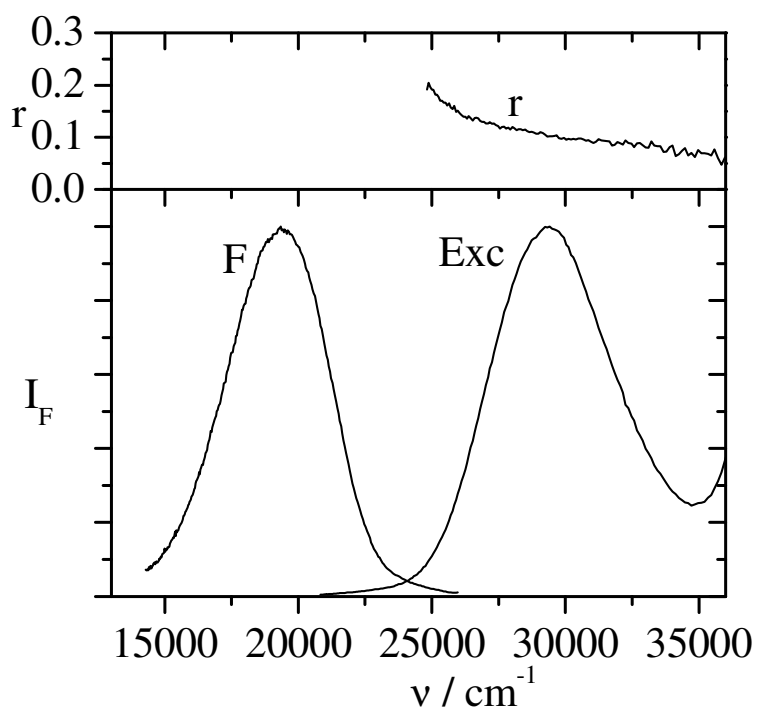


Fig. 90. Fluorescence, fluorescence excitation and fluorescence anisotropy spectra of the covalently bound DANSyl amide on silica 3. The fluorescence spectrum is excited at  $26700 \text{ cm}^{-1}$ ; the excitation and the anisotropy spectra are observed at  $20000 \text{ cm}^{-1}$ .

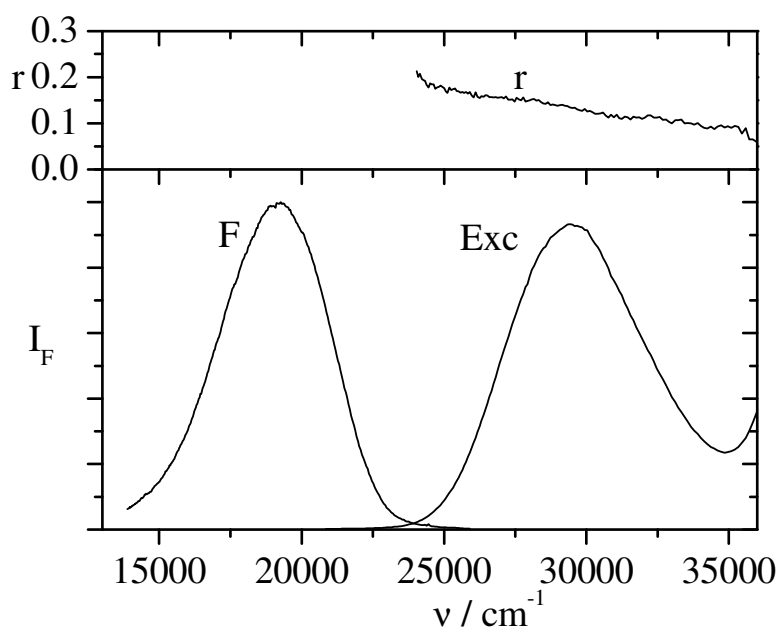


Fig. 91. Fluorescence, fluorescence excitation and fluorescence anisotropy spectra of the covalently bound DANSyl amide on silica 4. The fluorescence spectrum is excited at  $26700 \text{ cm}^{-1}$ ; the excitation and the anisotropy spectra are observed at  $20000 \text{ cm}^{-1}$ .

### 4.5.2.3. Reaction kinetics

The progress of the reaction of DANSyl chloride with the 3-aminopropyl groups of the four different types of silica 1-4 under investigation is monitored by fluorescence spectroscopy of the formed DANSyl amide according to the reaction in scheme 8 in 5.2. Figs. 92-95 show the increase of the fluorescence intensity of the formed DANSyl amide species on 6 mg of the four modified silica surfaces respectively as a function of time.

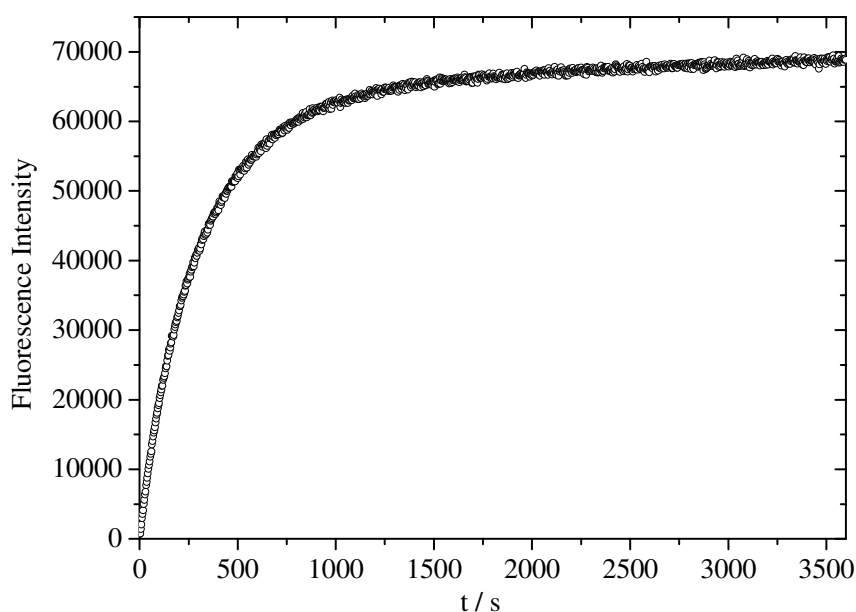


Fig. 92. Increase of fluorescence intensity of the adsorbed species with time of a stirred solution of DANSyl chloride (3 ml dichloromethane + 6 mg silica 1),  $\tilde{\nu}_{ex} = 26700 \text{ cm}^{-1}$ ,  $\tilde{\nu}_{em} = 20000 \text{ cm}^{-1}$ ,  $([B_o] = 0.17 \cdot 10^{-5} \text{ M})$ . Points are measured at time intervals of  $\Delta t = 3 \text{ s}$ .

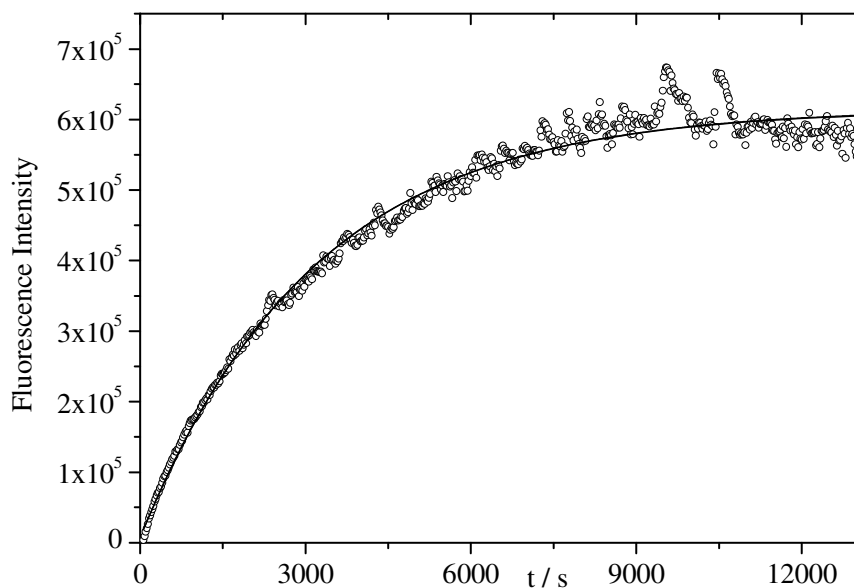


Fig. 93. Increase of fluorescence intensity of the adsorbed species with time of a stirred solution of DANSyl chloride (3 ml dichloromethane + 6 mg silica 2),  $\tilde{\nu}_{ex} = 26700 \text{ cm}^{-1}$ ,  $\tilde{\nu}_{em} = 20000 \text{ cm}^{-1}$ ,  $([B_o] = 0.08 \cdot 10^{-5} \text{ M})$ . Points are measured at time intervals of  $\Delta t = 10 \text{ s}$ .

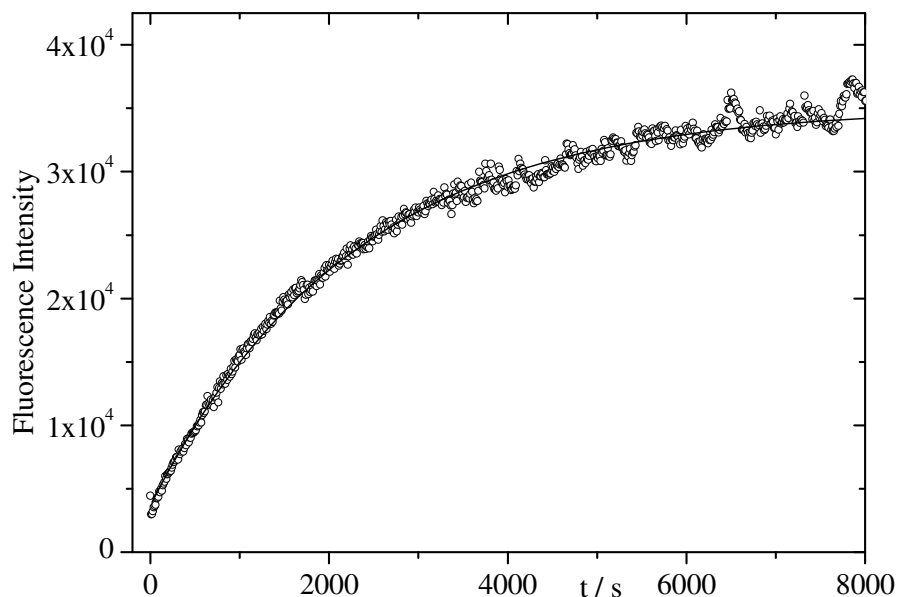


Fig. 94. Increase of fluorescence intensity of the adsorbed species with time of a stirred solution of DANSyl chloride (3 ml dichloromethane + 6 mg silica 3),  $\tilde{\nu}_{ex} = 26700 \text{ cm}^{-1}$ ,  $\tilde{\nu}_{em} = 20000 \text{ cm}^{-1}$ ,  $([B_o] = 0.10 \cdot 10^{-5} \text{ M})$ . Points are measured at time intervals of  $\Delta t = 10 \text{ s}$ .

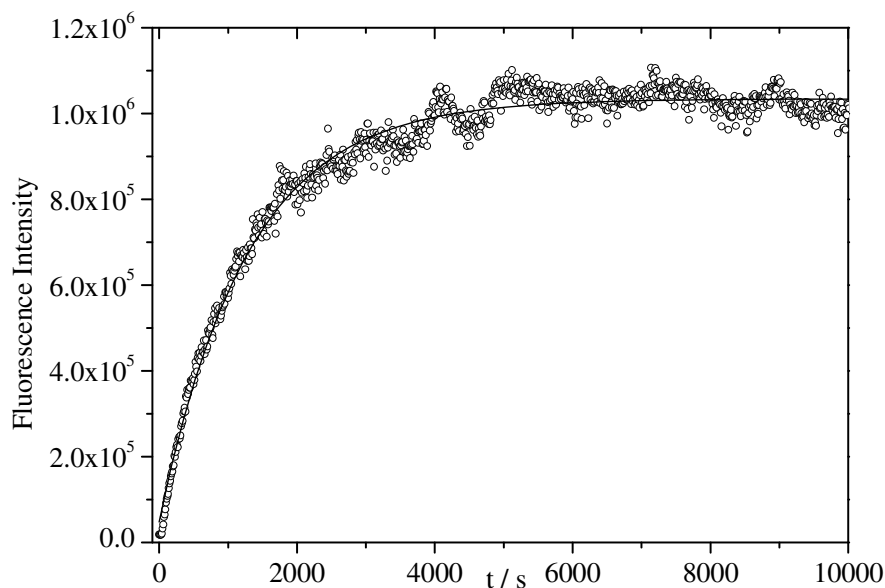


Fig. 95. Increase of fluorescence intensity of the adsorbed species with time of a stirred solution of DANSyl chloride(3 ml dichloromethane + 6 mg silica 4),  $\tilde{\nu}_{ex} = 26700 \text{ cm}^{-1}$ ,  $\tilde{\nu}_{em} = 20000 \text{ cm}^{-1}$ , ( $[B_o] = 0.4 \cdot 10^{-5} \text{ M}$ ). Points are measured at time intervals of  $\Delta t = 10 \text{ s}$ .

The kinetics of formation of DANSyl amide at the four different types silica surfaces is calculated by plotting  $\frac{(I_{F\infty} - I_{Ft})}{I_{F\infty}}$  (see Eq. 45. in the theory part) of DANSyl amide in a semi-logarithmic plot vs. time, Fig. 96. Here  $I_{Ft}$  is the fluorescence intensity at time  $t$  after DANSyl chloride injection and  $I_{F\infty}$  is the fluorescence intensity at equilibrium value (at time  $t \rightarrow \infty$ ). Table 25 shows the concentration of the amino groups at the surface, the effective rate constant,  $k_{eff}$  and the 2<sup>nd</sup>-order rate constant,  $k_b$  for each type of the modified silica.

The curves in Fig. 96 is approximately exponential and this is due to the concentration of the amino groups at the surface ( $[\text{NH}_2]$  in range of  $10^{-4} \text{ M}$ ) is much bigger than of initial concentration of DANSyl chloride ( $[B_o] \approx 10^{-6} \text{ M}$ ). This means also that only the most accessible amino groups are reacted. For 3-aminopropyl silica, the experiment is repeated three times and its always been nonexponential but the deviations are not very serious and may have different causes, e.g., inhomogeneity of the surface.

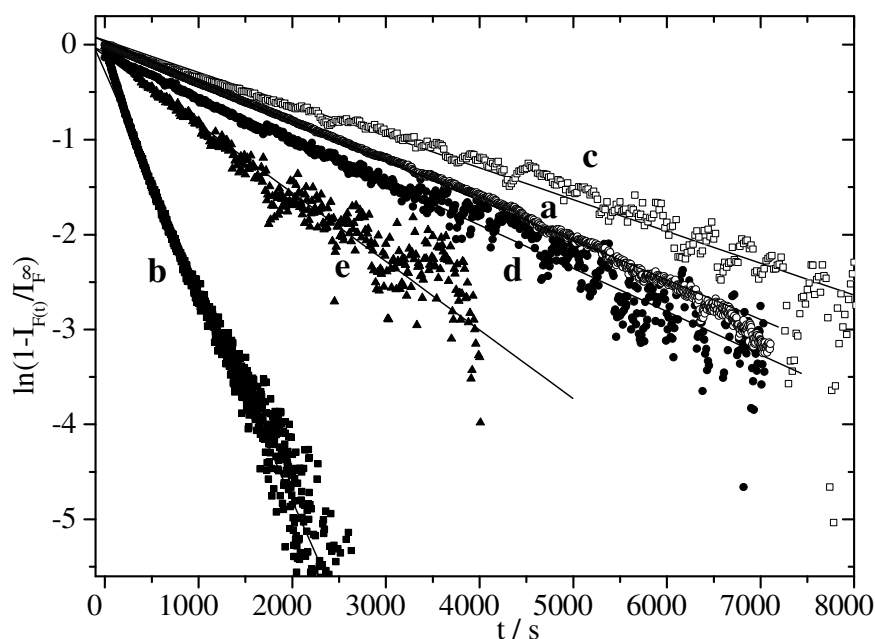


Fig. 96. Semi-logarithmic plot of covalently bound DANSyl amide on a) in solution, concentration of DANSyl chloride ( $[B_o] = 1.9 \cdot 10^{-6} M$ ) b) silica 1, concentration of DANSyl chloride ( $[B_o] = 1.7 \cdot 10^{-6} M$ ), c) silica 2, concentration of DANSyl chloride ( $[B_o] = 0.8 \cdot 10^{-6} M$ ), d) silica 3, concentration of DANSyl chloride ( $[B_o] = 1.0 \cdot 10^{-6} M$ ) and e) silica 4 concentration of DANSyl chloride ( $[B_o] = 0.40 \cdot 10^{-6} M$ ) at  $\tilde{\nu}_{ex} = 26700 \text{ cm}^{-1}$ ,  $\tilde{\nu}_{em} = 20000 \text{ cm}^{-1}$ .

Table 25. Concentration of the amino groups at the surface  $[NH_2] / M$ , the pseudo first order rate constant,  $k_{eff}$ , the 2<sup>nd</sup>-order rate constant  $k_b$  of covalently bound DANSyl amide and the ratio (reacted %) of reacted DANSyl chloride with the amino groups at the different types of modified silica surfaces.

Type of silica	$[NH_2] / 10^{-4} M$	$k_{eff} / 10^{-3} s^{-1}$	$k_b / M^{-1} s^{-1}$	reacted %
Solution	3.3	0.4	1.2	
1	7.4	2.3	3.1	≈ 100
2	2.1	0.3	1.4	≈ 96
3	3.9	0.5	1.3	≈ 84
4	2.8	0.7	2.2	≈ 92



## Discussion

DANSyl chloride dissolved in dry dichloromethane reacts readily and completely with the amino group in 3-aminopropyl, 3-aminopropyl + octyl, 3-aminopropyl + phenyl and 3-aminopropyl + butyric silica surface to form DANSyl amide. This is confirmed by comparing the fluorescence emission and fluorescence excitation spectra of DANSyl amide in dichloromethane (see Fig. 29) to those of the reacted DANSyl chloride at four different types of modified silica. The DANSyl amide which is formed at the surface shows an anisotropy value much higher than that of DANSyl amide in dichloromethane ( $r$  in DCM  $\approx 0$ , see Table 10), which proves that the formed DANSyl amide is actually immobilized at the silica surface. The anisotropy values are smaller than that of DANSyl amide in glycerol. This is due to solvation by dichloromethane which enhances the mobility of the surface anchored molecule [118].

The kinetics of reaction of DANSyl chloride with the amino groups at the modified silica surface is measured by increasing in the fluorescence intensity of the product, DANSyl amide at the surface. The reaction kinetics measurements show that the 2<sup>nd</sup>-order rate constants are in order of  $2 \text{ M}^{-1}\text{s}^{-1}$  which is not significantly different from that in homogeneous solution, i.e. the reaction of DANSyl chloride with the amino group is not hindered by the surface. There are minor differences between the various kinds of silica. This may be due to the surface concentration of the other modifiers used in these experiments. The reaction partners are mainly solvated by dichloromethane, not by silica supported modifiers. This interpretation is also supported by the independence of the DANSyl amide emission spectra of the type of silica.

## Summary

In this work, a comparative study of the surface acidities of different micro-porous solid media based on silicon dioxide (non-modified silica beads, silica beads modified with C30 alkyl chains, silica modified with polymers, and controlled porous glasses) is presented. For this purpose, conjugated molecules with additional electron-donor and proton-acceptor centres are used as adsorbates. Acridine (AC) and some of its derivatives 1,2,7,8-dibenzacridine (1-DBA), 3,4,5,6-dibenzacridine (3-DBA), and acridine orange (AO) are chosen for this study. These probes are used because they are fluorescent molecules with high quantum yields. The positions of the electronic transitions of these molecules are easily to determine. The spectra and photophysical properties of these molecules exhibit considerable changes upon protonation. Also, the molecules have long fluorescence lifetimes in the range of  $10^{-9} - 3 \cdot 10^{-8}$  s which are convenient to measure.

The absorption and fluorescence spectra of the probe molecules in solution are used to compare with the spectra of the adsorbed species, and to distinguish between various surface binding sites of different acidity. The mobilities of the adsorbed probe molecules on the surfaces are determined by the fluorescence anisotropy. The kinetics of the adsorption of the probes at the surfaces are measured by time-dependent absorbance and fluorescence spectroscopy. The accessibility of the adsorbed species at the surfaces to oxygen and the reaction with active groups on chemically modified silica surfaces (mainly amino groups) are also studied by fluorescence spectroscopy.

In the case porous Vycor glass surface as adsorbent and acridine as adsorbate, the excitation and emission spectra must be clearly assigned to the acridinium cation, i.e., the Vycor glass surface protonates acridine in the ground-state. Fluorescence anisotropy measurements reveal that the cationic acridine is immobilized at the porous Vycor glass surfaces. The fluorescence lifetime of adsorbed acridine at Vycor glass is more strongly quenched by oxygen than the respective species in solution (in water at  $\text{pH} \approx 1$ ). This means that the acridine at the solid/air interface are more exposed to oxygen than in solution. The reaction equilibrium is not observed for the adsorption of acridine at porous Vycor glass i.e., all acridine is adsorbed at porous Vycor glass surfaces after  $\approx 60$  min.

1,2,7,8-dibenzacridine is adsorbed at Vycor porous glass surfaces also exclusively in its protonated form as a result from the interaction between acidic surface centers and the free lone pair on the nitrogen. The depolarization measurements reveal that the adsorbed protonated 1,2,7,8-dibenzacridine is immobilized at the Vycor glass surfaces. The fluorescence lifetime of adsorbed 1,2,7,8-dibenzacridine at Vycor glass is more quenched by oxygen than the respective species in solution (in acidic ethanol). The reaction equilibrium can not be observed in case of adsorption of 1,2,7,8-dibenzacridine at porous Vycor glass surfaces.

The steady state fluorescence and fluorescence decays reveal that 3,4,5,6-dibenzacridine is adsorbed at Vycor porous glass and forms the protonated species at the surface. The fluorescence anisotropy spectrum demonstrates that the protonated species of 3,4,5,6-dibenzacridine are immobilized at the Vycor glass surface. A finite equilibrium is observed when 3,4,5,6-dibenzacridine is adsorbed at the porous Vycor glass surface.

The kinetics of adsorption of acridine, 1,2,7,8-dibenzacridine and 3,4,5,6-dibenzacridine at the porous Vycor glass surfaces are studied by measuring the absorbance of the adsorbed protonated species at porous Vycor glass surfaces. By comparing the values of the total rate constant of adsorption  $k_{tot}$ , which is calculated in a first-order approximation, it is noticed that the rates of the adsorption of the three compounds at PVG decrease in the following order; acridine > 1,2,7,8-dibenzacridine >> 3,4,5,6-dibenzacridine. This is due to the difference in the effective diffusion coefficient  $D_{eff}$  of the three compounds into the glass sheet. Since the effective diffusion coefficient which obtained from the algorithm in section 2.6. (theory part) shows that  $D_{eff}$  of the three compounds is decreases according to the following order: acridine > 1,2,7,8-dibenzacridine >> 3,4,5,6-dibenzacridine. This means that the adsorption of the three probes at porous Vycor glass surfaces is diffusion controlled.

1,2,7,8-dibenzacridine is adsorbed at the Geltech porous glass as protonated molecule and as H-bonded species which both are immobilized at the surface. Upon excitation the H-bonded species is transformed to the protonated form.

Non-modified silica beads are applied as adsorbent for acridine from solution in cyclohexane and the main surface product is H-bonded acridine (B....H) which is protonated in the excited singlet state. The fluorescence anisotropy spectrum demonstrates that the

adsorbed acridine is immobilized at silica surface. The fluorescence lifetime of adsorbed acridine, at non-modified silica is more strongly quenched by oxygen than the respective species in solution (in water at  $\text{pH} \approx 1$  for AC).

1,2,7,8-dibenzacridine is mainly assigned to protonated cations ( $\text{Si-O}^-\dots^+(\text{HB})$ ) and hydrogen-bonded complexes ( $\text{Si-OH}\dots\text{B}$ ) at non-modified silica surface. The ratio between the two species at the silica surface depends on the water coverage of the silica surface. The hydrogen-bonded species undergo protonation upon excitation. The fluorescence excitation anisotropy spectra and the fluorescence life times value it possible to distinguish between the two adsorbed species (protonated and hydrogen-bonded) of 1,2,7,8-dibenzacridine at the silica surface.

In case of non-modified silica as adsorbent and acridine and /or 1,2,7,8-dibenzacridine as adsorbates, a finite equilibrium is observed and calculated. This reaction equilibrium depends on the water coverage of the non-modified silica surface (and thus on the humidity of air).

In contrast, in case of porous Vycor glass as adsorbent, there is quantitative adsorption, i.e. no equilibrium is observed with acridine and 1,2,7,8-dibenzacridine. This is because of the strong binding to the surfaces that substantially reduces the rate of desorption.

The kinetic studies for the adsorption of acridine and 1,2,7,8-dibenzacridine at the non-modified silica beads surface from cyclohexane solution show that, the rate of adsorption of acridine is faster than the rate of adsorption of 1,2,7,8-dibenzacridine. This is may be due to the difference in the diffusion coefficient of acridine and 1,2,7,8-dibenzacridine into the silica particles. The effective diffusion coefficient of acridine which obtained from the algorithm in section 2.6. (theory part) is higher than that of 1,2,7,8-dibenzacridine.

3,4,5,6-dibenzacridine is not adsorbed from cyclohexane and not protonated at the silica beads surface, since the free electron pair on the nitrogen is sterically shielded by the benzo groups. AO is adsorbed at non-modified silica and is immobilized at the surfaces.

1,2,7,8-dibenzacridine is adsorbed at silica C30 from cyclohexane solution. There are two species formed at the silica C30 surface; the main one is the protonated form of 1,2,7,8-dibenzacridine and the other is the hydrogen-bonded species. The fluorescence excitation

anisotropy distinguishes the two adsorbed species on silica C30 surface. The oxygen quenching rate constant for protonated 1,2,7,8-dibenzacridine at silica C30 surface is slightly lower with respect to the non-modified surface and also with respect to the acidic solution. This is due to the lower mobility of oxygen in the interphase since, oxygen is not capable of penetrating between the alkyl chains.

1,2,7,8-dibenzacridine is not adsorbed at the silica modified with TBB-polymer (see Fig. 17) and the fluorescence anisotropy spectrum demonstrates that, since it has value of  $r \approx 0$  which is exactly the value for 1,2,7,8-dibenzacridine in cyclohexane. This means that the TBB coating shields most of surface silanol groups from the interaction with the probes.

Acridine orange is still adsorbed at silica modified with 200 mg of polymerized divinylbenzene (DVB-coated silica) and forms the protonated molecule due to the interaction with residual silanol groups. On the other hand, a very small amount of acridine orange is adsorbed at TBB-coated silica less than 5%. This means that the TBB coating shields most of the acidic surface silanol groups from the fluorescence analysis, whereas the DVB-coating shields only some of the surface silanol groups. The decrease of accessible surface silanol groups is in the series: non-modified silica  $\geq$  silica C30  $>$  DVB-coated silica  $>$  TBB-coated silica.

5-Dimethyl amine naphthalene-1-sulfon (DANSyl) chloride is used to quantify the reaction of silica modified with amino-groups, since DANSyl chloride is a non-fluorescent probe in dry dichloromethane. DANSyl chloride reacts with the amino-groups at the silica surface and forms DANSyl amide, which is a fluorescent probe. DANSyl chloride dissolved in dry dichloromethane reacts readily and completely with the amino group in 3-aminopropyl, 3-aminopropyl + octyl, 3-aminopropyl + phenyl and 3-aminopropyl + butyric silica surfaces to form DANSyl amide. The DANSyl amide which is formed at the surface shows an anisotropy value much higher than that of DANSyl amide in dichloromethane ( $r$  in DCM  $\approx 0$ ) which proves that the formed DANSyl amide is actually immobilized at the silica surface. The kinetics of reaction of DANSyl chloride with the amino groups at the modified silica surface is measured by the time-dependent increase in the fluorescence intensity of the product, DANSyl amide at the surface. The reaction kinetics measurements show that the 2<sup>nd</sup>-order rate constants are in order of  $2 \text{ M}^{-1}\text{s}^{-1}$  which is not significantly different from that in homogeneous solution.

## References

- [1] a) J. A. Marqusee and K. A. Dill, *J. Chem. Phys.*, **85**; 434 (1986).  
b) J. G. Dorsey and K. A. Dill, *Chem. Rev.*, **89**; 331 (1989).
- [2] L. C. Sander and S. A. Wise in *Retention and Selectivity Studied in HPLC* (Ed.: R. M. Smith), Elsevier, Amsterdam, pp. 337 (1994).
- [3] K. Albert, T. Lacker, M. Raitza, M. Prusch, H.-J. Egelhaaf, and D. Oelkrug, *Angew. Chem.*, **110**; 809 (1998); *Angew. Chem. Int. Ed.*, **37**; 778 (1998).
- [4] D. Oelkrug, M. Radjaipour, and H. Erbse, *Z. Phys. Chem. N.F.*, **88**; 23 (1974).
- [5] R. K. Bauer, P. de Mayo, W. R. Ware, and K. C. Wu, *J. Phys. Chem.*, **86**; 3781 (1981).
- [6] K. A. Zachariasse, in M. Anpo and T. Matsuura (Eds.), *Photochemistry on Solid Surfaces, Studies in Surface Science and Catalysis, Vol. 47*, Elsevier, Amsterdam; 48 (1989).
- [7] D. Oelkrug, H. Erbse, and M. Plauschinat, *Z. Phys. Chem. N.F.*, **96**; 283 (1975);  
D. Oelkrug and M. Radjaipour, *Z. Phys. Chem. N.F.*, **123**; 163 (1980).
- [8] D. Oelkrug, G. Schrem, and I. Andrä, *Z. Phys. Chem. N.F.*, **106**; 197(1977); K. Rempfer, S. Uhl and D. Oelkrug, *J. Mol. Struct.*, **114**; 225 (1984).
- [9] J. B. F. Lloyed, *Analyst*, **100**; 529 (1975).
- [10] P. Hite, R. Krasnansky, and J.K. Thomas, *J. Phys. Chem.*, **90**; 5795 (1986).
- [11] S. A. Samchuk, N. P. Smirnova, and A. M. Eremenko, *J. Appl. Spectrosc.*, **52**; 195 (1990);  
N. P. Smirnova, A. M. Eremenko and A.A. Chuiko, *J. Mol. Struct.*, **218**; 453 (1990).
- [12] S. Suzuki and T. Fujii, in M. Anpo and T. Matsuura (Eds.), *Photochemistry on Solid Surfaces*, Elsevier, Amsterdam; 79 (1989).
- [13] D. Oelkrug, W. Flemming, R. Füllemann, R. Günther, W. Honnen, G. Krabichler, M. Schäfer, and S. Uhl, *Pure & Appl. Chem.*, **58**; 1207 (1986).
- [14] J. J. Kirbland and C. H. Diks, J. and J. J. Destefano, *J. Chromatogr.*, **19**; 635 (1993).
- [15] J. Köhler, D. B. Chase, R. O. Farlee, A. J. Vega, and J. J. Kirbland, *J. Chromatogr.*, **275**; 352 (1986).
- [16] J. Köhler and J. J. Kirbland, *J. Chromatogr.*, **125**; 385 (1987).
- [17] B. Pfleiderer and E. Bayer, *J. Chromatogr.*, **67**; 468 (1989).
- [18] Li. Zengbiao and C. Rutan Sarah, *Anal. Chimica Acta*, **312**; 127 (1995).
- [19] L. T. Zhuravalev, *Colloids and Surfaces*, **173**; 1 (2000).
- [20] H. A. Benesi, *J. Am. Chem. Soc.*, **78**; 5490 (1956).
- [21] M. L. Hair and W. Hertl, *J. Phys. Chem.*, **47**; 91 (1970).

- [22] K. Marshall, G. L. Ridge Will, C. H. Rochester, and J. Simpson, *Chem. Ind. (London)* (1974).
- [23] T. Morimoto, J. Imai, and M. Nagao, *J. Phys. Chem.*, **78**; 704 (1974).
- [24] A. B. Morraw and A. I. Cody, *J. Phys. Chem.*, **79**; 761 (1975).
- [25] G. M. Whitesides, H. A. Biebuyck, J. P. Folkers, and K. L. Prime, Acid-bas interactions: in wetting. In K.L. Mittal and H. R. Anderson (Eds), *Acid-base interactions: Relevance to Adhesion Science and Technology*. VSP, Utrecht; 229 (1991).
- [26] A. Gervasini and A. Auroux, *J. Phys. Chem.*, **97**; 2628 (1993).
- [27] K. Tanabe, M. Risono, Y. Ono, and H. Hattori, *New Solid Acids and Bases: Their Catalytic Properties*. Elsevier, Amsterdam, (1989).
- [28] L. P. Hammett and A. J. Deyrup, *J. Am. Chem. Soc.*, **54**; 2721 (1932).
- [29] L. P. Hammett, *Chem. Rev.*, **16**; 67 (1935).
- [30] C. Walling, *J. Am. Chem. Soc.*, **72**; 1164 (1950).
- [31] H. A. Benesi, *J. Phys. Chem.*, **61**; 970 (1957).
- [32] F. M. Fowkes, H. A. Benesi, L. B. Ryland, W. M. Sawyer, K. D. Detling, E. S. Loeffler, F. B. Folchmer, M. R. Johnson, and Y. P. Sun, *Agric. Food Chem.*, **8**; 203 (1960).
- [33] J. G. Mason, R. Siriwardane, and J.P. Wightman, *J. Adhes.*, **11**; 315 (1981).
- [34] F. M. Fowkes, Characterization of solid surfaces by wet chemical techniques. In: F. M. Fowkes, L. A. Casper and C. J. Powell (Eds.), *Industrial Applications of Surface Analysis*. ACS symposium series 199; **69** (1982).
- [35] B. W. Glombitza, D. Oelkrug, and P. C. Schmidt, *Eur. J. Pharm. Biopharm.*, **40**; 289 (1994).
- [36] S. Uhl, K. Rempfer, H.-J. Eglhaaf, B. Leher, and D. Oelkrug, *Anal. Chim. Acta*, **303**; 17 (1995).
- [37] L. R. Snyder, J. J. Kirkl, and J. L. Glajch, *Practical HPLC Method Development*, second ed., Wiley, New York, pp. 178 (1977).
- [38] K. G. Wahlund and A. Sokolowski, *J. Chromatogr.*, **151**; 299 (1978).
- [39] B. A. Person and B. L. Karger, in H. Engelhardt (Ed.), *Practice of High Performance Liquid Chromatography*, Spring, Heidelberg, pp. 201 (1986).
- [40] S. M. Hansen, P. Helboe, and M. Thomson, *J. Chromatogr.*, **544**; 53 (1991).
- [41] J. Nawrocki and B. Buszewski, *J. Chromatogr.*, **449**; 1 (1988).
- [42] L. C. Tan and P. W. Carr, *J. Chromatogr. A*, **799**; 1 (1998).

- [43] B. Buszewski, Z. Suprynowicz, P. Staszczuk, K. Albert, B. Pfeleiderer, and E. Bayer, J. Chromatogr., **449**; 305 (1990).
- [44] L. Sander and S. A. Wise, LC GC Int., **3** No. 6; 24 (1990).
- [45] H. Engelhardt and A. M. Cunat-Walter, J. Chromatogr. A, **716**; 27 (1995).
- [46] B. Yan, J. Zhao, S. J. Brown, F. Blackwell and W. P. Carr, Anal. Chem., **72**; 1253 (2000).
- [47] J. Zhao and W. P. Carr, Anal. Chem., **71**; 5217 (1999).
- [48] E. Boschetti, J Chromatogr., **658**; 207 (1994).
- [49] D. Bentrop, J. Kohr, and J. Engelhardt, Chromatographia, **32**; 171 (1991).
- [50] S. Durie, K. Jerabek, C. Mason, and C. D. Sherrington, Macromolecules, **35**, 9665 (2002).
- [51] W. Halled, Application of controlled pore glass in solid phase biochemistry, in: W. H. Scouten (Ed.), Solid phase Biochemistry, Jhon Wiley and Sons, New York, 635 (1983).
- [52] R. Schnabel and P. Langer, J. Chromatogr., **544**; 137 (1991).
- [53] T. H. Elmer, Porous and reconstructed glasses, in: S. J. Schnieder, Jr. (Ed.), ASM Engineered Materials Handbook, vol. **4**, ASM, Materials Park, OH, 427 (1991).
- [54] W. Haller, Nature, **206**; 693 (1965).
- [55] A.L. Spatorico, J. Appl. Polym. Sci., **12**; 1610 (1975).
- [56] A. N. Sidorov. Opt. Spektrosk. ( Akad. Nauk SSSR, Otd. Fiz.-Mat. Nauk), **8**; 424 (1960) (English transiliation).
- [57] N. W. Cant and L.H: Little, Can. J. Chem., **42**; 802(1964); **43**; 1252 (1965).
- [58] D. Lev Gelb and K. E. Gubbins, Fundamentals of Adsorption, **6**; 551 (1999).
- [59] J. K. Thomas, J. Phys. Chem., **91**; 267 (1987).
- [60] R. Krasnansky and J. K. Thomas, Langmuir, **10**; 4551 (1994).
- [61] G. Fischer and U. Pindur. Pharmazie, **54**; 83 (1999).
- [62] J. J. Aaron, M. Maafi, C. Párkányi, and C. Bonface, Spectrochim. Acta , **51A**;603 (1995).
- [63] R. M. Acheson, Heteroaromatic cyclic compounds, Wiley Interscience, New York (1973).
- [64] K. Kasama, K. Kikuchi, Y. Nishida, and H. Kokubun, J. Phys. Chem.,**85**; 4148 (1981).
- [65] L. A. Diverdi and M.R. Topp, J. Phys. chem., **88**; 3447 (1984).
- [66] K. Kasama, K. Kikuchi, S. Yamamoto, K. Vjite, Y. Nishidy, and H. Kokubun, J. Phys. Chem., **85**; 1291 (1981).
- [67] K. Kasama, K. Kikuchi, K. Uji-Ie, S. Akiyamamoto, and H. Kokubun, J. Phys. Chem., **86**; 4733 (1982).



- [68] O. R. Pons, L. S. Andres, and M. Merchan, *J. Phys. Chem. A*, **105**; 9664 (2001).
- [69] N. Mataga, Y. Kailu, and M. Koizumi, *Bull. Chem. Soc. Jpn.*, **29**; 373 (1956).
- [70] N. Mataga and S. Tsuno, *Bull. Chem. Soc. Jpn.*, **30**; 368 (1959).
- [71] E. J. Bowen, N. J. Holder, and G. B. Woodger, *J. Phys. Chem.*, **66**; 2991 (1962).
- [72] Y. Hirata and I. Janaka, *Chem. Phys. Lett*, **41**;336 (1976).
- [73] V. Sundstrom, P. M. Rentzepis, and E. C. Lim, *J. Chem. Phys.*, **66**; 4287 (1977).
- [74] D. Oelkrug, S. Uhl, M. Gregor, R. Lege, G. Kelly, and F. Wilkinson, *J. Mol. Struct.*, **218**; 435 (1990).
- [75] D. Oelkrug, M. Gregor, and S. Reich, *Photochem. and Photobiol.*, **54** (4); 539 (1991).
- [76] I. Negron-Encarnacion, R. Arce, and M. Jimenez, *J. Phys. Chem. A*, **109**; 787 (2005).
- [77] S. A. Samchuk, N. P. Smirnova, and A. M. Eremenko, *J. Appl. Spectr.*, **52**; 195 (1990).
- [78] N. P. Smitnova, S. A. Samchuk, A. M. Yeremenko, and A. A. Chuiko, *J. Mol. Struct.*, **218**; 453 (1990).
- [79] A. M. Eremenko, N. P. Smirnova, V. M. Ogenko, and A. A. Chuiko, *Res. Chem. Intermed.*, **19** (9); 855 (1993).
- [80] T. Shimosaka, T. Sugii, and T. Hobo, J. B. Alexanged Ross and K. Uchiyama, *Anal. Chem.*, **72**; 3532 (2000).
- [81] S. Tsuneda, T. Endo, K. Saito, K. Sugita, K. Horie, T. Yamashita, and T. Sugo, *Chem. Phys. Lett.*, **275**; 203 (1997).
- [82] A. Weller, *Z. Elektrochem. Ber. Bunsenges. Phys. Chem.*, **61**; 956 (1957).
- [83] A. Gafni and L. Brand, *Chem. Phys. Lett.*, **58**; 346 (1978).
- [84] V. Zanker, *Z. phys. chem.*, **199**; 225 (1952).
- [85] M. Pursch, L. C. Sander, and K. Albert, *Anal. Chem.*, **68**; 4107 (1996).
- [86] M. Pursch, S. Strohschein, H. Händel, and K. Albert, *Anal. Chem.*, **68**; 386 (1996).
- [87] B. F. Gisi., *Anal. Chim. Acta*, **58**; 248 (1972).
- [88] Geltech Cooperation, 3267 Progress Dr. Orlando, FL 32826.
- [89] H.-H. Perkampus, A. Knop, and J. V. Knop *Spectrochim. Acta*, **25A**, 1584 (1969).
- [90] V. Zanker, P. Schimdt, *Chem. Ber.*, **92**; 615 (1959).
- [91] S. Uhl, Ph. D. Thesis, Tübingen University, (1994).
- [92] M. E., Lamm and D.M., Neville, *J. Phys. Chem.*, **69**; 3872 (1965).
- [93] B. H. Robinson, A. Loeffler, and G. Schwarz, *J. Chem. Soc. Faraday Trans.*, **69**; 56 (1973).
- [94] A. B. Demyashkevich and M.g. Kuzmin, *Russian J. Phys. Chem.*, **53**; 699 (1979).
- [95] L. A. Diverdi and M. R. Topp, *J. Phys. Chem.*, **88**; 3447 (1984).

- [96] K. J. Choi, L. A. Hallidy, and M. R. Topp, in: R. Hochstrasser, W. Kaiser, C.V. Skank (Eds.), *Picosesond Phenomena II*; Springer Verlag, Berlin, Heidelberg, New York; 131 (1980).
- [97] P. Lühring and A. Schumpe, *J. Chem. Eng. Data*, **34**; 250 (1989).
- [98] J. R. Lakowicz, *Principles of fluorescence spectroscopy*, Kluwer Academic / Plenum, New York; 238 (1999).
- [99] I. N.-Encarnacion, M. J.-Perez, and R. Arce, *J. Division of Enviromental Chemistry*, **42 (1)**; 1 (2002).
- [100] R. S. Mulliken, *J. Am. Chem. Soc.*, **74**; 811 (1952).
- [101] M. J. Basila, *Chem. Phys. Lett*, **35**; 1151 (1961).
- [102] L. R. Snyder, *J. Phys. Chem.*, **67**; 9622 (1963).
- [103] P. Hobza, J. Saud, C. Morgeneyer, J. Hurych, and R.J. Zanradnik, *Phys. Chem. Lett.*, **85**; 4061 (1981).
- [104] W. J. Pohle, *J. Chem. Soc., Faraday Trans. 1*; 78 (1982).
- [105] E. J. Bowen, N. J. Holder, and G. B. Woodger, *J. Phys. Chem.*, **66**; 2491 (1962).
- [106] G. B. Cox, *J. Chromatgr., A*, **656**; 353 (1993).
- [107] O. S. Wolfbeis and G. Boide, *Applications of optochemical sensors for measuring chemical quantities*, Vol. **3**, S. 893f., in: W. Göpel, J. Hesse, and J. N. Zemel (Eds.), *Sensors. A comprehensive survey*, VCH, Weinheim (1992).
- [108] W. Trettnal, *Optical sensors based on fluorescence quenching*, S. 81, in: O. S. Wolbeis (Ed.), *Fluorescence spectroscopy. New methods and applications*, Springer, Berlin-Heidelberg (1993).
- [109] O. S. Wolbeis, *Nacher. Chem. Tech. Lab*. **43**; 313 (1995).
- [110] Th. Wolff, F. Akbarain, and G. V. Büнау, *Ber. Bunsenges. Phys. Chem.*, **94**; 833 (1990).
- [111] S. Wolfgang and H. D. Gagney, *J. Phys. Chem.*, **87**; 5395 (1983).
- [112] R. Krasnansky, K. Koike, and J. K. Thomas, *J. Phys. Chem.*, **94**; 4521 (1990).
- [113] E. Holder, D. Oelkrug, H.-J. Egelhaaf, H. A. Mayer, and E. Linder, *J. Fluorescence*, **12**, Nos. 3/4; 383 (2002).
- [114] L. Sander and S. A. Wise, *LC · GC Int.*, **3** No. 6; 24 (1990).
- [115] R. E. Majors, *J. Chromatogr.*, **18**; 489 (1980).
- [116] R. E. Majors, *LC · GC Int.*, **3** No. 6; 12 (1990).
- [117] L. Sander and S. A. Wise, *CRC Crti. Rev. Anal. Chem.*, **18**; 299 (1987).
- [118] B. Lehr, H.-J. Egelhaaf, H. Fritz, W. Rapp, E. Bayer, and D. Oelkrug, *Macromolecules*, **29**; 7931 (1996).

Meine akademischen Lehrer waren - neben Prof. Dr. D. Oelkrug and H.-J. Egelhaaf in Tübingen and Prof. Dr. Ahmed B. Zaki and Prof. Dr. Ali H. Gemeay in Tanta, Ägypten- die Dozenten und Professoren:

K. Albert, H. Bertagnolli, F. Brandstetter, H.-J. Egelhaaf, E. Linder, H. A. Mayer, K. Müller, U. Nagel, C. Ochsenfeld, W. Rosenstiel, V. Schurig, B. Speiser, L. Wesemann, K.-H. Wiesmüller.

## Lebenslauf

**Name** : Abeer Salah Eldeen Elsherbiny.

**Geburtstag** : 27/10/1973.

**Geburtsort** : Damrow- Gharbia Governorate, Ägypten.

### Schulbildung :

1979-1985 Grundschole in Damrow, Elmehalla Elkubra, Ägypten.

1985-1988 Vorbereitungsschole in Damrow, Elmehalla Elkubra, Ägypten.

1988- 1991 Gymnasium in Elsaída Zinab, Elmehalla Elkubra, Ägypten.

1991- 1995 B. Sc., in Chemie , Fakultät für Naturwissenschaften,  
Tanta Universtät.

1995- 1996 Post-graduate courses.

1996-1999 M. Sc. in Chemie (Physikalische Chemie)  
(Kinetic study of the interaction between montmorillonite  
and some organic compounds).

**Promotion:** Antfertigung der vorliegenden Dissertation am Institut für  
2002-2006 Physikalische und Theoretische Chemie der Unverstät Tübingen  
unter Anleitung von Herrn Prof. Dr. D. Oelkrug.

**Arbeit** : Assistent lecturer in Chemie Abteilung, Tanta Universtät, Ägypten.

**Familien stand** : Verheiratet , zwei kinder.